

**GAS-PHASE FRAGMENTATION MECHANISMS  
OF PROTONATED PEPTIDES VIA TANDEM  
MASS SPECTROMETRY**

**A Thesis Submitted to  
the Graduate School of Engineering and Sciences of  
İzmir Institute of Technology  
in Partial Fulfillment of the Requirements for the Degree of**

**DOCTOR OF PHILOSOPHY**

**in Chemistry**

**by  
Çağdaş TAŞOĞLU**

**December 2013  
İZMİR**

We approve the thesis of **Çağdaş TAŞOĞLU**

**Examining Committee Members:**

---

**Prof. Dr. Talat YALÇIN**

Department of Chemistry, Izmir Institute of Technology

---

**Prof. Dr. Şefik SÜZER**

Department of Chemistry, Bilkent University

---

**Prof. Dr. Bekir SALİH**

Department of Chemistry, Hacettepe University

---

**Prof. Dr. Levent ARTOK**

Department of Chemistry, Izmir Institute of Technology

---

**Prof. Dr. Nuran ELMACI**

Department of Chemistry, Izmir Institute of Technology

20 December 2013

---

**Prof. Dr. Talat YALÇIN**

Supervisor, Department of Chemistry  
Izmir Institute of Technology

---

**Assist. Prof. Dr. Alper ARSLANOĞLU**

Co-Supervisor, Department of Molecular  
Biology and Genetics  
Izmir Institute of Technology

---

**Prof. Dr. A. Emin EROĞLU**

Head of the Department of  
Chemistry

---

**Prof. Dr. R. Tuğrul SENGER**

Dean of the Graduate School of  
Engineering and Sciences

## ACKNOWLEDGEMENTS

First of all, I owe my sincere gratitude to Prof.Dr. Talat YALÇIN for not only his guidance, motivation, enthusiasm, wisdom, persistent assistance, understanding, and patience but also for his endless knowledge in any subject and sharing his life experience whenever I need... His expertise extends far beyond mass spectrometry so that I could not have imagined having a better supervisor and mentor for my Ph.D. study. I am also grateful to the rest of my thesis committee; Prof.Dr. Şefik SÜZER, Prof.Dr. Bekir SALİH, Prof.Dr. Levent ARTOK and Prof.Dr. Nuran ELMACI for their invaluable contributions, useful suggestions, and constructive comments on my thesis study.

I am appreciative of the financial support from The Scientific and Technological Research Council of Turkey (TÜBİTAK) for research projects (Project No: 109T430 – 112T558), and providing me the graduate scholarship for four years (TÜBİTAK BİDEB 2211: National Scholarship Program for Ph.D. Students). The State Planning Organization, DPT, (Project No: 2008K120730) is also gratefully acknowledged for its financial assistance for the foundation of İYTE Mass Spectrometry Facility.

Moreover, I would particularly like to thank to Dr. Filiz YEŞİLIRMAK for her endless help, moral support, and being with me in my hard times. I also thank to my friends and labmates; Sila KARACA, Melda GÜRAY, Melike DİNÇ, and Özge GÖRGÜN for their kind friendship, help, and all we have had in the last five years. Without their presence, labwork would have been boring and harder, too.

Last but not the least; I am greatly indebted to my father; Mahmut TAŞOĞLU who has always been a source of inspiration and encouragement to me throughout my life... Life has become more unbearable without you... Then, I would like to express my gratitude to my both mothers; Lütfiye TAŞOĞLU for her spiritual protection throughout my life, and Şaduman TAŞOĞLU for growing me up. I also thank my lovely sister Özlem TAŞOĞLU for being my best friend all my life. Finally, my deepest and most heartfelt appreciation goes to Elvan HANGÜNEY, my twin flame and little Calimero, for changing my life and making me believe in miracles after all...

# ABSTRACT

## GAS-PHASE FRAGMENTATION MECHANISMS OF PROTONATED PEPTIDES VIA TANDEM MASS SPECTROMETRY

Protein identification based on enzymatic digestion of proteins and tandem mass spectrometric (MS/MS) analysis of peptide fragments has become a more popular method than classical approaches like Edman degradation. However, today's protein sequencing tools have been constructed on a limited basis of peptide fragmentation chemistry such that some peptides can fragment in unusual ways that may not be predicted by the current bioinformatics software. Thus, erroneous assignments can be done in protein identification, which can lead to vital problems. Herein, it was aimed to reveal the rich chemistry lying behind the gas-phase fragmentation of peptides containing specific residues using MS/MS and collision induced dissociation (CID) analysis. As a result, the implementation of more detailed peptide fragmentation mechanisms into bioinformatics algorithms will no doubt help to improve database search tools.

Results clearly indicate that  $b_6$  and  $b_7$  ions have higher tendency towards macrocyclization when compared to  $b_5$  ions. Besides it was observed that neighboring amino acid influences the selective opening of the macrocyclic structure and no preferential cleavage order can be specified depending on the amino acid residue. Next study showed that proline-containing peptides have high tendency to place the proline residue in the N-terminal position during the ring opening of macrocyclic structure. This is then followed by dipeptide elimination of proline with its adjacent C-terminal residue. Moreover, we demonstrated that sequence-scrambling exists for all histidine-containing peptides whatever the residue position and neighbor residue is. Additionally, we suggest that  $\alpha$ -amino- $\epsilon$ -caprolactam formation at the side chain of lysine prevents macrocyclization reaction of  $b_7$  when K is positioned at the C-terminus. Finally, it was observed that macrocyclization reaction proceeds for peptides containing arginine when arginine gets closer to the C-terminus. Besides arginine was found to behave like lysine and forms ornithine when located at the C-terminus.

## ÖZET

### PROTONLANMIŞ PEPTİTLERİN SIRALI KÜTLE SPEKTROMETRESİ İLE GAZ-FAZI PARÇALANMA MEKANİZMALARI

Proteinlerin enzimle parçalanması ve bunun sonucunda oluşan peptit parçalarının tandem kütle spektrometresiyle analizine dayalı protein tanımlanması, Edman degradasyonu gibi klasik yaklaşımlardan daha popüler bir metot haline gelmiştir. Fakat günümüz protein sekanslama araçları, sınırlı bir peptit parçalanma kimyasına dayalı olarak oluşturulmuştur, öyle ki; bazı peptitler geçerli biyoinformatik yazılımlarınca tahmin edilemeyen olağandışı şekillerde parçalanabilmektedir. Bu nedenle protein tanımlamasında hayati problemlere neden olabilecek hatalı belirlemeler yapılabilir. Bu noktada spesifik amino asitler içeren peptitlerin gaz fazı parçalanmalarının arkasında yatan zengin kimyanın MS/MS ve CID analizleri kullanarak ortaya çıkarılması amaçlanmıştır. Sonuç olarak, daha detaylı peptit parçalanma mekanizmalarının biyoinformatik algoritmalara uyarlanması, veritabanı araştırma araçlarının geliştirilmesine şüphesiz yardımcı olacaktır.

Sonuçlar  $b_7$  ve  $b_6$  iyonlarının  $b_5$  iyonlarına kıyasla makrohalkalaşmaya daha eğilimli olduğunu açıkça gösterdi. Ayrıca komşu amino asitin, makrohalkalı yapının seçici açılmasını etkilediği ve amino asite bağlı herhangi bir tercihten parçalanma sıralamasının yapılamayacağı gözlemlendi. Sonraki çalışma, prolin içeren peptitlerin makrohalkalı yapıda halka açılımı sırasında prolini N-terminal pozisyona yerleştirmeye oldukça eğilimli olduğunu gösterdi. Bu, daha sonra prolin ve ona C-terminal'den bağlı amino asitin ikili bir peptit olarak kopması ile devam eder. Diğer taraftan histidin içeren tüm peptitlerde amino asit pozisyonu ve komşu amino asit ne olursa olsun sekans bozulmasının var olduğunu kanıtladık. Buna ek olarak lizin C-terminal'deyken fonksiyonel gruptaki  $\alpha$ -amino- $\epsilon$ -caprolactam oluşumunun,  $b_7$ 'nin makrohalkalaşma reaksiyonunu engellediğini öne sürüyoruz. Son olarak arjinin içeren peptitlerde, arjinin C-terminus'a yaklaştıkça makrohalkalaşma reaksiyonunun gerçekleştiği gözlemlendi. Ayrıca arjininin C-terminaldeyken lizin gibi davrandığı ve ornitin oluşturduğu bulundu.

*To the memory of my father, Mahmut Taşođlu...*

*'Every man dies, not every man really lives.'*

*Randall Wallace*

# TABLE OF CONTENTS

ACKNOWLEDGEMENTS .....	iii
ABSTRACT.....	iv
ÖZET .....	v
TABLE OF CONTENTS.....	vii
LIST OF FIGURES .....	x
LIST OF SCHEMES .....	xii
LIST OF TABLES .....	xiii
LIST OF ABBREVIATIONS.....	xiv
CHAPTER 1. INTRODUCTION TO MASS SPECTROMETRY .....	1
1.1. What is Mass Spectrometry? .....	1
1.2. Ionization Sources.....	3
1.2.1. Electrospray Ionization (ESI).....	3
1.2.2. Matrix-Assisted Laser Desorption/Ionization (MALDI) .....	5
1.3. Mass Analyzers.....	5
1.3.1. Linear Quadrupole Mass Analyzer .....	6
1.3.2. Ion-Trap Mass Analyzer .....	7
1.3.3. Time-of-Flight Mass Analyzer.....	8
1.3.4. Fourier Transform Ion Cyclotron Resonance Mass Analyzer .....	9
1.4. Ion Detectors.....	10
CHAPTER 2. MASS SPECTROMETRY OF PROTONATED PEPTIDES.....	11
2.1. Amino Acids and Peptides.....	11
2.2. Peptide Fragmentation .....	12
2.3. Side Chain Effects .....	17
2.4. Tandem Mass Spectrometry and Collision-Induced Dissociation...	20
2.5. Aim of the Study.....	21
CHAPTER 3. EXPERIMENTAL.....	23
3.1. Materials .....	23
3.2. Mass Spectrometry .....	23

CHAPTER 4. INVESTIGATION OF PEPTIDE SIZE, RESIDUE POSITION, NEIGHBOR AMINO ACID AND SIDE CHAIN EFFECT ON MACROCYCLIZATION OF $b_n$ ( $n = 5 - 7$ ) IONS.....	26
4.1. Introduction.....	26
4.2. Experimental.....	27
4.3. Results and Discussion .....	27
4.3.1. Influence of Neighbor Amino Acid on Preferential Opening of Macrocyclic b Ion .....	27
4.3.2. Effects of Peptide Size, Residue Position, Neighbour Residue, and Side Chain on Preferential Opening of Macrocyclic b Ion.....	31
CHAPTER 5. EFFECT OF PROLINE ON PEPTIDE FRAGMENTATION.....	36
5.1. Introduction.....	36
5.2. Experimental.....	37
5.3. Results and Discussion .....	37
5.3.1. CID Studies of $MH^+$ Ions of YAGFLVP-NH <sub>2</sub> , YPVGFLA-NH <sub>2</sub> , and PYAGFLV-NH <sub>2</sub> .....	37
5.3.2. CID Studies of $b_7$ Ions of PAAAAAA-NH <sub>2</sub> Series.....	40
5.3.3. CID Studies of $b_7$ Ions of PYAGFLV-NH <sub>2</sub> Series .....	41
5.3.4. CID Studies of $b_7$ Ions of AAPXAAA-NH <sub>2</sub> Series and AAXPAAA-NH <sub>2</sub> Series (where X is C, D, F, G, L, V, and Y) ....	46
CHAPTER 6. EFFECT OF BASIC RESIDUES ON PEPTIDE FRAGMENTATION.	52
6.1. Fragmentation Behavior of Histidine Residue.....	52
6.1.1. Introduction.....	52
6.1.2. Experimental .....	52
6.1.3. Results and Discussion.....	53
6.2. Fragmentation Behavior of Lysine Residue .....	58
6.2.1. Introduction.....	58
6.2.2. Experimental .....	58
6.2.3. Results and Discussion.....	58
6.3. Fragmentation Behavior of Arginine Residue .....	65
6.3.1. Introduction.....	65



6.3.2. Experimental .....	65
6.3.3. Results and Discussion.....	66
CHAPTER 7. CONCLUSION .....	74
LITERATURE CITED .....	76

# LIST OF FIGURES

<u>Figure</u>	<u>Page</u>
Figure 1.1. Discovery of neon isotopes on a photographic plate by Thomson in 1913 ...	1
Figure 1.2. Basic schematic of a mass spectrometer .....	2
Figure 1.3. Schematic of ESI process .....	4
Figure 1.4. Simple diagram of a linear quadrupole analyzer .....	7
Figure 1.5. Schematic of a quadrupole ion-trap.....	8
Figure 2.1. Amino acid structure in its unionized form.....	11
Figure 2.2. Nomenclature of peptide fragmentation for a tetrapeptide .....	13
Figure 2.3. Proposed structures for $b_2$ ion; (a) diketopiperazine, (b) oxazolone .....	15
Figure 2.4. Basic concepts of tandem mass spectrometry .....	21
Figure 3.1. Thermo Scientific LTQ XL linear ion trap MS system.....	24
Figure 3.2. AB SCIEX 4000 QTRAP MS system.....	24
Figure 4.1. CID spectra of $b_6$ ions derived from permuted isomers of YAGFLV-NH <sub>2</sub> . Each precursor peptide sequence is shown with its related spectrum. CE is 24eV.....	28
Figure 4.2. Breakdown graphs for $b_6$ ions derived from permuted isomers of YAGFLV- NH <sub>2</sub> . Nondirect sequence ions are shown only.....	29
Figure 4.3. CID spectra of $b_6$ ions of derived from FAYVGL-NH <sub>2</sub> , GVIYALF-NH <sub>2</sub> , and VFYLAG-NH <sub>2</sub> . CE is 24 eV. ....	30
Figure 4.4. Breakdown graphs for $b_6$ ions derived from FAYVGL-NH <sub>2</sub> , GVIYALF-NH <sub>2</sub> , and VFYLAG-NH <sub>2</sub> . Nondirect sequence ions are shown only. ....	30
Figure 4.5. Breakdown graphs for elimination of X from XYAGFLV-NH <sub>2</sub> and YAGXFLV-NH <sub>2</sub> , (X = D, E).....	32
Figure 4.6. Breakdown graphs for elimination of X from XYAGFLV-NH <sub>2</sub> and YAGXFLV-NH <sub>2</sub> (X = H, K) .....	32
Figure 4.7. Breakdown graphs for elimination of X from XYAGFLV-NH <sub>2</sub> and YAGXFLV-NH <sub>2</sub> (X = M, P, and W).....	34
Figure 4.8. Breakdown graphs for elimination of X from XYAGFLV-NH <sub>2</sub> and YAGXFLV-NH <sub>2</sub> (X = C, N, Q, S, and T) .....	35
Figure 5.1. CID spectrum of MH <sup>+</sup> ion derived from YAGFLVP-NH <sub>2</sub> .....	38

Figure 5.2. CID spectrum of MH <sup>+</sup> ion derived from YPVGFLA-NH <sub>2</sub> ( <i>b</i> ions shown only) .....	38
Figure 5.3. CID spectrum of MH <sup>+</sup> ion derived from PYAGFLV-NH <sub>2</sub> .....	39
Figure 5.4. CID spectra of <i>b</i> <sub>7</sub> ions derived from isomers of PAAAAAA-NH <sub>2</sub> .....	41
Figure 5.5. CID spectra of <i>b</i> <sub>7</sub> ions derived from isomers of PYAGFLV-NH <sub>2</sub> .....	43
Figure 5.6. Comparison of CID spectra of dipeptide elimination from <i>b</i> <sub>7</sub> of PYAGFLV-NH <sub>2</sub> isomers versus <i>b</i> <sub>5</sub> of YAGFLV-NH <sub>2</sub> isomers .....	45
Figure 5.7. CID spectra of <i>b</i> <sub>7</sub> ions derived from isomers of PYAFLVG-NH <sub>2</sub> where G is N-terminal to P .....	46
Figure 5.8. Comparison of CID spectra of <i>b</i> <sub>7</sub> of AAPXAAA-NH <sub>2</sub> isomers versus <i>b</i> <sub>7</sub> of AAXPAAA-NH <sub>2</sub> isomers (X = C, D, F, G, L, V, and Y) .....	48
Figure 5.9. Breakdown graphs of <i>b</i> <sub>7</sub> of AAPXAAA-NH <sub>2</sub> series (X= C, D, F, L, V, and Y) .....	49
Figure 5.10. Breakdown graphs of <i>b</i> <sub>7</sub> of AAXPAAA-NH <sub>2</sub> series (X= C, D, F, L, V, and Y) .....	50
Figure 6.1. CID spectra of <i>b</i> <sub>7</sub> of (a) HAAAAAA-NH <sub>2</sub> isomers, (b) HYAGFLV-NH <sub>2</sub> isomers .....	53
Figure 6.2. Breakdown graphs of <i>b</i> <sub>7</sub> of HAAAAAA-NH <sub>2</sub> isomers .....	56
Figure 6.3. Breakdown graphs of <i>b</i> <sub>7</sub> of HYAGFLV-NH <sub>2</sub> isomers .....	57
Figure 6.4. CID spectra of <i>b</i> <sub>7</sub> ions derived from isomers of KAAAAAA-NH <sub>2</sub> .....	59
Figure 6.5. CID spectra of <i>b</i> <sub>7</sub> ions derived from isomers of KYAGFLV-NH <sub>2</sub> .....	60
Figure 6.6. Comparison of CID spectra of <i>b</i> <sub>7</sub> ions derived from YAGFLVK-NH <sub>2</sub> and YAGFLVK(Ac)-NH <sub>2</sub> .....	61
Figure 6.7. CID spectra of 651 <i>m/z</i> from different peptide series .....	62
Figure 6.8. CID spectra of largest <i>b</i> ions of YAGFLVK <sub>n</sub> series (n = 2 to 7) .....	64
Figure 6.9. CID spectra of <i>b</i> <sub>7</sub> ions derived from isomers of RAAAAAA-NH <sub>2</sub> .....	67
Figure 6.10. CID spectra of <i>b</i> <sub>7</sub> ions derived from isomers of RYAGFLV-NH <sub>2</sub> .....	68
Figure 6.11. CID spectra of <i>b</i> <sub>n</sub> - 42 ion from isomers of AAAAAAR-NH <sub>2</sub> .....	69
Figure 6.12. CID spectra of <i>b</i> <sub>n</sub> - 42 ion from isomers of YAGFLVR-NH <sub>2</sub> .....	70
Figure 6.13. Structures of Lysine and Arginine .....	71
Figure 6.14. CID spectra of largest <i>b</i> ions of YAGFLVR <sub>n</sub> series (n = 2 to 7) .....	73

## LIST OF SCHEMES

<u>Scheme</u>	<u>Page</u>
Scheme 2.1. Classification of Peptide Fragmentation Models .....	14
Scheme 2.2. Mechanism of oxazolone formation and $b_x - y_z$ pathway.....	16
Scheme 2.3. Formation of <i>direct</i> and <i>non-direct</i> sequence ions for a hypothetical peptide ‘PEPTIDE’ .....	17
Scheme 2.4. Histidine Effect .....	18
Scheme 2.5. Lysine Effect .....	19
Scheme 2.6. Arginine Effect.....	20
Scheme 5.1. Proposed reaction mechanism and pathways for the formation of P+R <sub>2</sub> dipeptide and its loss from $b_7$ ion .....	51
Scheme 6.1. Mechanism of macrocyclization and formation of nondirect sequence ions for HYAGFLV-NH <sub>2</sub> .....	55
Scheme 6.2. Proposed mechanism for CID of $b_7$ produced from YAGFLVK-NH <sub>2</sub> .....	63
Scheme 6.3. Proposed mechanism for loss of 42 from $b$ ions with C-terminal arginine	72

## LIST OF TABLES

<b><u>Table</u></b>	<b><u>Page</u></b>
Table 1.1. Methods used in sample introduction, ionization, separation, and detection ..	3
Table 1.2. Comparison of various mass analyzer .....	6
Table 2.1. Molecular masses of naturally occurring amino acid residues .....	12
Table 5.1. Relative intensities of <i>b</i> ions of YPVGFLA-NH <sub>2</sub> at various collision energies .....	39
Table 5.2. Matched ion pairs chosen to prove dipeptide elimination .....	44

## LIST OF ABBREVIATIONS

a.u.	arbitrary units
CE	Collision Energy
CID	Collision-Induced Dissociation
Da	Dalton
DC	Direct Current
EPI	Enhanced Product Ion
ESI	Electrospray Ionization
FT-ICR	Fourier Transform – Ion Cyclotron Resonance
HPLC	High Performance Liquid Chromatography
IRMPD	Infrared Multiple Photon Dissociation
IT	Ion Trap
LIT	Linear Ion Trap
<i>m/z</i>	mass to charge ratio
MALDI	Matrix-Assisted Laser Desorption / Ionization
MP	Mobile Proton
MS	Mass Spectrometry
PIC	Pathways In Competition
QIT	Quadrupole Ion Trap
RF	Radio Frequency
TOF	Time-of-Flight

# CHAPTER 1

## INTRODUCTION TO MASS SPECTROMETRY

### 1.1. What is Mass Spectrometry?

In the last century, mass spectrometry (MS), the science of measuring mass-to-charge ratio ( $m/z$ ) of gaseous ions, has emerged as a fast growing and indispensable analytical technique allowing quantitation of atoms or molecules and providing structural information by revealing dissociation patterns. This method is applied to a broad range of fields such as biotechnology, clinical testing, pharmaceutical analysis, environmental analysis, and geology. It is widely accepted as a universal tool for chemical analysis because of its fundamental ability to measure all atomic and molecular masses. MS has its roots in gas discharge studies of Sir J.J. Thomson in 1897 (1). After sending a neon beam through electric and magnetic fields, he observed two different parabolas of deflection on the photographic plate, corresponding to isotopes of neon-20 and neon-22, respectively (Figure 1.1). This was the first experimental use of

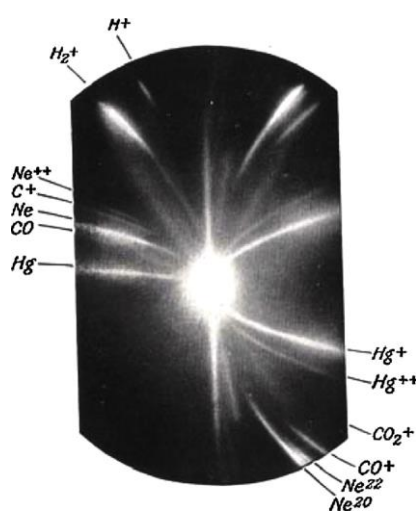


Figure 1.1. Discovery of neon isotopes on a photographic plate by Thomson in 1913

mass spectrometry which was then improved significantly by F.W. Aston and A. Dempster. Although scientists did not notice the importance of MS for long years, its use in petroleum industry, organic chemistry and biology paved the way for instrumental improvement of this method.

A typical mass spectrometer consists of three main functional units as conceptualized in Figure 1.2. After introducing the sample into the system either by direct infusion or chromatographic methods, you need to create gas-phase ions from neutral analyte atoms/molecules to be able to control their motion. Ions are then accelerated and focused to mass analyzer, the heart of a mass spectrometer, where they are separated with respect to their  $m/z$  ratio with the help of electric / magnetic fields. In the end, electronic detection of the separated ion is performed and these ion currents are converted into a mass spectrum. The whole system is operated under high vacuum ( $10^{-5}$  –  $10^{-8}$  torr) to create a suitable low-pressure environment so that mean free path of ions are large enough to avoid neutralization by collisions and the ions can reach the detector with a sufficient amount. Various types of methods used in each functional unit are displayed in Table 1.1. Sensibility, mass accuracy, and resolution are three essential properties that determine the overall performance of a mass spectrometer in addition to combined performance of the individual parts.

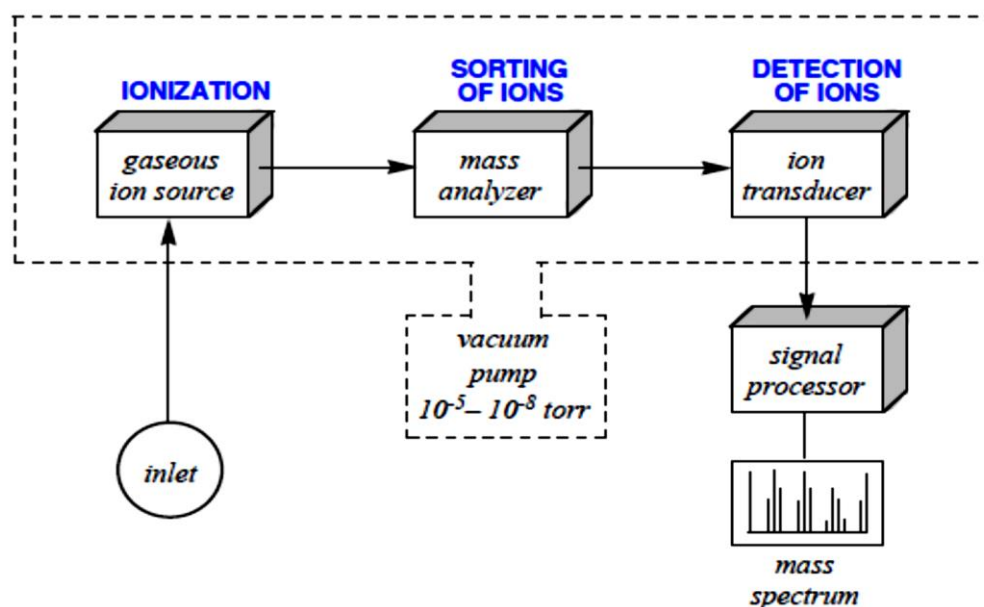


Figure 1.2. Basic schematic of a mass spectrometer



Table 1.1. Methods used in sample introduction, ionization, separation, and detection

Sample Introduction	Ionization Sources	Mass Analyzers	Detectors
<ul style="list-style-type: none"> <li>- Direct Infusion</li> <li>- Gas Chromatography (GC)</li> <li>- Liquid Chromatography (LC)</li> <li>- Capillary Electrophoresis (CE)</li> </ul>	<ul style="list-style-type: none"> <li>- Electrospray Ionization (ESI)</li> <li>- Matrix Assisted Laser Desorption Ionization (MALDI)</li> <li>- Electron Impact (EI)</li> <li>- Chemical Ionization (CI)</li> <li>- Atmospheric Pressure Chemical Ionization (APCI)</li> <li>- Fast Atom Bombardment (FAB)</li> <li>- Field Desorption (FD)</li> <li>- Field Ionization (FI)</li> <li>- Plasma Desorption (PD)</li> <li>- Thermospray Ionization (TS)</li> </ul>	<ul style="list-style-type: none"> <li>- Linear Quadrupole</li> <li>- Quadrupole Ion Trap</li> <li>- Time of Flight</li> <li>- Magnetic Sector</li> <li>- Fourier Transform Ion Cyclotron Resonance</li> <li>- Orbitrap</li> <li>- Hybrid Types</li> </ul>	<ul style="list-style-type: none"> <li>- Electron Multiplier</li> <li>- Photographic Plate</li> <li>- Faraday Cup</li> <li>- Microchannel Plate</li> </ul>

## 1.2. Ionization Sources

The success of a mass spectrometric analysis is strongly dependent on converting neutral analyte atoms or molecules into gas-phase ionic species. In addition to creating ions, ionization sources also have the function of accelerating the ions into mass analyzer for ultimate separation. For this purpose, all the ions should have same kinetic energy distribution (monoenergetic) so that there is an equal opportunity for both low and high mass ions being sent to the analyzer. The mode of ion generation is chosen according to the nature of sample investigated. In this chapter, electrospray ionization (ESI) and matrix-assisted laser desorption/ionization (MALDI) will be considered only because these are the ionization methods used for the majority of protein/peptide analysis.

### 1.2.1. Electrospray Ionization (ESI)

ESI is a very gentle ionization technique applicable to a wide range of compounds in mass analysis. In 1968, this method was first introduced by Dole's group (2) who showed that intact gas-phase macromolecules can be generated from a solution.

However, it was 1980s when Fenn et al. (3) managed to couple ESI to MS so that capabilities of mass spectrometry have been significantly improved. It is also commonly utilized as an interface between high performance liquid chromatography (HPLC) and MS. Due to its ‘‘soft’’ characteristics, ESI method is particularly important for the analysis of large biomolecules without degradation, which was previously a problematic case because of their fragile nature.

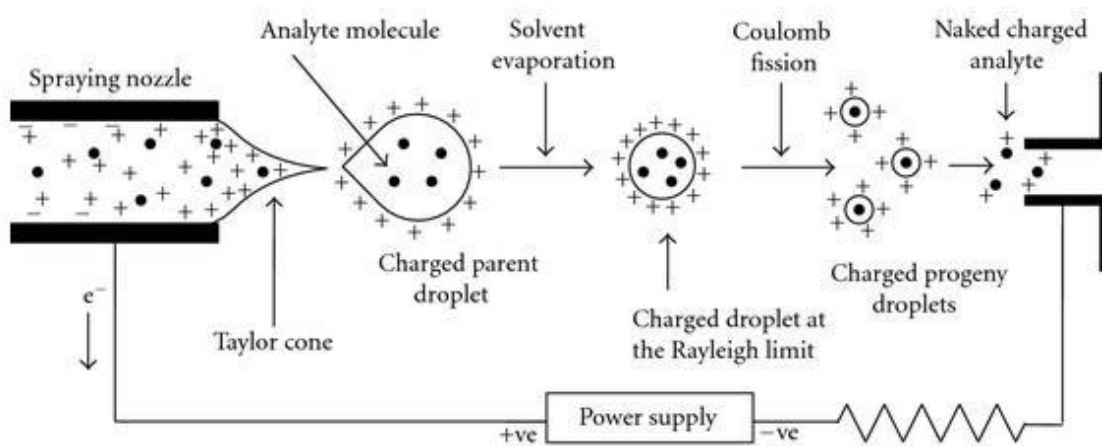


Figure 1.3. Schematic of ESI process (4)

The main principle of ESI can be described through a simple diagram represented in Figure 1.3. The sample solution mixed with a 1:1 mixture of water and an organic solvent (typically methanol, isopropanol, or acetonitrile) containing a 1% of suitable acid (acetic acid or formic acid) is pumped through a capillary tube at a continuous flow rate of several  $\mu\text{L}/\text{min}$ . A high voltage of 3-4 kV is applied between the capillary and counter electrode to create a fine spray of charged droplets forming a ‘‘Taylor cone’’. A flow of drying nitrogen gas at the interface promotes evaporation of the solvent from the charged droplets. There comes a moment when the repulsive Coulombic forces exceeds surface tension of the droplet (Rayleigh limit) to cause the formation of smaller daughter droplets (Coulomb fission). Finally, gas-phase analyte ions are produced upon further evaporation, and directed to the mass analyzer with the help of ion optics.

### 1.2.2. Matrix-Assisted Laser Desorption/Ionization (MALDI)

The MALDI technique is another soft ionization method in the mass analysis of large biomolecules and organic macromolecules. It was discovered simultaneously by two research groups, Karas and Hillenkamp (5), and Tanaka et al. (6) in 1988. Invention of MALDI is a kind of revolution that opened mass spectrometry to the study of proteins and other biopolymers with masses in excess of 200 kDa. A primary aspect of MALDI is mixing of the sample with a ‘matrix’, a low-molecular weight energy-absorbing organic material. Matrix is the heart of MALDI process since it serves as laser energy absorbent and an energy transfer agent in order to prevent direct interaction of laser energy with the sample. In principal, the analyte is dispersed in a large excess of matrix material (in the ratio of one-to-several thousands) which can strongly absorb energy at the wavelength of the laser radiation (typically a nitrogen laser at 337 nm). The analyte and matrix is then dissolved in an organic solvent, placed on a metallic probe or sample target, and allowed to dry. Evaporation of the solvent leaves matrix crystals surrounding analyte molecules. After the target is placed in the vacuum chamber of the mass spectrometer, a high energy laser beam is directed at the sample plate with about  $10^6$  W/cm<sup>2</sup> irradiance power. Most of the laser energy is efficiently absorbed by the matrix crystals causing evaporation of the matrix, and this energy is transferred to the analyte as heat in a controlled manner such that no fragmentation occurs. In this way, analyte molecules are converted into gas-phase ions, and then sent to the mass analyzer.

### 1.3. Mass Analyzers

The mass analyzer, the heart of the mass spectrometer, basically serves to separate the gas-phase ion based on their  $m/z$  value applying appropriate electric and magnetic fields to control their motion. The ions can be transmitted, focused, and mass-resolved depending on their kinetic energy, velocity, and momentum through a mass analyzer. The main capability of a mass analyzer is characterized by certain parameters, such as mass accuracy (uncertainty in  $m/z$  values), mass range (max. analyzable  $m/z$  allowed), resolution (ability to separate two neighbour  $m/z$  values), scan speed,

detection sensitivity (min. amount of analyte that can be detected at a certain confidence level) in addition to ability to be coupled with chromatographic tools.

Various designs of mass analyzers have been developed; of these, magnetic sector, linear quadrupole, quadrupole ion-trap (QIT), time-of-flight (TOF), and Fourier transform-ion cyclotron resonance (FT-ICR) are widely used types. Several important characteristics of those analyzers are compared in Table 1.2. Although there is no ideal mass analyzer applicable to all samples, FT-ICR and magnetic sector instruments provide the highest resolution values; therefore, they are the most expensive analyzer types. Linear quadrupole and ion-trap will be explained in detail in this chapter since these analyzers are utilized during this thesis study.

Table 1.2. Comparison of various mass analyzers (7)

Characteristic	Magnetic Sector	Quadrupole	QIT	TOF	FT-ICR
Mass range (Da)	15,000	4,000	100,000	Unlimited	$>10^6$
Resolution	200,000	Unit	30,000	15,000	$>10^6$
Dynamic range	++++	+++	+++	+++	++
MS/MS	++++	+++	+++	+++	++
LC (or CE)MS	+	++++	+++	++	++
Cost	\$\$\$\$	\$	\$	\$\$	\$\$\$\$

### 1.3.1. Linear Quadrupole Mass Analyzer

The linear quadrupole mass analyzer is very commonly used design of mass spectrometer which was invented by Paul and Steinwedel in 1953 (8). It mainly utilizes the stability of the trajectories in oscillating electric fields for mass separation of the ions. The analyzer consists of a set of four parallel metal rods to which fixed DC and alternating RF potentials applied as demonstrated below in Figure 1.4. Ions produced in the source are focused on the center of the region between quadrupole rods by a small accelerating potential. Each mass-to-charge ratio has a fixed set of DC/RF value. At a specific combination of DC and RF voltages applied to the rods, only ions of certain  $m/z$  value have stable trajectories and hence pass through the rods to the detector. On the other hand, the remainder of the ions have unstable trajectories, are discharged on the

rods so that they cannot be detected. RF voltage is continuously varied to force other ions to follow a stable trajectory so that a mass spectrum can be obtained. The resolution of the analyzer is directly related to the combination of DC and RF voltages. The linear quadrupole is usually operated at unit mass resolution.

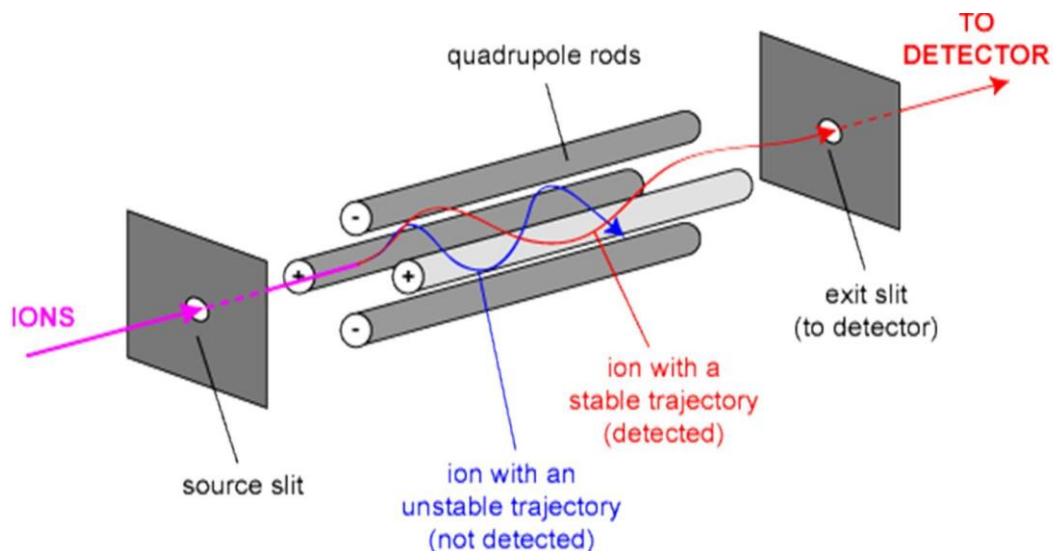


Figure 1.4. Simple diagram of a linear quadrupole analyzer (9)

### 1.3.2. Ion-Trap Mass Analyzer

Ion-traps (IT) are modern type of mass analyzers that utilize oscillating electric field to store and manipulate ions in time rather than in space. Trapping of ions is performed by applying RF quadrupole electric field in two or three dimension; therefore, ion-traps can be categorized in two groups: 3D ion-trap and 2D ion-trap.

3D ion traps, also known as quadrupole ion-trap (QIT) or Paul traps, were first described by Paul and Steinwedel at the same time with linear quadrupoles (8); however, its popularity was increased after Stafford's group improved this analyzer with some modifications (10). QIT employs a cylindrical ring electrode and two ellipsoid end-cap electrodes as shown in Figure 1.5. Following to the introduction of ions to the analyzer, ions of all masses are trapped and stored on a 3D eight-shaped oscillating trajectory. Helium gas ( $10^{-3}$  Torr) is used as a bath gas to improve ion-

trapping efficiency by stabilizing ion trajectories. Ramping RF voltage at the ring electrode results in unstable trajectories and thus ions of a specific  $m/z$  are expelled from the trap towards the outside detector. Ions with different  $m/z$  are ejected from the trap at different voltages and times since oscillating frequencies are a function of ion masses.

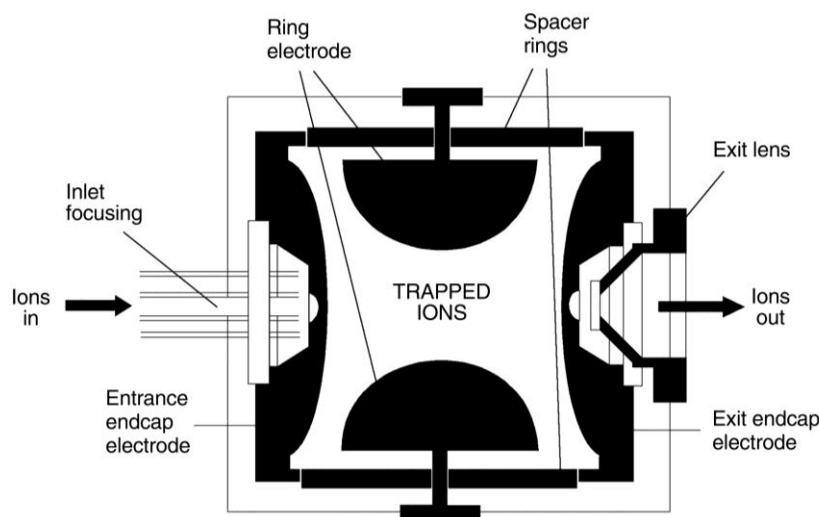


Figure 1.5. Schematic of a quadrupole ion-trap (11)

2D ion traps, which are also named as linear ion-traps (LIT) are more sophisticated mass analyzers in comparison to QITs. They are made up of four-rod quadrupole ending in lenses. Ions are confined radially by RF field, and axially by stopping potentials applied to the end electrodes. Once symmetrically applied, voltages at each part keep ions in the center of the quadrupole field. LITs are generally preferred for their higher ion-trapping capacity, enhanced sensitivity, and minimized space-charge effects.

### 1.3.3. Time-of-Flight Mass Analyzer

A theory of time-of-flight (TOF) mass analyzer was proposed by Stephens in 1946 (12). Since the late 1980s, it has been coupled with MALDI to handle the pulse of ions. TOF is a type of speed analyzer which separates ions according to their different

velocities. A short pulse of ions exiting the source is given the same kinetic energy to accelerate them towards the detector; hence, it is obvious that ions carrying the same charge with different mass will travel through a flight tube at different velocities; thus, it takes different amount of time to travel the same distance. The lighter ions travel down a field-free region faster and reach the detector earlier due to their higher velocity while it takes longer time for heavier ions because of their lower velocity. So flight times of ions required to move through a field-free region between the source and the detector are measured, and packets of isomass ions are quantified. Conversion of time spectrum into a mass spectrum is managed by calibrating the analyzer through measuring the flight times of ions of known mass.

In early days, TOF had a disadvantage of low resolution reasoned by inhomogeneous kinetic energy distribution of the ions; hence, different arrival times are recorded for ions of same mass. However, this kinetic energy problem is solved by the introduction of an energy-correcting device, named as ‘‘reflectron’’. A retarding field created by the reflectron provides larger pathways for more energetic ions to reach the detector at the same time with less energetic ions of the same mass so that mass resolution is improved.

#### **1.3.4. Fourier Transform Ion Cyclotron Resonance Mass Analyzer**

Fourier transform ion cyclotron resonance (FT-ICR) mass spectrometry was developed by A. Marshall and M. Comisarow in the early 1970s (13). This technique has been accepted as a sophisticated mass analyzer due to its unique capabilities like ultrahigh resolution, high mass range/accuracy, and ion-trap nature. The ions are confined in a cubic cell where they are trapped in a fixed strong magnetic field combined with an electric field perpendicular to each other. This cell is made up of two opposite trapping plates, two opposite excitation plates, and two opposite detector (receiver) plates. Then, the ions are excited by means of radio-frequency pulse to follow a circular orbital motion where the cyclotron frequency of each ion is a function of its  $m/z$  value. The coherent movement of the ions induces an alternating current in the detector plates. Varying RF frequencies are applied to excitation plates so that frequency vs. time spectrum is obtained. Finally, this time domain spectrum is converted into regular mass spectrum with the help of Fourier transformation method.

## 1.4. Ion Detectors

After passing through the mass analyzer, ion currents are detected and transformed into a usable signal by a detector. Different types of detectors are used in mass spectrometers. The most widely used ones are explained below.

The first type is *photographic plate* which has been used since the development of early mass spectrometers. Ions of same  $m/z$  reach the detector at the same location, and their  $m/z$  values are found based on the position of this location.

*Faraday cup* is another detector type which consists of a metal cup with a small orifice. An ion current is produced as a result of collision of ions with the walls of the cup while accepting or donating electrons to be neutralized. Thus, the discharge current is amplified and detected.

The recent detector design is *electron multiplier*, in which the ions gain high velocity for better detection efficiency using conversion dynode at a potential difference with an opposite charge to ions. Secondary electrons are emitted by excitation of the first dynode, and they are multiplied in a cascade by the following dynodes to be detected.

*Multichannel plate (MCP)* is a sophisticated design of electron multiplier that has millions of independent channels. Each ion entering the channel produces electrons from the walls of channel. These secondary electrons move in parabolic trajectories and collide with the channel surface to generate more secondary electrons. This cycle occurs again and again so that several thousands of electrons are emitted to be detected.



## CHAPTER 2

### MASS SPECTROMETRY OF PROTONATED PEPTIDES

#### 2.1. Amino Acids and Peptides

Amino acids, which are classically known as the building blocks of proteins, are essential molecules for organisms to be able to survive. There exist 20 naturally occurring amino acid residues whose abbreviations and molecular masses are listed in Table 2.1. Human body can produce only ten of those amino acids since we do not have all the enzymes required for their synthesis; therefore, the remaining ones must be supplied in the food.

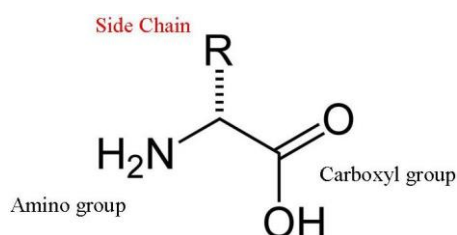


Figure 2.1. Amino acid structure in its unionized form

The general chemical structure of amino acids is given in Figure 2.1. As the name “amino acid” implies, they all contain at least one amino and one acid (carboxyl) group. It is the “side chain groups” (R) what differentiate the amino acids so that they can be categorized into three main groups: nonpolar, uncharged polar and charged polar residues. The biological activity of the proteins is determined directly by the chemical properties of the side chains as much as the peptide length.

Amino acids can be polymerized to produce peptides through a condensation reaction (via elimination of a H<sub>2</sub>O molecule). The bond formed between the resulting CO-NH linkage is named as peptide bond. In mass spectrometric analysis of proteins,

they are digested with specific enzymes such as trypsin, chymotrypsin, pepsin, and elastase that cut the protein at certain peptide bonds. For instance, trypsin cleaves the peptide bond at the C-terminal side of lysine and arginine residues. This process produces smaller peptide fragments which are easier to be analyzed by mass spectrometry technique.

Table 2.1. Molecular masses of naturally occurring amino acid residues

<b>Residue</b>	<b>Abbreviation</b>		<b>Monoisotopic Mass</b>	<b>Immonium Ion Mass</b>
<b>Glycine</b>	Gly	G	57.0215	30
<b>Alanine</b>	Ala	A	71.0371	44
<b>Serine</b>	Ser	S	87.0320	60
<b>Proline</b>	Pro	P	97.0528	70
<b>Valine</b>	Val	V	99.0684	72
<b>Threonine</b>	Thr	T	101.0477	74
<b>Cysteine</b>	Cys	C	103.0092	76
<b>Leucine</b>	Leu	L	113.0841	86
<b>Isoleucine</b>	Ile	I	113.0841	86
<b>Asparagine</b>	Asn	N	114.0429	87
<b>Aspartic Acid</b>	Asp	D	115.0269	88
<b>Glutamine</b>	Gln	Q	128.0586	101
<b>Lysine</b>	Lys	K	128.0950	101
<b>Glutamic Acid</b>	Glu	E	129.0426	102
<b>Methionine</b>	Met	M	131.0405	104
<b>Histidine</b>	His	H	137.0589	110
<b>Phenylalanine</b>	Phe	F	147.0684	120
<b>Arginine</b>	Arg	R	156.1011	129
<b>Tyrosine</b>	Tyr	Y	163.0633	136
<b>Tryptophan</b>	Trp	W	186.0793	159

## 2.2. Peptide Fragmentation

With the invention of soft ionization techniques, namely ESI (14-16) and MALDI (5; 17), mass spectrometry has become one of the most attractive techniques for proteomics studies. It is well-demonstrated that low-energy environment generally help the cleavage of amide bond on the protonated peptide, and then produce sequence-

informative *b* and *y* fragment ions in greater abundance (18; 19). Nomenclature of peptide fragmentation is demonstrated in Figure 2.2.

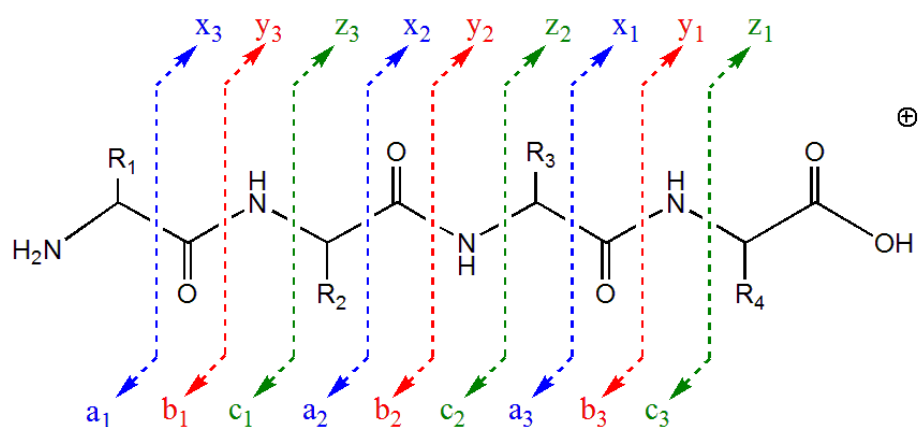
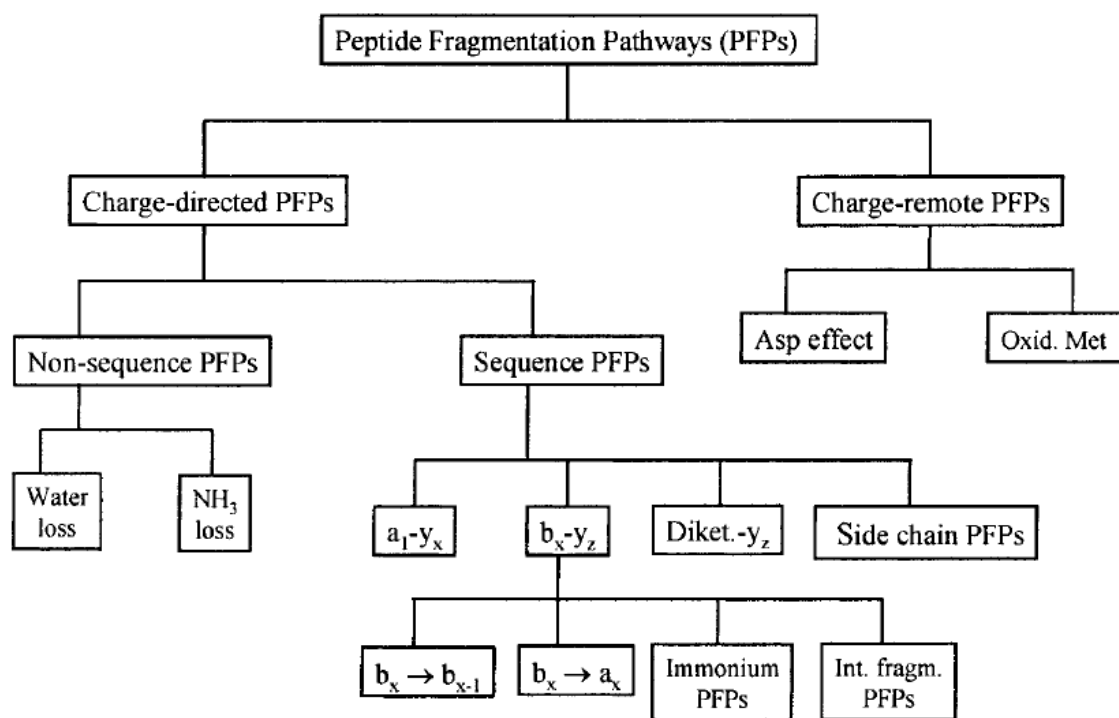


Figure 2.2. Nomenclature of peptide fragmentation for a tetrapeptide

*Mobile proton* (MP) (20; 21) and its explicit extension, *pathways in competition* (PIC) (22), are the current models interpreting the chemistry of peptide fragmentation where excitation occurs by first retainment of ionizing proton by sites of higher basicity, including N-terminal amino group, amide carbonyl oxygen, and side chain groups of arginine, histidine and lysine. Considering the singly-charged peptides, this mobile proton is retained by these main protonation sites so that *charge-directed fragmentation pathway* is followed. However, if the peptide is doubly-charged, the additional proton can be sequestered to thermodynamically less favored sites causing *charge-remote fragmentation* (Scheme 2.1.).

Consequently, bioinformatics algorithms such as SEQUEST (23) and Mascot (24) make use of the masses of *b* and *y* ions directly to reveal peptide sequence information. Those bioinformatics tools compare and relate experimental mass spectra to theoretical (predicted) mass spectra of candidate protein sequences derived from protein database. Unfortunately, these advanced algorithms have been constructed based on a very limited peptide dissociation chemistry which might lead to wrong assignments in protein identification (25; 26). It is obvious that deduction of underlying dissociation chemistry and incorporation of complete fragmentation mechanisms into current algorithms will improve MS-based identification of unknown proteins.



Scheme 2.1. Classification of Peptide Fragmentation Models (22)

Because of the close relation between peptide structure and dissociation chemistry, a large variety of studies has been performed to determine the structure of the fragment ions. While C-terminal  $y$  ions are established to be linear truncated peptides (27; 28), situation is a little bit complex for the complementary N-terminal  $b$  ions. Contrary to the earlier studies (18; 19; 29-31) proposing an acylium structure for  $b$  ions, Yalcin and his coworkers (32; 33) first established a five-membered oxazolone ring structure for these ions, which is formed via nucleophilic attack of an adjacent backbone carbonyl oxygen to a carbonyl carbon. The mechanism of oxazolone formation and related  $b_x - y_z$  pathway is shown in Scheme 2.2. Proposal of oxazolone structure has then been further corroborated by various groups utilizing not only CID experiments (34-36), but also isotopic labeling (37-39), theoretical calculations (40; 41), and very recent infrared multiple photon dissociation (IRMPD) spectroscopic studies (42-46). Other possible structural form suggested especially for  $b_2$  ions is diketopiperazine ring which is a six-membered ring produced by a nucleophilic attack of N-terminal amino group on the second carbonyl carbon (28; 47). Apart from

oxazolone and diketopiperazine, alternative structures can also be produced with participation of side chains in fragmentation (48).

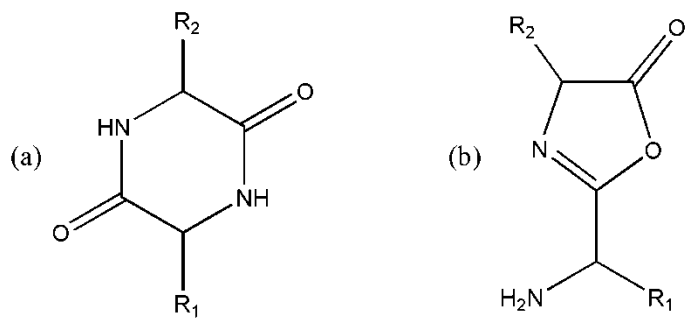
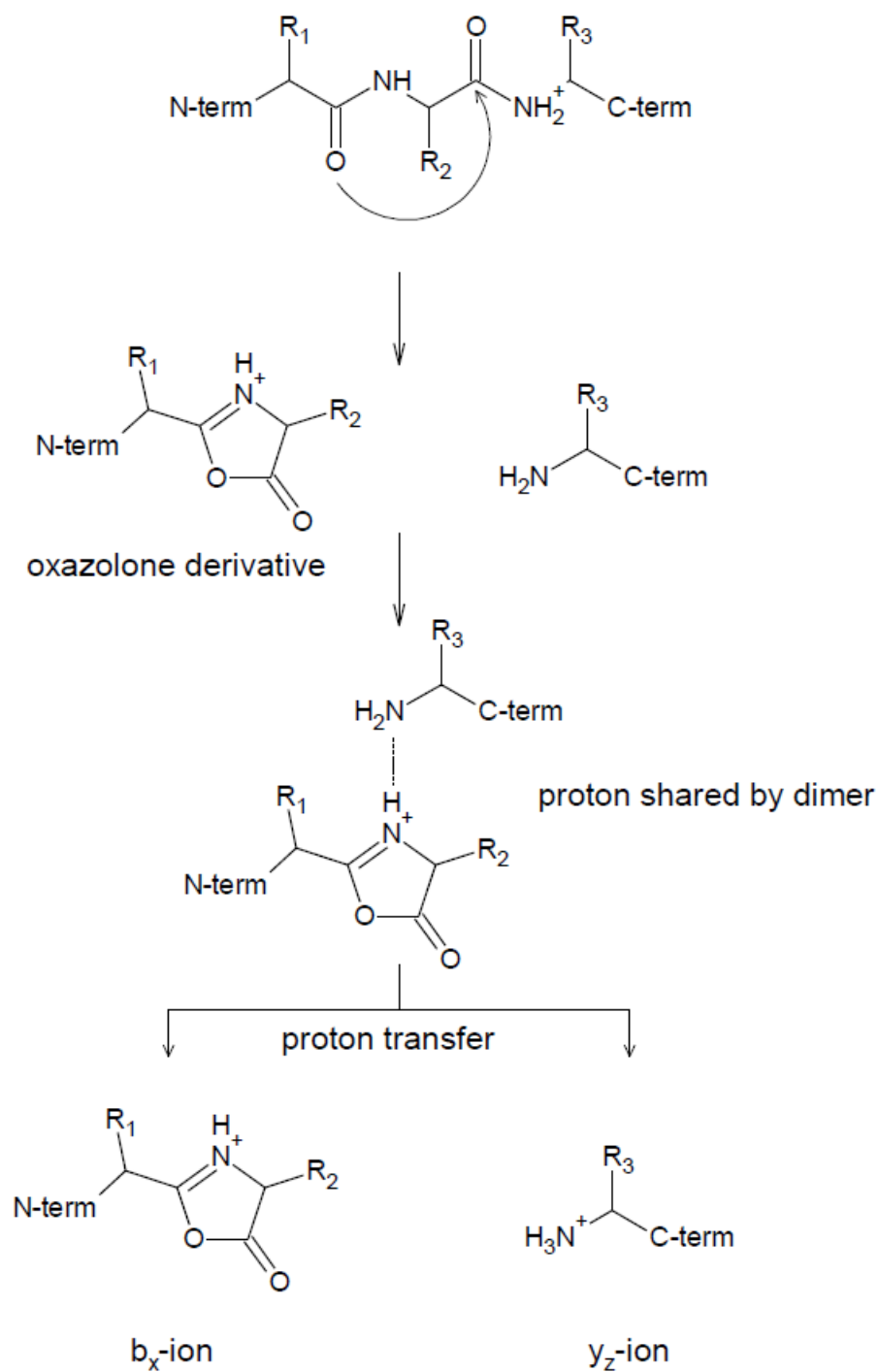


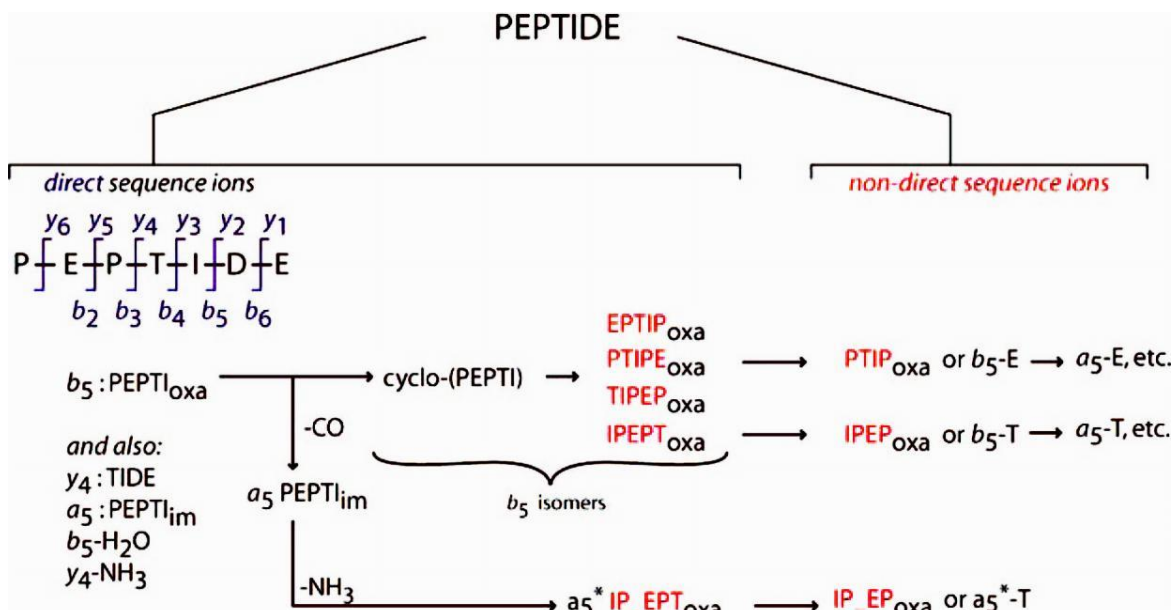
Figure 2.3. Proposed structures for  $b_2$  ion; (a) diketopiperazine, (b) oxazolone



Scheme 2.2. Mechanism of oxazolone formation and  $b_x - y_z$  pathway

More recently, an alternative structure has been considered for larger  $b_n$  ions ( $n \geq 5$ ) in which N-terminal amine group attacks the oxazolone ring nucleophilically forming a *macrocyclic* structure. Potential reopening of this cyclic model at various

amide bonds produces rearranged (scrambled or permuted) isomeric linear oxazolone *b* ions which is the main cause of *non-direct* sequence fragment ions upon further dissociation in addition to direct sequence ions as shown in Scheme 2.3. (49-56). Consideration of these non-direct sequence fragment ions and evaluation of their importance in CID analysis is considered to prevent confusion in peptide sequencing.

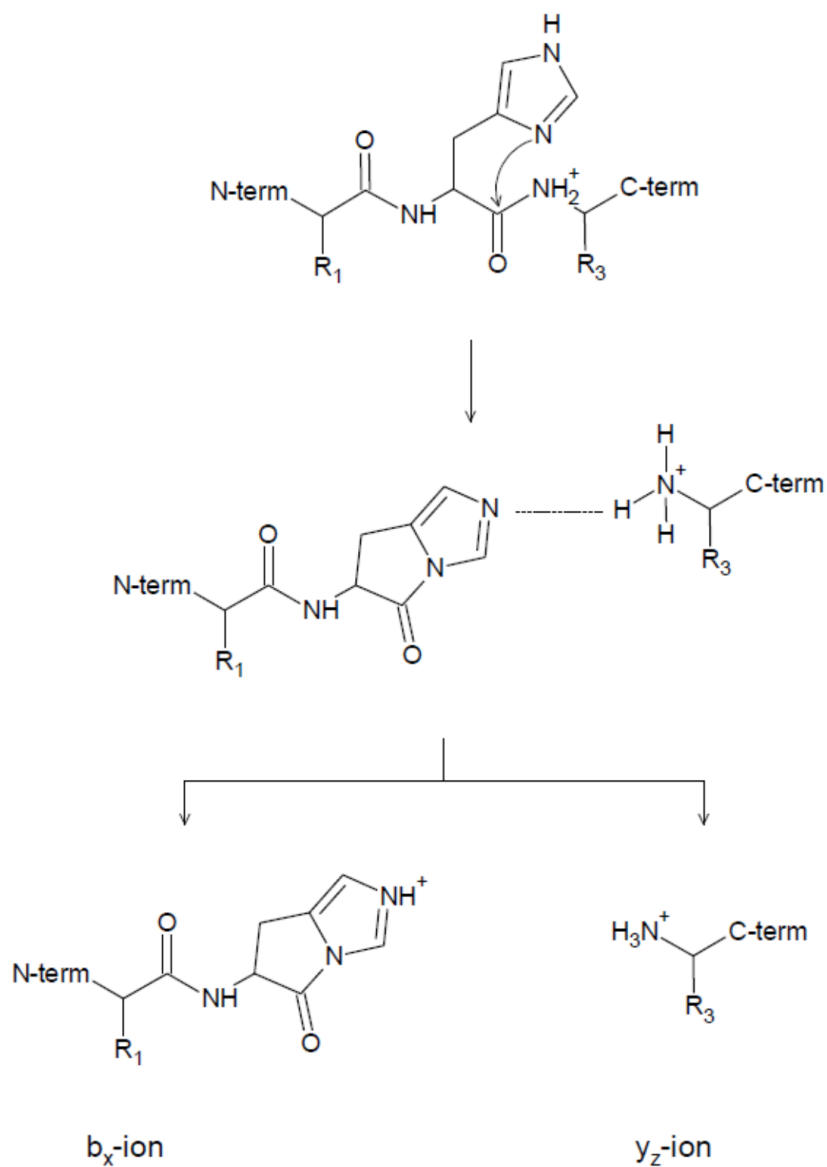


Scheme 2.3. Formation of *direct* and *non-direct* sequence ions for a hypothetical peptide "PEPTIDE" (53)

### 2.3. Side Chain Effects

In addition to peptide fragmentation pathways reasoned by backbone nucleophiles such as amide oxygen N-terminal nitrogen, some peptides can follow side chain-specific routes. Histidine effect is one of such pathways that involves charge-directed pathway. Cleavage C-terminal to histidine occurs when the number of protons is greater than the number of arginine residues in the peptide. The proton retained by the histidine side chain migrates to peptide bond C-terminal to the histidine. Next, the imidazole nitrogen nucleophilically attacks to carbonyl carbon. The complex formed

allows proton transfer between N- and C-terminal fragments so that both  $b_x$  and  $y_z$  ions are formed (Scheme 2.4).

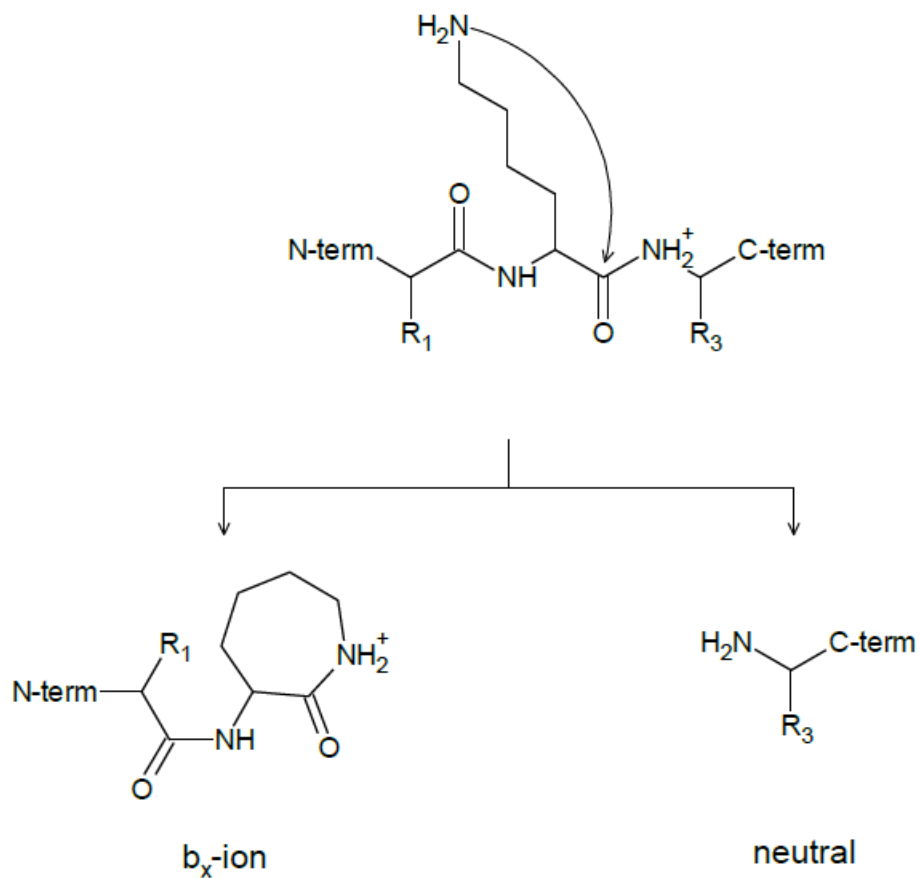


Scheme 2.4. Histidine Effect

Lysine effect is observed when the proton at highly basic  $\epsilon$ -amino group migrates to the carbonyl carbon C-terminal to the lysine residue. Then, peptide dissociation can proceed via nucleophilic attack of the lysine side chain. As a result, a

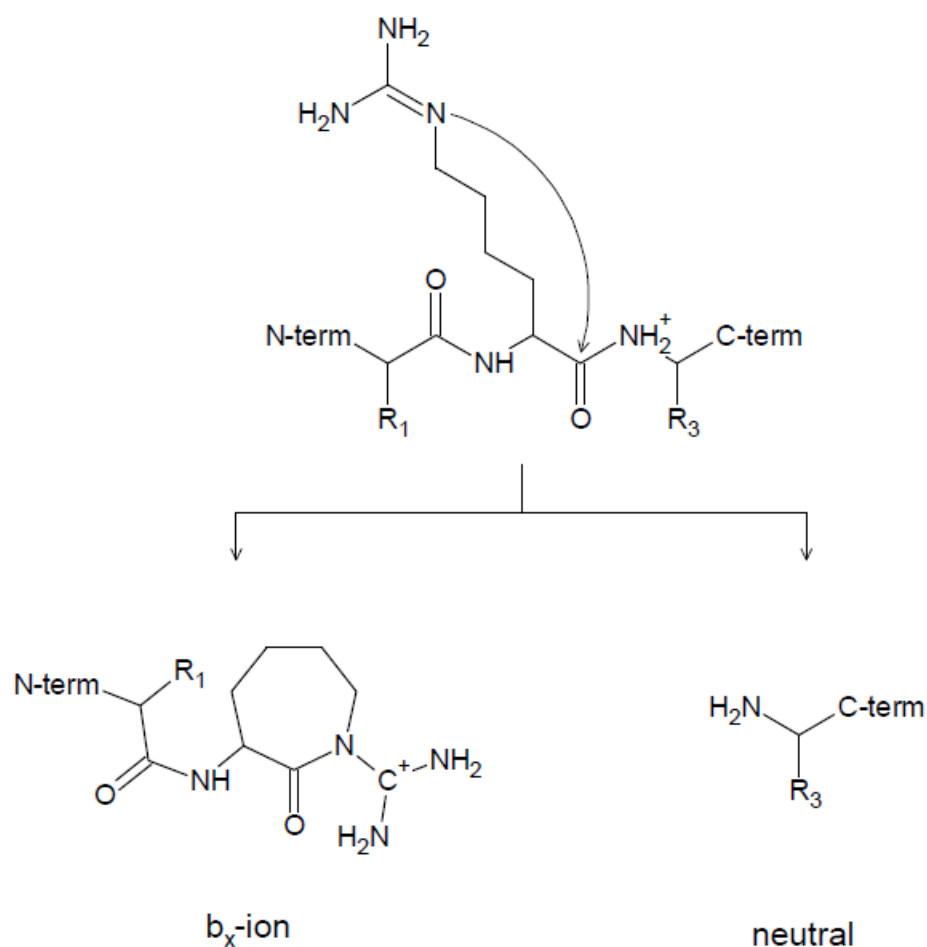


charged caprolactam derivative of  $b_x$  ion and neutral C-terminal peptide fragment are produced as demonstrated in Scheme 2.5.



Scheme 2.5. Lysine Effect

Another side chain-related mechanism is arginine effect which occurs by the migration of the proton at the arginine side chain to the amide nitrogen C-terminal to the arginine residue. This proton transfer leads to the nucleophilic attack of the guanidine group on the carbonyl carbon as shown in Scheme 2.6. In the end, a non-classical  $b_x$  ion with a six-membered ring is formed.



Scheme 2.6. Arginine Effect

## 2.4. Tandem Mass Spectrometry and Collision-Induced Dissociation

Tandem mass spectrometry (MS/MS) is basically defined as the coupling of two mass spectrometers in space or time which aims to reveal further structural information of a sample of interest. In other words, it is known as a mass spectrum of a mass spectrum. A typical tandem mass spectrometer consists of at least two stages of mass analysis. In MS/MS, there are three fundamental processes; mass selection, fragmentation, and mass analysis (Figure 2.4). In the first stage of mass analysis (MS-1), ion of interest is mass-separated from all other ions formed in the ion source. The intermediate region is called as ‘collision cell’ where the selected ion (also named as *precursor or parent ion*) undergoes fragmentation by collisions with non-reactive gas such as helium or argon (excitation / activation of precursor ion). This process is named

as ‘‘collision-induced dissociation’’ (CID) that generates *product or daughter ions* to be mass-analyzed in the second stage of tandem mass spectrometry (MS-2). In tandem mass spectrometric analysis of peptides, daughter ions give information about amino acid sequence, which in turn provides protein identification.

Different types of instrumental designs have been developed for tandem mass spectrometric analysis. The common examples of these hybrid style instruments are triple quadrupole (QQQ), quadrupole/ion trap (QIT), Fourier transform-ion cyclotron resonance (FT-ICR), magnetic/electric sector, quadrupole/time-of-flight (Q-TOF), and time-of-flight/time-of-flight (TOF/TOF).

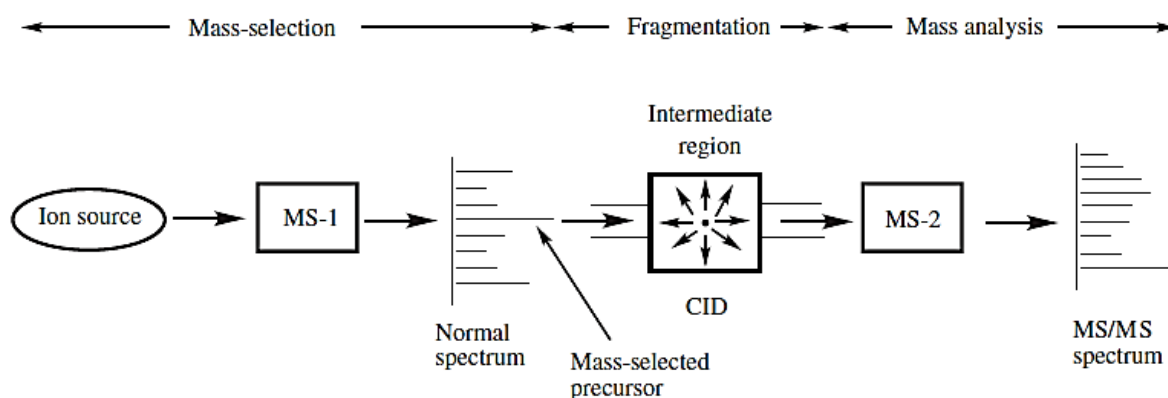


Figure 2.4. Basic concepts of tandem mass spectrometry (7)

## 2.5. Aim of the Study

As discussed in previous paragraphs, today’s automated protein sequencing algorithms are based on rudimentary peptide dissociation models; thus, they discard rich chemistry lying behind peptide fragmentation. These limitations may result in uncertainty in the interpretation of the obtained mass spectra so that erroneous assignment can be done in peptide / protein identification. In the light of these facts, we herein aimed to gain further insight into the peptide fragmentation characteristics of various sets of model peptides containing specific residues using MS/MS and CID

analysis. A better understanding of gas-phase peptide dissociation chemistry and implementation of more detailed peptide fragmentation mechanisms into bioinformatics algorithms will no doubt help to improve database search tools so that more accurate protein identification can certainly be done.

## CHAPTER 3

### EXPERIMENTAL

#### 3.1. Materials

All synthetic model peptides were obtained from GL Biochem (Shanghai, China) and used as received with no further purification. HPLC grade methanol and formic acid were supplied by Merck (Darmstadt, Germany). The water used was ultrapure grade (Arium 611 UV, Sartorius AG, Goettingen, Germany). Stock solutions of peptides were prepared by dissolving solid material in a 1:1 (v/v) mixture of methanol and water to a concentration of  $10^{-2}$  M. Peptide samples at micromolar concentration level were prepared by diluting stock solutions with 1:1 CH<sub>3</sub>OH: H<sub>2</sub>O containing 1% formic acid.

#### 3.2. Mass Spectrometry

All low-energy CID experiments were conducted on a LTQ XL linear ion trap mass spectrometer (Thermo Scientific, NJ, USA) while energy dependence of fragmentation studies were performed on a hybrid triple quadrupole/linear ion trap 4000 QTRAP instrument (Applied Biosystems/MDS Sciex, Ontario, Canada) both of which are equipped with an electrospray ionization source. Protein samples at micromolar concentration level were dissolved in 1:1 CH<sub>3</sub>OH: H<sub>2</sub>O with 1% formic acid and infused into electrospray source at a 5  $\mu$ L/min flow rate using an incorporated syringe pump for the linear ion trap system and a syringe pump from Harvard Apparatus (model 11 plus, Natick, MA, USA) for the triple quadrupole/linear ion trap system.

The linear ion trap MS analyses were performed in the following conditions: All the instrumental parameter settings (lens voltages, multipole offsets, etc.) were optimized to get maximum parent ion transmission to the ion trap mass analyzer using the autotune routine within the LTQ Tune program. Ion spray voltage was kept at 5.00



Figure 3.1. Thermo Scientific LTQ XL linear ion trap MS system



Figure 3.2. AB SCIEX 4000 QTRAP MS system

kV and nitrogen was used as a sheath gas (10 a.u.), auxiliary gas (1 a.u.), and sweep gas (1 a.u.) for spray while helium was used as a bath/buffer gas (cooler gas) to improve trapping efficiency.

The hybrid triple quadrupole/linear ion trap MS analysis was carried out as follows. Nitrogen was used as nebulizer, curtain, and collision gas. Q1 scan was applied first to adjust declustering potential for the generation of the most intense ion signal with best Gaussian distribution peak shape, which was then followed by enhanced product ion (EPI) scan for MS/MS experiments. EPI scan studies were operated using the following instrumental parameters: curtain gas (CUR), 10.00 arb; ion spray voltage (IS), 5500.00; temperature (TEM), 0.00 °C; ion source gas 1 (GS1), 19.00; ion source gas 2 (GS2), 0.00; interface heater (ihe), On; collision gas (CAD), 6.00 arb; collision energy spread (CES), 0.00; collision energy (CE), 14.0-42.0 eV (with increments of 4.0 eV) , quadrupole 1 ion energy (IE1), 0.800; Q1 resolution, unit; detector (CEM), 2200.0; scan rate, 1000 Da/s; LIT fill time, 20 ms. All MS/MS data were collected as a sum of 50 MCA scans. Analyst 1.5 software was used for instrument control, data acquisition and processing while interpretation of whole data was performed using Igor Pro 3.13 (WaveMetrics Inc., Oregon, USA).

## CHAPTER 4

# INVESTIGATION OF PEPTIDE SIZE, RESIDUE POSITION, NEIGHBOR AMINO ACID AND SIDE CHAIN EFFECT ON MACROCYCLIZATION OF $b_n$ ( $n = 5 - 7$ ) IONS

### 4.1. Introduction

Recently, the effect of peptide size (57) on the macrocyclization of  $b$  ions and the effect of amino acid nature (58) on the potential ring opening of this cyclic model at various amide bonds have been studied by Stipdonk et al. However, they have only considered a single isomeric series of the YAGFLVG model to monitor the macrocyclization of  $b$  ions, and focused only on the  $b_5$  ions produced from YAXFLG (where X = G, K, E, D, N, Q) to obtain information about the side chain effect. In addition, Polfer et al. published a detailed study about  $b_2$ - $b_8$  ions to predict the influence of the peptide size on cyclization (59). It was observed that the smaller  $b$  fragments ( $b_2$  and  $b_3$ ) form an oxazolone structure; in contrast midsized ones ( $b_4$ - $b_7$ ) generate a combination of oxazolone and macrocyclic structures.

In this work, we have carried out a more comprehensive systematic study to examine the effects of peptide size, residue position, neighboring amino acid, and side chain on the macrocyclization and the potential ring opening of macrocyclic  $b_n$  ( $n = 5$  to  $7$ ) ions.

---

This chapter serves as a review of the following publication: Tasoglu, C.; Gorgulu, G.; Yalcin, T. ‘‘ Investigation of peptide size, residue position, neighbor amino acid and side chain effect on macrocyclization of  $b_n$  ( $n = 5-7$ ) ions’’ *International Journal of Mass Spectrometry*, 2012. 316-318: 108-116.



## 4.2. Experimental

The study utilized two sets of model peptides. The first set was isomeric peptide series of YAGFLV-NH<sub>2</sub> to examine the neighboring amino acid effect on the ring cleavage of macrocyclic *b* ions. The second set was XYAGFLV-NH<sub>2</sub> and YAGXFLV-NH<sub>2</sub> where X denotes C, D, E, H, K, M, N, P, Q, S, T, and W amino acid residues. The position of the X amino acid residue was varied to examine the influence of the amino acid position and side chain on the ring formation and cleavage (*b*<sub>5</sub>-X, *b*<sub>6</sub>-X and *b*<sub>7</sub>-X) of macrocyclic *b* ions. Moreover, the collision energy dependence of the preferential cleavage of macrocyclic *b* ions was also studied. The details of MS conditions and all other parameters are given in Chapter 3.

## 4.3. Results and Discussion

### 4.3.1. Influence of Neighbor Amino Acid on Preferential Opening of Macrocyclic *b* Ion

The MS/MS spectra of *b*<sub>6</sub> (651 *m/z*) ions derived from YAGFLV-NH<sub>2</sub>, AGFLVY-NH<sub>2</sub>, GFLVYA-NH<sub>2</sub>, FLVYAG-NH<sub>2</sub>, LVYAGF-NH<sub>2</sub>, and VYAGFL-NH<sub>2</sub> are presented in Figure 4.1. They produce both direct and non-direct sequence ions in agreement with the literature studies (50; 53; 55-57), and display nearly an identical fragmentation pattern. This is because the *b*<sub>6</sub> ions derived from the isomeric peptides form the same macrocyclic structure due to the generation of the same amino acid sequence order upon cyclization. The main product ions include H<sub>2</sub>O elimination (633 *m/z*), *a*<sub>6</sub> ion (623 *m/z*), and *a*<sub>6</sub>\* ion (606 *m/z*). Additionally, all the spectra show significant non-direct sequence ions as the eliminations of Y (488 *m/z*), A (580 *m/z*), F (504 *m/z*), L (538 *m/z*), and V (552 *m/z*). It was noticed that in previous studies the MS/MS experiments concerning the macrocyclization of *b* ions were performed at a single collision energy value. Therefore, the collision energy dependence of the preferential cleavage of macrocyclic *b* ions was also investigated. Figure 4.2 shows the breakdown graph of these isomeric peptides considering non-direct sequence ions only. However, it should be noted that some of the non-direct sequence amino acid eliminations might overlap with the direct sequence ions (e.g., *b*<sub>6</sub>-V from YAGFLV

might overlap with the  $b_5$  ion). As one can easily see, they all follow nearly the same dissociation pattern regardless of the peptide sequence. Interestingly, the elimination tendency of each internal amino acid residue from the  $b_6$  ion is same for all model peptides. A decreasing trend was shown in the order of  $Y > V > L > F \sim A$ . The internal elimination of tyrosine was observed to be the most dominant event ( $\sim 7\%$  of total ion current at maxima) compared to the other eliminations. The results suggested that the ring-opening from the A-Y bond forming AGFLVY<sub>oxa</sub> linear hexapeptide isomer is

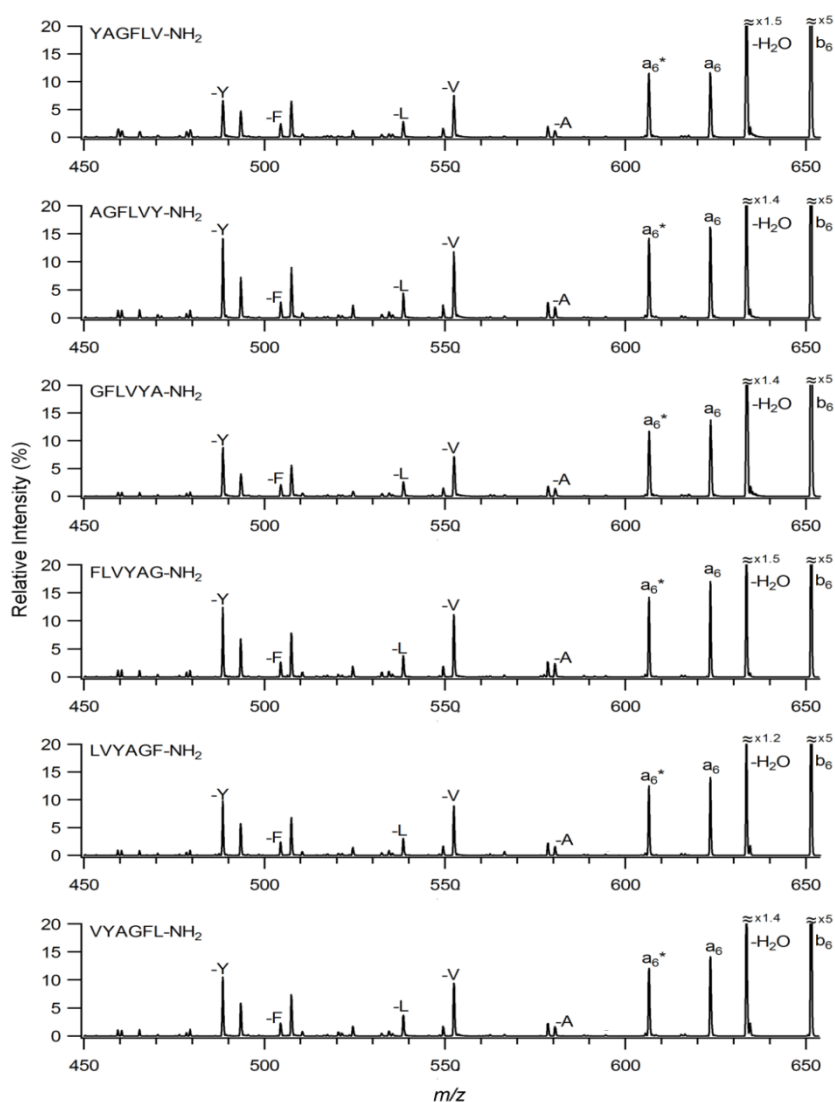


Figure 4.1. CID spectra of  $b_6$  ions derived from permuted isomers of YAGFLV-NH<sub>2</sub>. Each precursor peptide sequence is shown with its related spectrum. CE is 24eV.

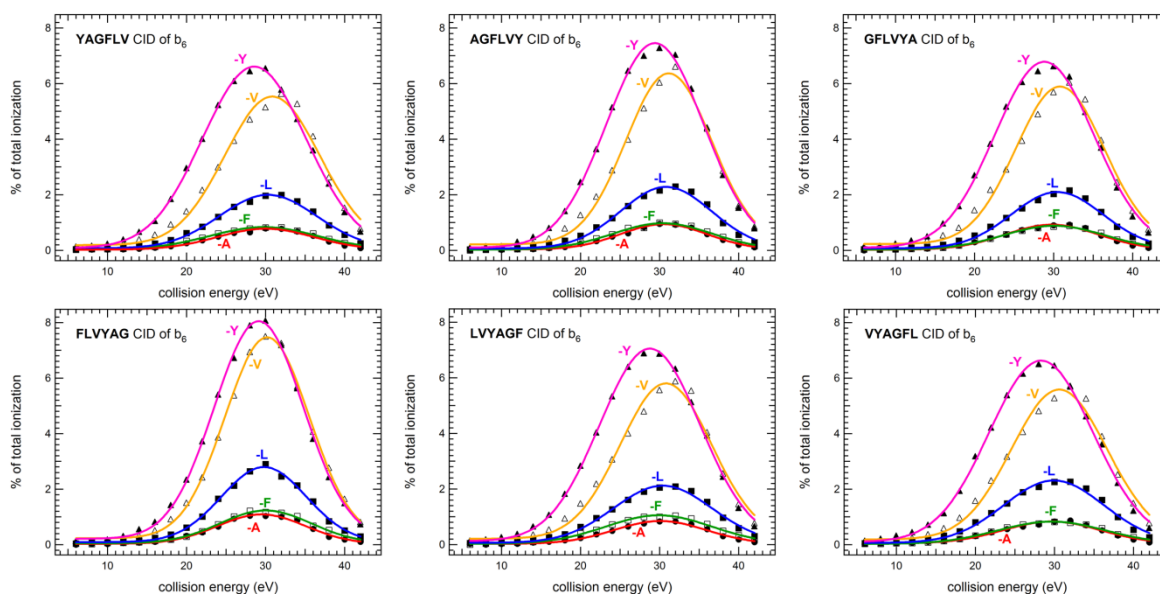


Figure 4.2. Breakdown graphs for  $b_6$  ions derived from permuted isomers of YAGFLV-NH<sub>2</sub>. (Nondirect sequence ions are shown only)

energetically the most favored pathway and is in excellent agreement with the work previously published by Harrison et al. (53). Their potential energy surface (PES) scan studies have revealed that the energetically most favored ring-opening transition structure is AGFLY<sub>oxa</sub>. However, the relative intensities of non-direct sequence ions in both the MS/MS spectra Figure 4.3 and breakdown graphs Figure 4.4 of  $b_6$  ions derived from FAYVGL-NH<sub>2</sub>, GVYALF-NH<sub>2</sub>, and VFYLAG-NH<sub>2</sub> show different distributions within each other. As can be seen in Figure 4.3, the distribution of the non-sequence ion intensities are also different from the other series shown in Figure 4.1 even though they are all isomeric peptides. This could be due to the formation of a different amino acid sequence order in the cyclic forms of these peptides. It was clearly shown that neighboring amino acid has influenced the selective opening of the macrocyclic  $b_6$  ion. The breakdown graphs of these peptides (as shown in Figure 4.4) have totally different distributions when compared to each other and the results which are shown in Figure 4.2. Based on these findings, the single residue elimination orders are observed as V > Y > L ~ F > A, Y > L > F > V > A, and L > V > F ~ Y > A for FAYVGL-NH<sub>2</sub>, GVYALF-NH<sub>2</sub>, and VFYLAG-NH<sub>2</sub>, respectively. Nevertheless, alanine has the lowest tendency to be eliminated from the macrocycle regardless of the sequence.

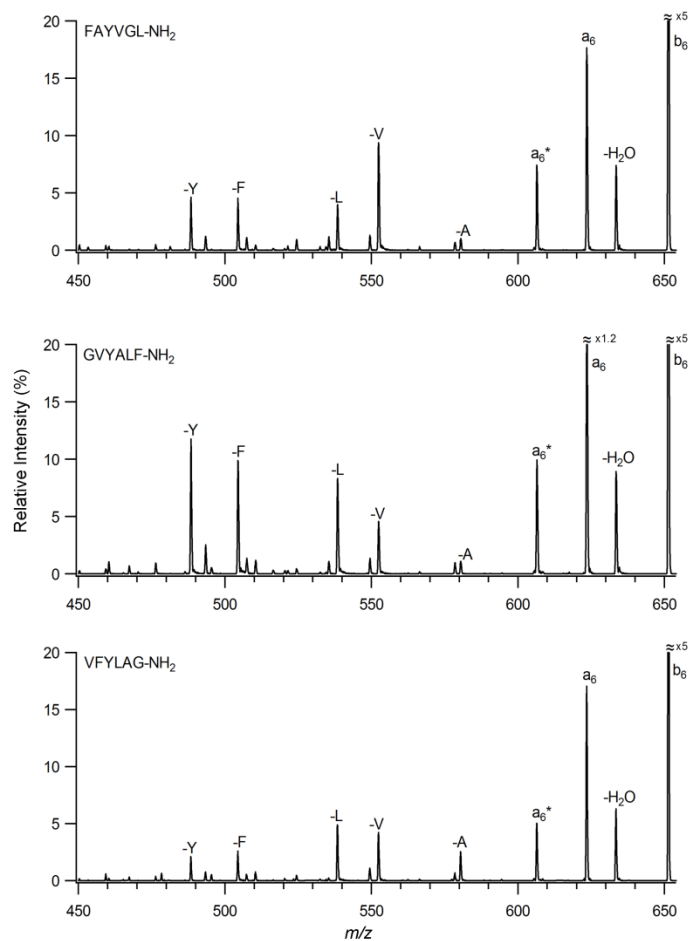


Figure 4.3. CID spectra of  $b_6$  ions of derived from FAYVGL-NH<sub>2</sub>, GVIYALF-NH<sub>2</sub>, and VFYLAG-NH<sub>2</sub>. CE is 24 eV.

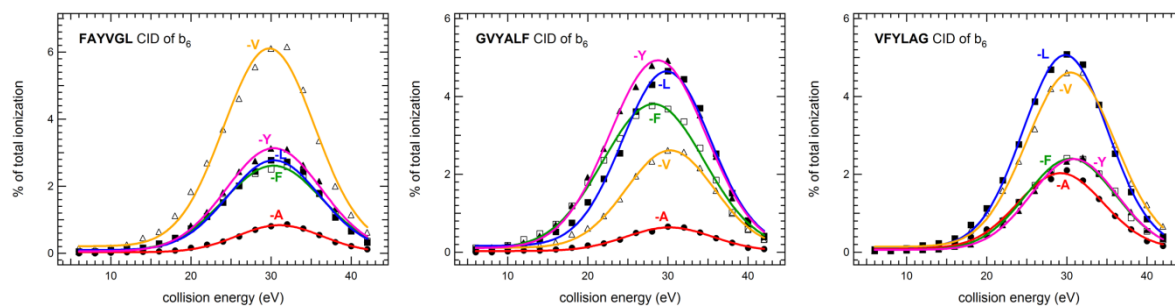


Figure 4.4. Breakdown graphs for  $b_6$  ions derived from FAYVGL-NH<sub>2</sub>, GVIYALF-NH<sub>2</sub>, and VFYLAG-NH<sub>2</sub>. Nondirect sequence ions are shown only.

### 4.3.2. Effects of Peptide Size, Residue Position, Neighbour Residue, and Side Chain on Preferential Opening of Macrocyclic $b$ Ion

Recently, Stipdonk et al. have demonstrated that the preferential opening of the macrocyclic  $b$  ion structure is directly affected by the peptide size (57) and the nature of the amino acid side chain (58). They have performed a CID of the  $b_5$  ion derived from YAXFLG model sequence (where X is G, K, E, D, N, Q), and compared the peak intensities related to the loss of X from the  $b_5$  ion. Using this approach, the  $b_5$ -X trend is found to follow the order of  $Q > K > D > N \sim E$  (no G elimination observed). However, they have only considered a single  $b$  ion size ( $b_5$ ), a single residue position, and a limited number of amino acid residues. In this study, on the other hand, we have extended this approach by examining the effect of the amino acid side chain using a variety of residues, changing the residue position, and investigating the  $b$  ion size ( $b_5$  to  $b_7$ ) on the ring formation and cleavage ( $b_5$ -X,  $b_6$ -X, and  $b_7$ -X) of macrocyclic  $b$  ions. For this purpose, the peptide series have been designed as XYAGFLV-NH<sub>2</sub> and YAGXFLV-NH<sub>2</sub> where X denotes C, D, E, H, K, M, N, P, Q, S, T, and W amino acid residues. The model peptides are divided into four main groups based on the side-chain nature of X residue such as acidic (D, E), basic (H, K), nonpolar (M, P, W), and polar (C, N, Q, S, T) groups. The collision energy dependence of the preferential cleavage of acidic, basic, nonpolar and polar peptide series are shown in Figure 4.5, Figure 4.6, Figure 4.7, and Figure 4.8, respectively. As is apparent in the graphs, the N-terminal position and the central position of all the residues mentioned above were considered. The results clearly show that  $b_6$  and  $b_7$  ions have a higher tendency towards macrocyclization compared to the  $b_5$  ions with the exception of QYAGFLV-NH<sub>2</sub> showing  $b_5$ -Q  $>$   $b_7$ -Q profile. There is no such an observation for asparagine although its side chain is similar to glutamine. This interesting behavior of glutamine is presently under investigation in our laboratory. In addition, it has been observed that the selective ring opening is also dependent on the size of the  $b$  ions and the position of the amino acid residue. In Figure 4.5, it was shown that N-terminally positioned aspartic acid or glutamic acid cleavage from  $b_6$  or  $b_7$  is favored compared to their cleavages when centrally positioned. Furthermore, both  $b_6$ -X and  $b_7$ -X (where X= D or E) profiles showed similar distributions except for EYAGFLV-NH<sub>2</sub>.

X: ACIDIC

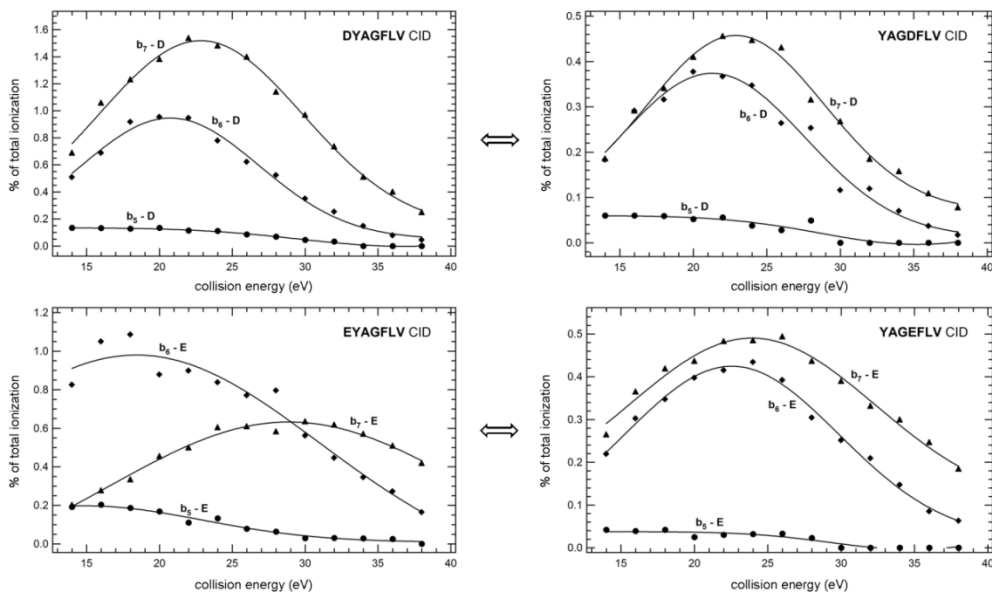


Figure 4.5. Breakdown graphs for elimination of X from XYAGFLV-NH<sub>2</sub> and YAGXFLV-NH<sub>2</sub>, (X = D, E)

X: BASIC

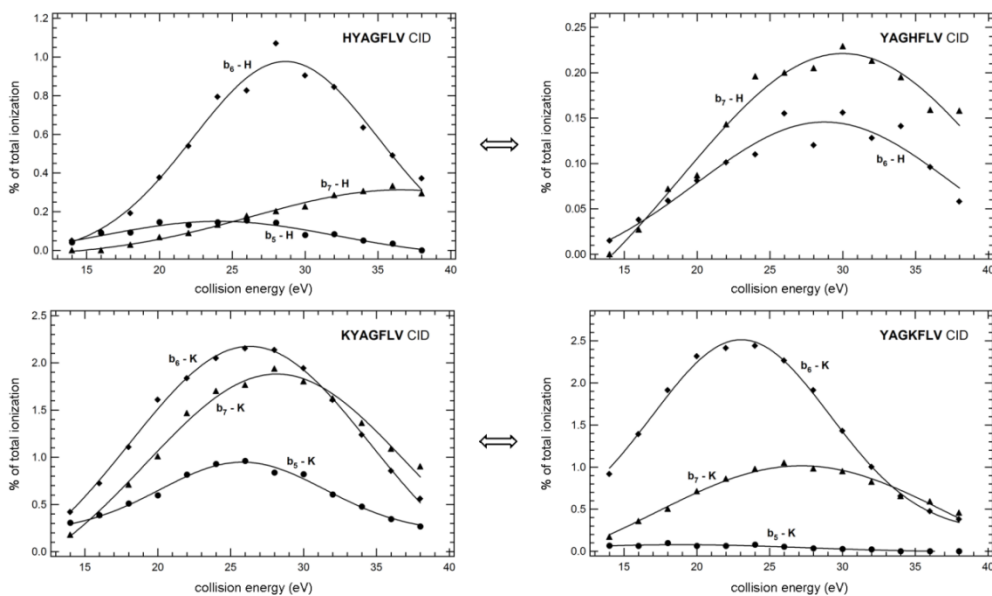


Figure 4.6. Breakdown graphs for elimination of X from XYAGFLV-NH<sub>2</sub> and YAGXFLV-NH<sub>2</sub> (X = H, K)

In Figure 4.6, the N-terminal and central position of the lysine residue showed a similar  $b_6$ -K distribution. But the  $b_7$ -K elimination from the N-terminal and the central position did not show a similar distribution. The preferential cleavage of  $b_5$ -K showed a different profile when N-terminal position is compared to the central position. It is also shown that the  $b_6$ -H cleavages from the N-terminal and central position are similar. By contrast, the  $b_7$ -H cleavage from the N-terminal and central position showed different distributions. In addition, the  $b_5$ -H cleavage from N-terminal position is in low abundance and is in agreement with the report by Harrison et al. (60). However, no acceptable signal was observed for the central position.

Among the nonpolar residues, preferential cleavage of the proline residue from  $b_5$ ,  $b_6$ , and  $b_7$  showed similar distributions no matter where the position of the proline residue is (Figure 4.7). However, N-terminal and central position of the methionine showed a similar distribution when considering  $b_6$  ions; although,  $b_7$  showed a different distribution. The major difference observed for tryptophan is the preferential cleavage from  $b_7$ -W for the N-terminal and central position.

Considering the polar residues, the position of asparagine and threonine did not influence the  $b_5$ -X,  $b_6$ -X and  $b_7$ -X distributions. Nonetheless, internal eliminations of cysteine, glutamine, and serine showed completely different distributions when their positions were changed from N-terminus to the center of the peptide (Figure 4.8).

Finally, among the all amino acid residues, Q, W, K, and M were found to be more favored eliminations from the macrocyclic  $b_6$  ion. Different from Stipdonk et al. (57; 58), our results have shown that no preferential cleavage order can be specified depending on the nature of amino acid side chain.

X: NONPOLAR

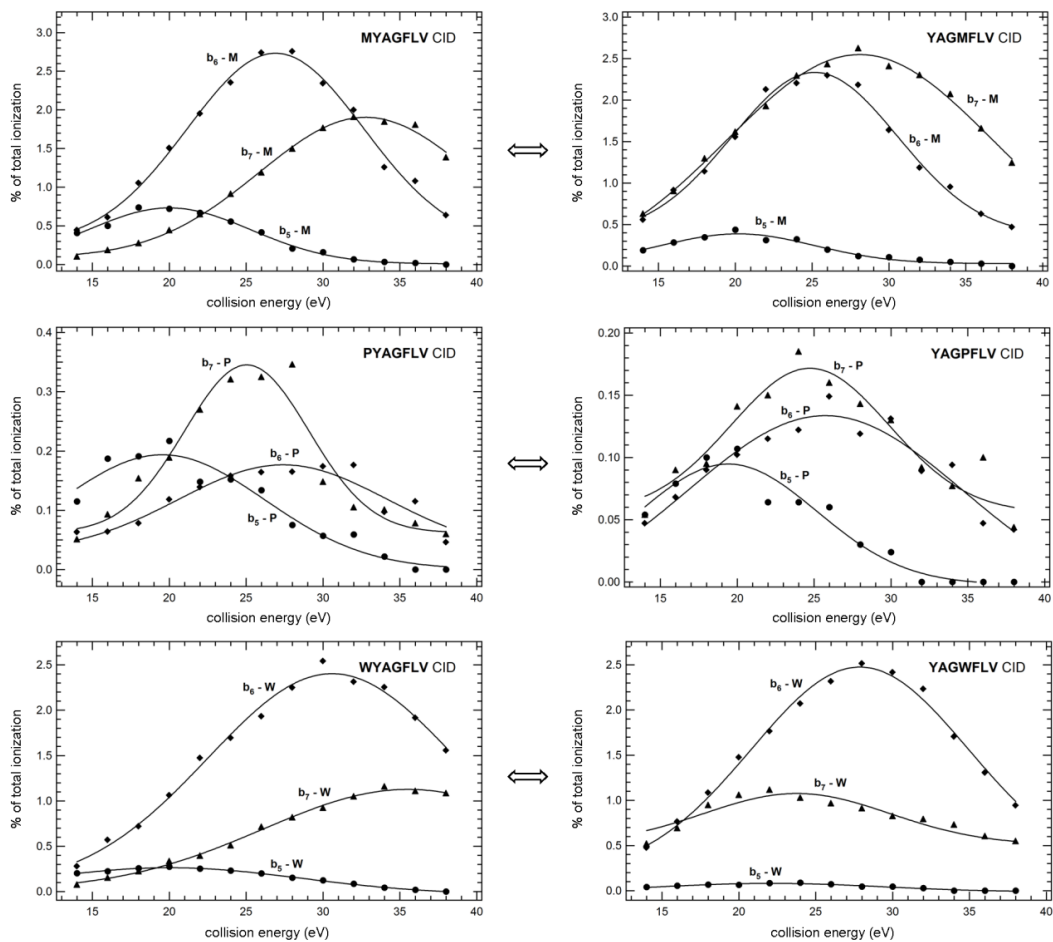


Figure 4.7. Breakdown graphs for elimination of X from XYAGFLV-NH<sub>2</sub> and YAGXFLV-NH<sub>2</sub> (X = M, P, and W)



X: POLAR

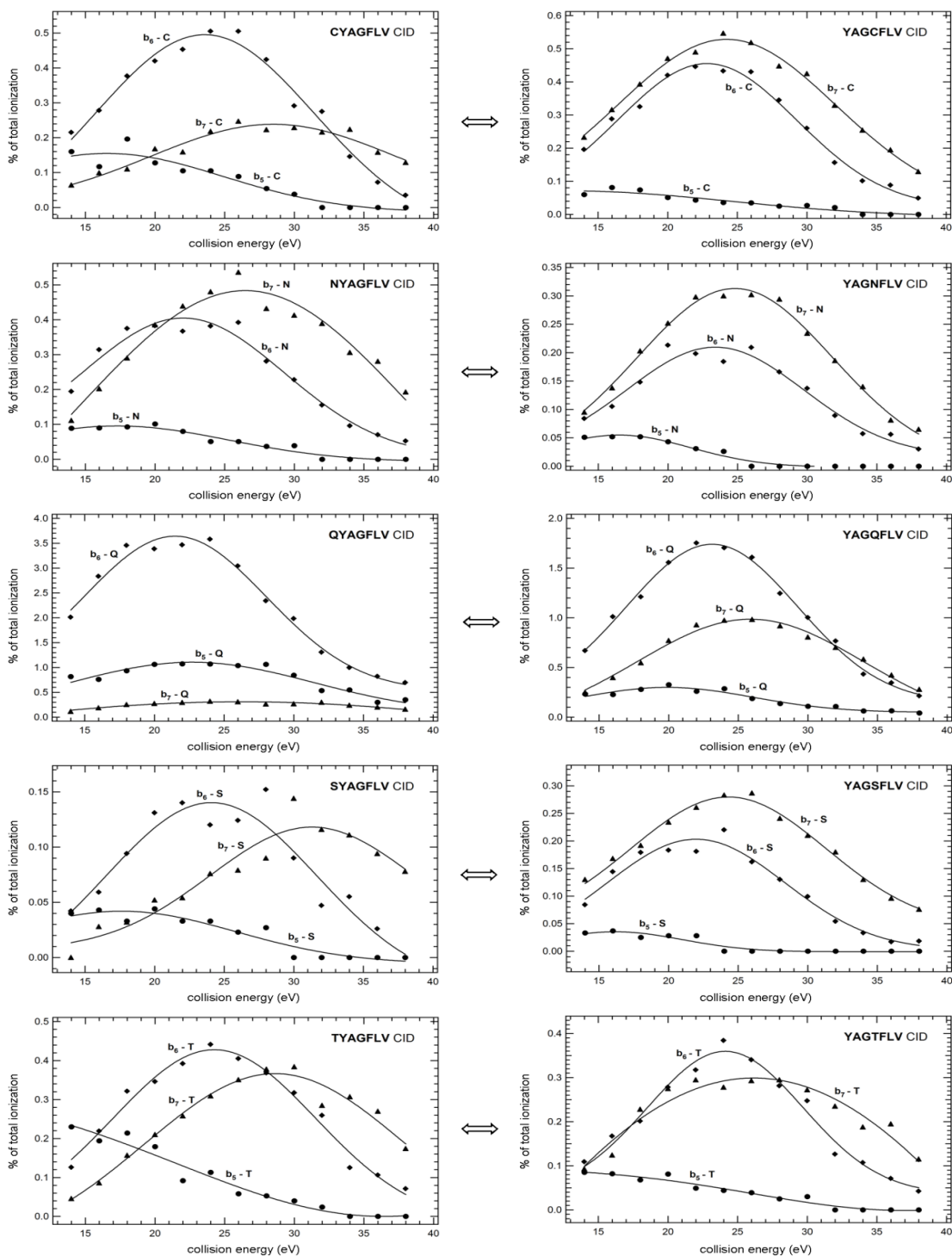


Figure 4.8. Breakdown graphs for elimination of X from XYAGFLV-NH<sub>2</sub> and YAGXFLV-NH<sub>2</sub> (X = C, N, Q, S, and T)

## CHAPTER 5

# EFFECT OF PROLINE ON PEPTIDE FRAGMENTATION

### 5.1. Introduction

Proline residue is of particular importance for tandem mass spectrometric analysis of peptides/proteins due to its influence on the course of peptide dissociation. Among amino acid residues without basic functional groups, proline has the highest proton affinity (61). A number of studies (62-69) have been reported to demonstrate ‘proline-directed fragmentations’ that produce very prominent  $y$  ions in the consequence of cleavage N-terminal to proline residue (proline effect). The position of proline has also been found to have a direct role at the cleavage site of protonated peptides (70) and deprotonated ones too (71). Moreover, structure of peptide fragments containing proline residue is of considerable subject to researchers. It was Eckart’s group who gave first experimental and theoretical clues of alternative gas-phase structure for  $b_2$  ion of GP rather than oxazolone (72). Wysocki’s Laboratory then suggested a diketopiperazine structure for a VP  $b_2$  ion (73). Quite recently, Wysocki et al. (74) have utilized action infrared multiphoton dissociation (IRMPD) spectroscopy, hydrogen-deuterium exchange (HDX), and density functional theory (DFT) calculations to examine the effect of N-terminal residue on the structure of proline-containing  $b_2$  ions. They found that GP, AP, IP, and VP  $b_2$  ions from tripeptides primarily exist as oxazolone in addition to small portions of diketopiperazine form while HP, synthetic cyclic HP and

---

This chapter represents the combination of a publication and a manuscript: (A) Harrison, A.G.; Tasoglu, C.; Yalcin, T. “Non-direct sequence ions in the tandem mass spectrometry of protonated peptide amides— an energy-resolved study” *Journal of The American Society for Mass Spectrometry*, 2013. 24(10): 1565-1572. (B) Tasoglu, C.; Harrison, A.G.; Yalcin, T. (to be sent to *Journal of The American Society for Mass Spectrometry*).

cyclic VP produce diketopiperazine only. Inspired by these studies, we investigated the fragmentation characteristics of proline-containing peptides.

## 5.2. Experimental

The study used C-terminal amidated model peptides as PA<sub>6</sub>, APA<sub>5</sub>, A<sub>2</sub>PA<sub>4</sub>, A<sub>3</sub>PA<sub>3</sub>, A<sub>4</sub>PA<sub>2</sub>, A<sub>5</sub>PA, A<sub>6</sub>P, PYAGFLV, PAGFLVY, PGFLVYA PFLVYAG, PLVYAGF, PVYAGFL, YPAGFLV, YAPGFLV, YAGPFLV, YAGFPLV, YAGFLPV, YAGFLVP, YPVGFLA, A<sub>2</sub>PXA<sub>3</sub>, and A<sub>2</sub>XPA<sub>3</sub> (where X = C, D, F, G, L, V, and Y, respectively). The details of MS conditions and all other parameters are given in Chapter 3. Only the MH<sup>+</sup> spectra of YAGFLVP, YPVGFLA, and PYAGFLV were collected using quadrupole/time-of-flight (QqTOF) mass spectrometer (QStar XL, SCIEX, Concord, Canada).

## 5.3. Results and Discussion

### 5.3.1. CID Studies of MH<sup>+</sup> Ions of YAGFLVP-NH<sub>2</sub>, YPVGFLA-NH<sub>2</sub>, and PYAGFLV-NH<sub>2</sub>

Fragmentation of MH<sup>+</sup> ion of YAGFLVP-NH<sub>2</sub> mainly gives *b*<sub>6</sub> ion by elimination of proline amide under low CID environment. Increasing the collision energy to 36 eV leads to minor formation of *y*<sub>1</sub> and *y*<sub>2</sub> ions and a large variety of *b*<sub>*n*</sub> ions as seen in Figure 5.1. It is obvious that the *b*<sub>6</sub> ion has undergone extensive macrocyclization and rearrangement prior to fragmentation. The distribution of *b*<sub>*n*</sub> ions is essentially the same as one observes for fragmentation of the *b*<sub>6</sub> ion directly. It is not possible to derive sequence information for this peptide amide from MS/MS studies of the MH<sup>+</sup> ion.

Figure 5.2 shows the CID spectrum of the MH<sup>+</sup> ion from YPVGFLA-NH<sub>2</sub> at 44 eV where *b* ions are considered only. Table 5.1 records the *b*<sub>*n*</sub> ion signals as a function of collision energy over the range 36 to 46 eV collision energy. At the lowest collision energy studied signals are observed for the sequence ions *b*<sub>7</sub>, *b*<sub>6</sub> and *b*<sub>5</sub> ions and, surprisingly, the *b*<sub>2</sub> ion at *m/z* 261. With increasing collision energy this ion becomes the major ion in the product ion mass spectrum. Accurate mass measurements

confirmed the ion as a YP (or PY)  $b_2$  ion of unknown structure. The observation of this product at low collision energies suggests the possibility that it may arise, in part, directly by fragmentation of the  $MH^+$  ion.

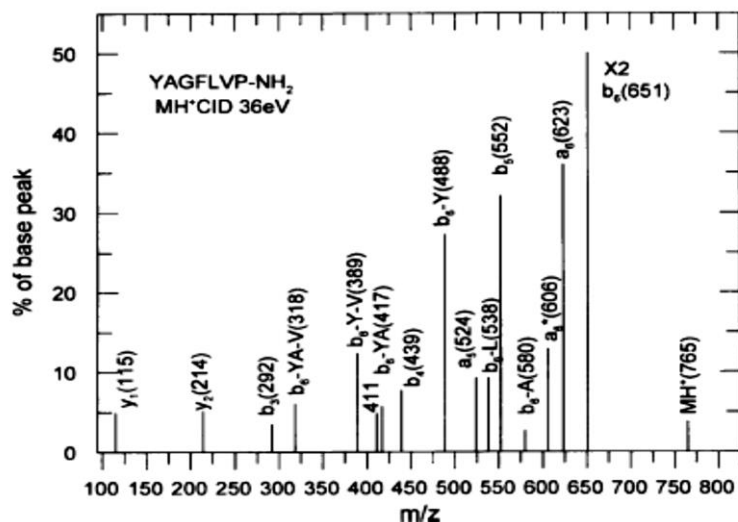


Figure 5.1. CID spectrum of  $MH^+$  ion derived from YAGFLVP-NH<sub>2</sub>

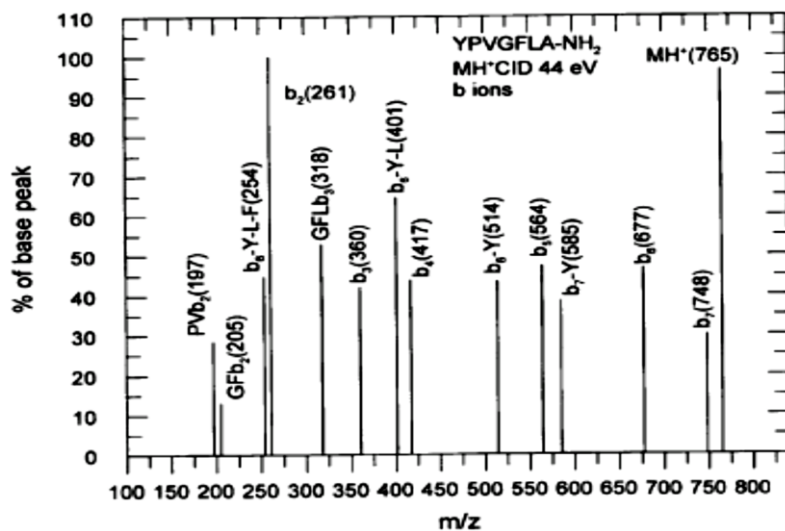


Figure 5.2. CID spectrum of  $MH^+$  ion derived from YPVGFLA-NH<sub>2</sub> ( $b$  ions shown only)

Table 5.1. Relative intensities of *b* ions of YPVGFLA-NH<sub>2</sub> at various collision energies

(Ion intensities as % of base peak)									
<i>m/z</i>	36 eV	38 eV	40 eV	42 eV	44 eV	46 eV	Ion	Residues	
765	100	100	100	100	96.4	43.0	MH <sup>+</sup>		
748	11.3	14.7	19.6	24.8	29.8	15.8	<i>b</i> <sub>7</sub>	YPVGFLA	
677	9.7	15.3	23.0	34.5	46.6	28.6	<i>b</i> <sub>6</sub>	YPVGFL	
585	—	5.3	11.8	22.7	38.5	29.6	<i>b</i> <sub>7</sub> -Y	PVGFLA	
564	5.5	9.0	16.8	29.5	47.2	35.8	<i>b</i> <sub>5</sub>	YPVGF	
514	—	4.8	10.0	22.6	43.4	36.6	<i>b</i> <sub>6</sub> -Y	PVGFL	
417	—	5.3	10.1	22.2	43.8	42.0	<i>b</i> <sub>4</sub>	YPVG	
401	—	5.6	12.8	30.5	64.6	65.5	<i>b</i> <sub>6</sub> -Y-L	PVGF	
360	—	7.7	13.8	25.2	42.0	33.4	<i>b</i> <sub>3</sub>	YPV	
318	—	4.9	11.1	24.6	52.8	49.5	GFL- <i>b</i> <sub>3</sub>	GFL	
261	3.9	8.7	19.5	46.1	100	100	<i>b</i> <sub>2</sub>	YP	
254	—	4.4	7.6	19.3	44.8	49.5	<i>b</i> <sub>6</sub> -Y-L-F	PVG	
205	—	—	—	5.2	13.0	15.0	GF- <i>b</i> <sub>2</sub>	GF	
197	—	3.1	4.8	12.0	28.4	32.0	PV- <i>b</i> <sub>2</sub>	PV	

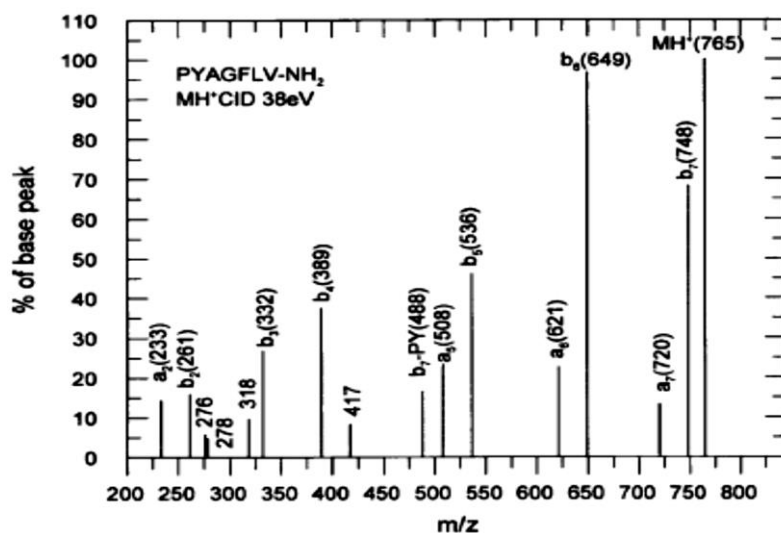


Figure 5.3. CID spectrum of MH<sup>+</sup> ion derived from PYAGFLV-NH<sub>2</sub>

The results in Figure 5.2 show the complete series of direct sequence ions *b*<sub>7</sub>, *b*<sub>6</sub>, *b*<sub>5</sub>, *b*<sub>4</sub>, *b*<sub>3</sub> and *b*<sub>2</sub>. In addition, there are non-direct sequence ions corresponding to *b*<sub>7</sub>-Y (585), *b*<sub>6</sub>-Y (514), *b*<sub>6</sub>-Y-L (401) and *b*<sub>6</sub>-Y-L-F (254). These result from macrocyclization of the *b*<sub>7</sub> and *b*<sub>6</sub> ions with preferential reopening of the macrocycle to put the proline residue at the N-terminus of the oxazolone so-formed. A recent study (75) of the fragmentation of *b*<sub>5</sub> ions containing proline provided qualitative evidence for the preference of the proline residue to be in the N-terminal position upon the opening of the macrocycle form.

The CID spectrum of the  $MH^+$  ion from PYAGFLV-NH<sub>2</sub> at 38 eV collision energy is given in Figure 5.3. Not surprisingly there is essentially no evidence for non-direct sequence ions in the spectrum. Because of the preference for the proline residue to be in the N-terminal position, any macrocyclic ions formed will reopen to give oxazolones with the original amino acid sequence.

### 5.3.2. CID Studies of $b_7$ Ions of PAAAAAA-NH<sub>2</sub> Series

The CID mass spectra of  $b_7$  (524  $m/z$ ) ions produced from protonated heptapeptides containing six alanine residues and one proline residue with the position of proline varied are given in Figure 5.4. Nearly identical fragmentation patterns are obtained for all the isomers, which is the direct evidence of head-to-tail macrocyclization reaction prior to re-opening at various amide bond positions regardless of original sequence. The obtained results are in good agreement with recent work of Harrison (75) showing identical CID spectra of  $b_5$  ions derived from PAAAA, AAPAA, and AAAAP series. In addition to the major product ions which are H<sub>2</sub>O loss (506  $m/z$ ),  $a_7$  (496  $m/z$ ), and  $a_7^*$  (479  $m/z$ ), we also observed non-direct sequence ions as eliminations of A (453  $m/z$ ), 2A (382  $m/z$ ), 3A (311  $m/z$ ), 4A (240  $m/z$ ), 5A (169  $m/z$ ), P (427  $m/z$ ), P+A (356  $m/z$ ), P+2A (285  $m/z$ ), and P+3A (214  $m/z$ ) for all isomers. These findings clearly show that position of proline does not influence the course of fragmentation as long as alanine is used as a spacer residue. Among the product ions, proline-based eliminations are of particular interest because they give us a clue about different fragmentation characteristics of proline-containing peptides. Hence, we examined different type of peptide series to reveal the mechanism lying behind this unique behavior in the next section.

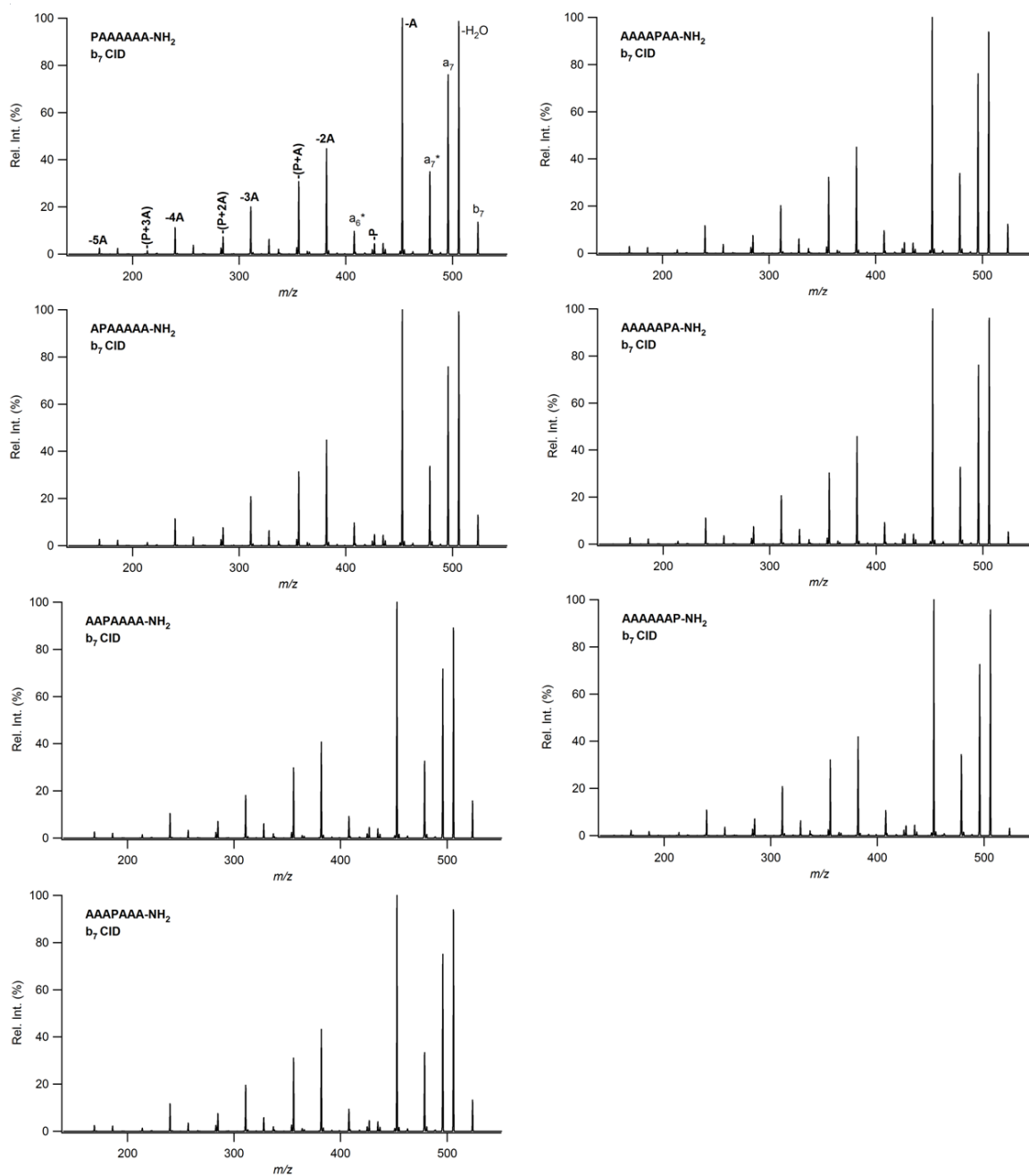


Figure 5.4. CID spectra of  $b_7$  ions derived from isomers of PAAAAAA-NH<sub>2</sub>

### 5.3.3. CID Studies of $b_7$ Ions of PYAGFLV-NH<sub>2</sub> Series

To determine the neighbor residue effect on fragmentation of proline-containing peptides, we carried out CID analysis of  $b_7$  ion (748  $m/z$ ) generated from PYAGFLV-NH<sub>2</sub> and its permuted isomers (Figure 5.5). Fragmentation of all heptapeptides yielded

H<sub>2</sub>O loss (730 *m/z*) and a<sub>7</sub> ion (720 *m/z*) as major product ions in addition to internal residue eliminations of P, Y, A, G, F, L, and F corresponding to 652, 586, 678, 692, 602, 636, and 650 *m/z*, respectively (red-labeled peaks). Internal losses can only be possible in the presence of macrocyclization reaction as known. To investigate the effect of proline position, we compared CID of *b*<sub>7</sub> ions derived from PYAGFLV-NH<sub>2</sub> isomers, and obtained very similar spectra for the following pairs: PYAGFLV-YAGFLVP, PAGFLVY-YPAGFLV, PGFLVYA-YAPGFLV, PFLVYAG-YAGPFLV, PLVYAGF-YAGFPLV, and PVYAGFL-YAGFLPV. As can be seen, each pair has the same ring sequence when macrocycled. Therefore, we can suggest that the position of proline does not seem to be important for product ion distribution as long as the connectivity of residues in the macrocycle is same.

An interesting observation is high-abundant P+X elimination peaks (X: Y, A, G, F, L, and V) where X residue is C-terminally connected to proline (blue-labeled peaks). Even though single proline elimination from *b*<sub>7</sub> is not a preferred route, loss of P+X dipeptide is generally observed to be more favored. Particularly, P+Y (60%) and P+V (50%) eliminations from *b*<sub>7</sub> ions of related peptides are highly dominant. In view of these observations, we extended our study by comparing the MS/MS spectra of the peptide fragment pairs in Table 5.2 to verify the identity of remaining peptide fragment after P+X elimination from *b*<sub>7</sub>. As apparent in Figure 5.6, the pairs gave exactly the same product ion distribution so that neutral dipeptide elimination from *b*<sub>7</sub> ion can be rationalized. They all yielded main product ion losses of H<sub>2</sub>O, CO, and CO+NH<sub>3</sub> from remaining pentapeptide fragments. In addition, internal single residue eliminations are clearly indicative of macrocyclization/re-opening pattern for remaining pentapeptide.



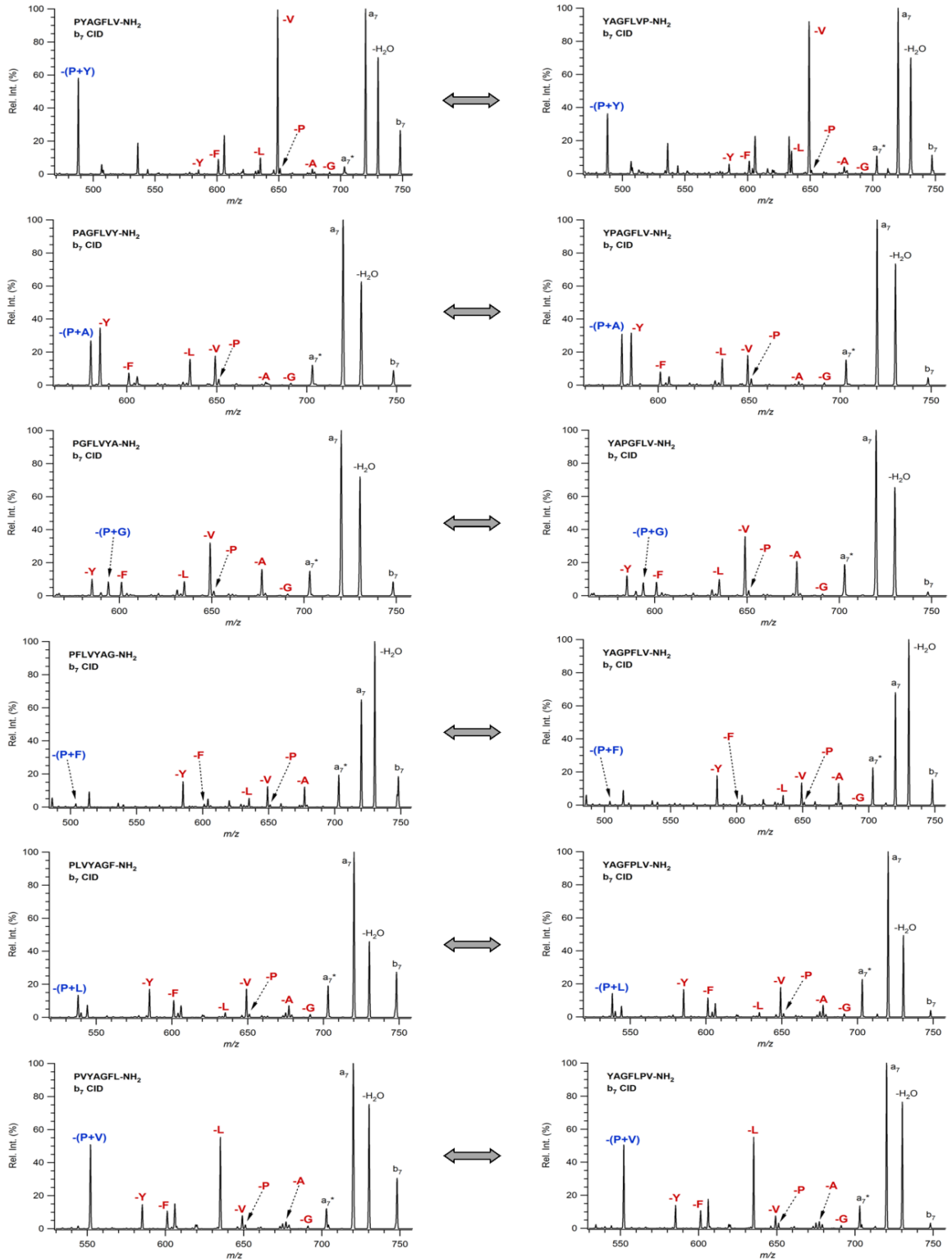


Figure 5.5. CID spectra of  $b_7$  ions derived from isomers of PYAGFLV-NH<sub>2</sub>

Table 5.2. Matched ion pairs chosen to prove dipeptide elimination

Series A	Series B	<i>m/z</i> matched
<i>b</i> <sub>7</sub> -(P+Y) from PY <b>AGFLV</b>	<i>b</i> <sub>5</sub> of <b>AGFLVY</b>	488 <i>m/z</i>
<i>b</i> <sub>7</sub> -(P+A) from PA <b>GFLVY</b>	<i>b</i> <sub>5</sub> of <b>GFLVYA</b>	580 <i>m/z</i>
<i>b</i> <sub>7</sub> -(P+G) from PG <b>FLVYA</b>	<i>b</i> <sub>5</sub> of <b>FLVYAG</b>	594 <i>m/z</i>
<i>b</i> <sub>7</sub> -(P+F) from PF <b>LVYAG</b>	<i>b</i> <sub>5</sub> of <b>LVYAGF</b>	504 <i>m/z</i>
<i>b</i> <sub>7</sub> -(P+L) from PL <b>VYAGF</b>	<i>b</i> <sub>5</sub> of <b>VYAGFL</b>	538 <i>m/z</i>
<i>b</i> <sub>7</sub> -(P+V) from PV <b>YAGFL</b>	<i>b</i> <sub>5</sub> of <b>YAGFLV</b>	552 <i>m/z</i>

A noticeable exception is low-abundant P+F elimination peak from *b*<sub>7</sub> when glycine is N-terminal to proline in PFLVYAG - YAGPFLV peptide pair (Figure 5.5). We examined this behavior for different isomers where glycine is N-terminal to proline again. Figure 5.7 illustrates that CID analysis of *b*<sub>7</sub> of PYAFLVG-NH<sub>2</sub> and its isomers all followed the same trend where P+Y or P+V losses from *b*<sub>7</sub> are minimized. We also examined whether position of proline affect this pathway by comparing CID of *b*<sub>7</sub> of PYAFLVG to LVGPYAF, PVLFYAG to YAGPVLV, and PYLTVAG to VAGPYLV. As seen, pairs produce very similar spectra where P+X losses are not significant any more. This observation is most possibly due to the minimal proton affinity of glycine residue so that mobile proton cannot be retained at the cleavage site of G-P bond (glycine effect). Thus, the intensity of P+X dipeptide elimination from *b*<sub>7</sub> is significantly decreased.

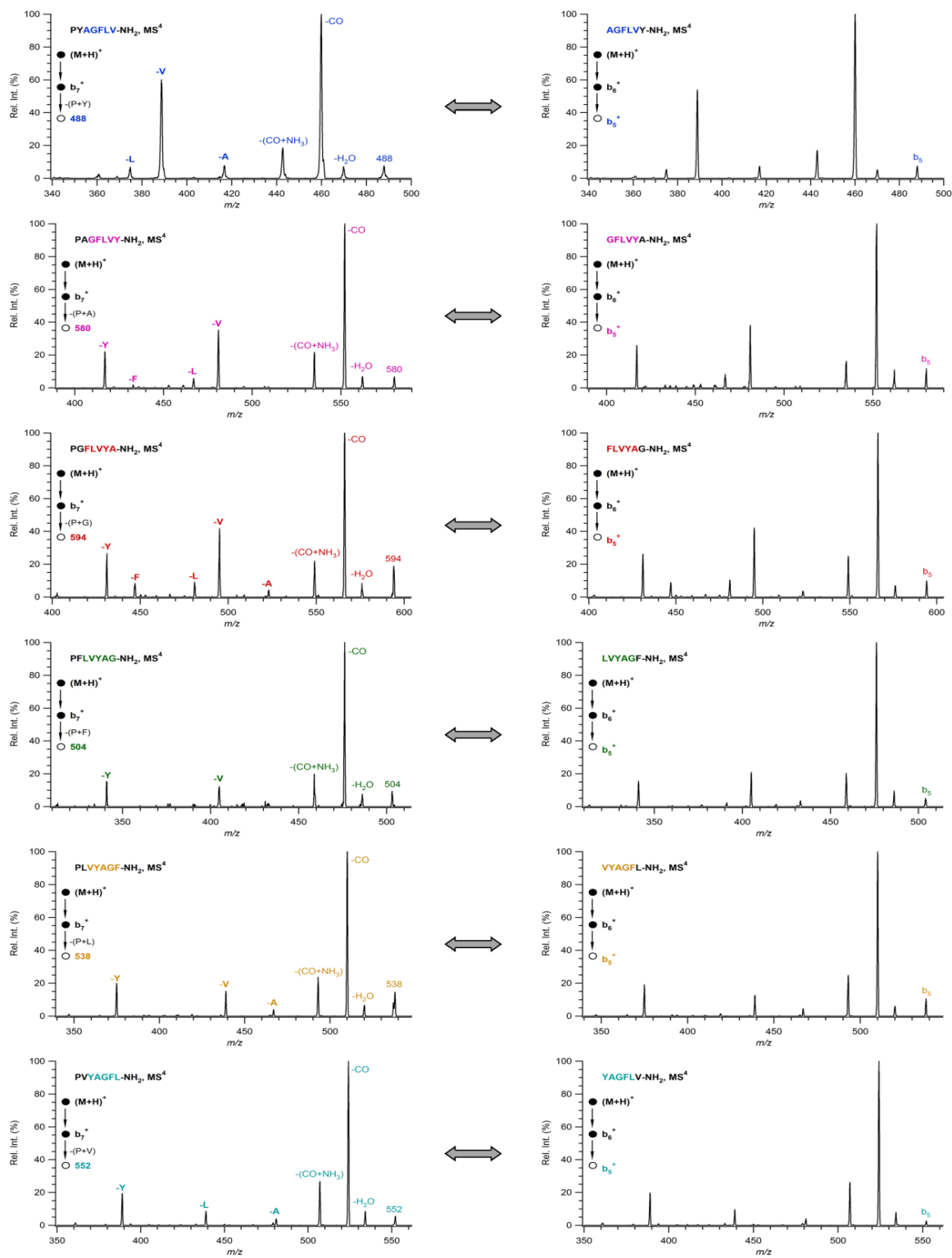


Figure 5.6. Comparison of CID spectra of dipeptide elimination from  $b_7$  of PYAGFLV-NH<sub>2</sub> isomers versus  $b_5$  of YAGFLV-NH<sub>2</sub> isomers

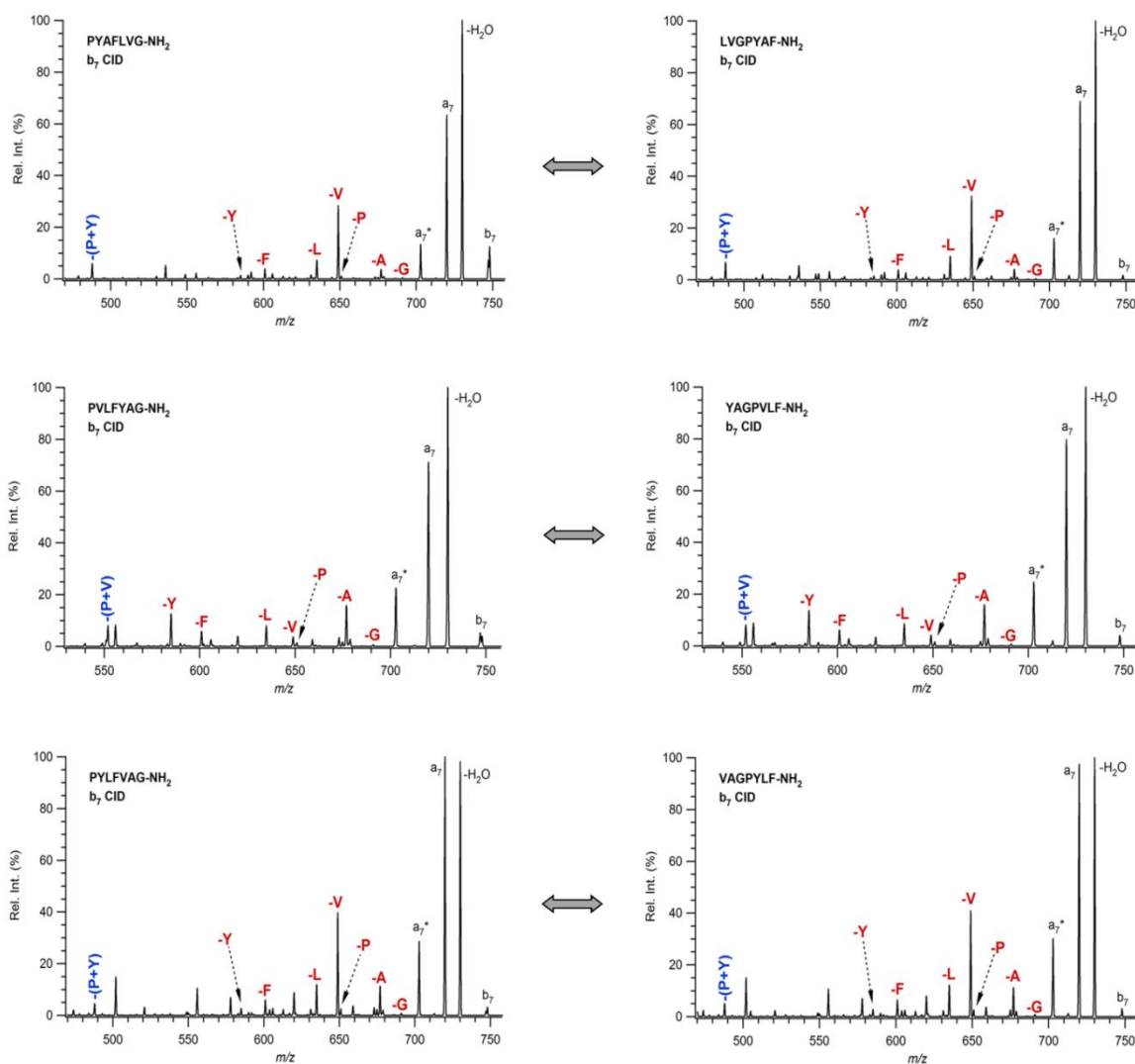


Figure 5.7. CID spectra of  $b_7$  ions derived from isomers of PYAFLVG-NH<sub>2</sub> where G is N-terminal to P

### 5.3.4. CID Studies of $b_7$ Ions of AAPXAAA-NH<sub>2</sub> Series and AAXPAAA-NH<sub>2</sub> Series (where X is C, D, F, G, L, V, and Y)

In order to further investigate the occurrence of neutral elimination of P+X from  $b_7$  when X is located C-terminal to P, and also to eliminate possible neighbour residue effects coming from the PYAGFLV series, we designed a different set of model peptides as AAXPAAA and AAPXAAA, where A is used as a spacer residue and X stands for C, D, F, G, L, V, Y residues. These series are much more objective models in

terms of comparing behavior of each residue adjacent to proline since neighbour residues are all alanine. The CID spectra produced from the respective  $b_7$  ions are displayed in Figure 5.8. As expected, losses of very intense P+X dipeptide (blue-labeled peaks) were observed for  $b_7$  of AAPXAAA models but not for that of AAXPAAA series. Instead, P+A eliminations were dominant in  $b_7$  spectra of AAXPAAA peptides, which is consistent with our previous observations suggesting that proline and its adjacent C-terminal residue is lost as a dipeptide no matter their position in the peptide backbone. This suggestion is well-supported by increased intensity levels of single X eliminations from  $b_7$  when X is N-terminal to P residue. For instance, loss of V from  $b_7$  is the base peak for AAVPAAA whereas it is only 10% for AAPVAAA case. We have a major elimination of alanine from  $b_7$  (base peak) of AAPVAAA instead. Same trend was also valid for other model peptides. Dominant single losses of residues N-terminal to proline can be explained by a preference of proline to be positioned at N-terminus so that this residue can be located at C-terminus.

Lastly, we also carried out detailed CID studies of  $b_7$  of AAPXAAA and AAXPAAA, where the fragmentation of major losses of P, X, P+X, and P+A were investigated as a function of collision energy range. Breakdown graphs in Figure 5.9 and Figure 5.10 indicate that elimination of P+X is highly favored for AAPXAAA models while -X is found to be a dominant loss for AAXPAAA series. In the end, these results made us think that preferential rearrangement occurs in peptide sequence during the ring opening of macrocyclic structure in such a way that proline is always located at N-terminus no matter its original position in the peptide backbone. Then, we propose that the peptide can follow three main pathways as outlined in Scheme 5.1. Path I (blue) includes the cleavage of second amide bond to form a deprotonated oxazolone  $b_2$  (P+R<sub>2</sub>), which explains dipeptide elimination from  $b_7$ . The remaining fragment is oxazolone  $b_5$  producing five-membered macrocycle which can also be formed directly by Path II (green). Path III (red), on the other hand, is the direct formation of macrocyclic  $b_7$  ion that opens up at various amide bonds to cause scrambling of original sequence. This explains the internal losses of single residues (red-labeled) from  $b_7$  ions.

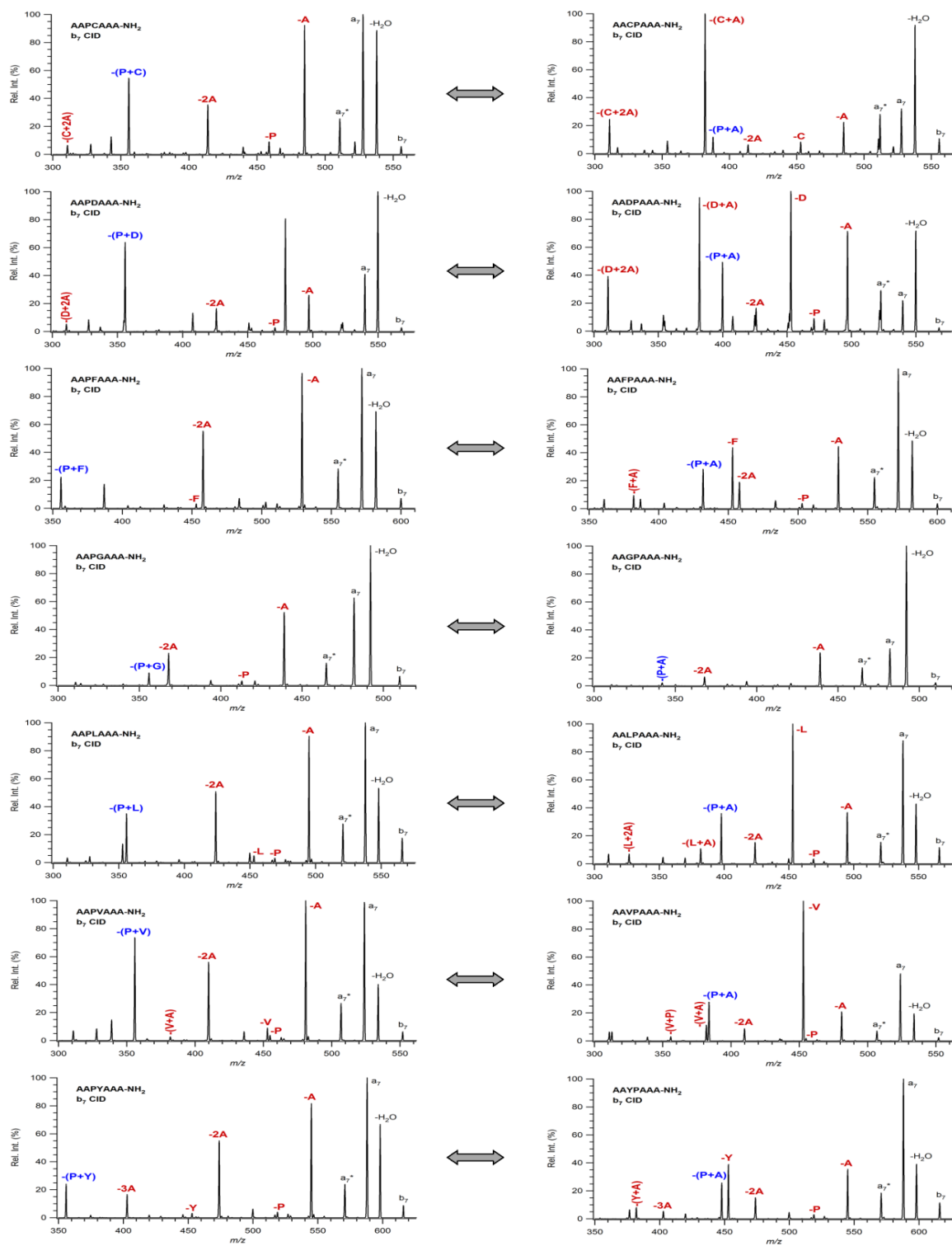


Figure 5.8. Comparison of CID spectra of  $b_7$  of AAPXAAA-NH<sub>2</sub> isomers versus  $b_7$  of AAXPAAA-NH<sub>2</sub> isomers (X = C, D, F, G, L, V, and Y)

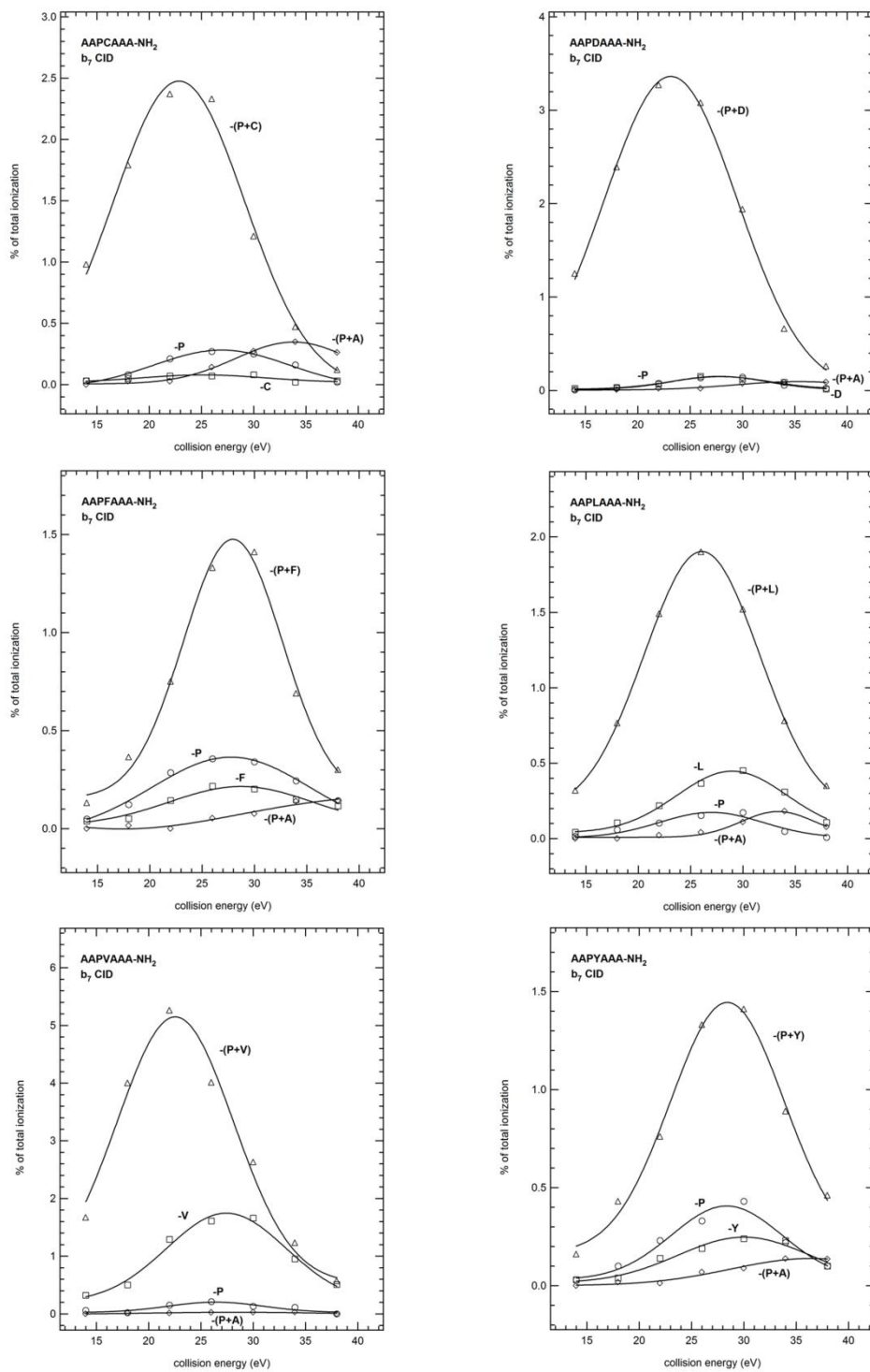


Figure 5.9. Breakdown graphs of  $b_7$  of AAPXAAA-NH<sub>2</sub> series (X= C, D, F, L, V, and Y)

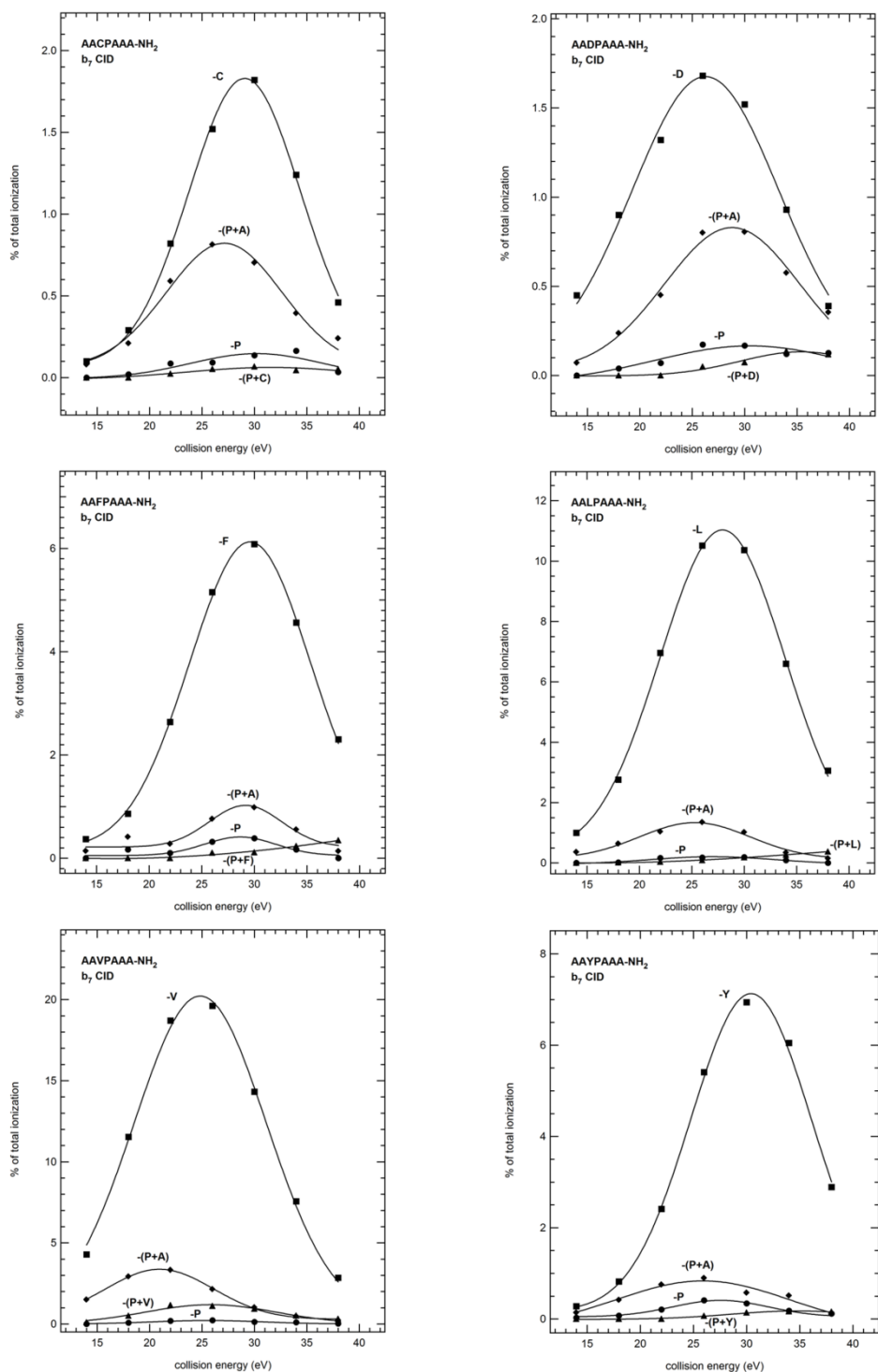
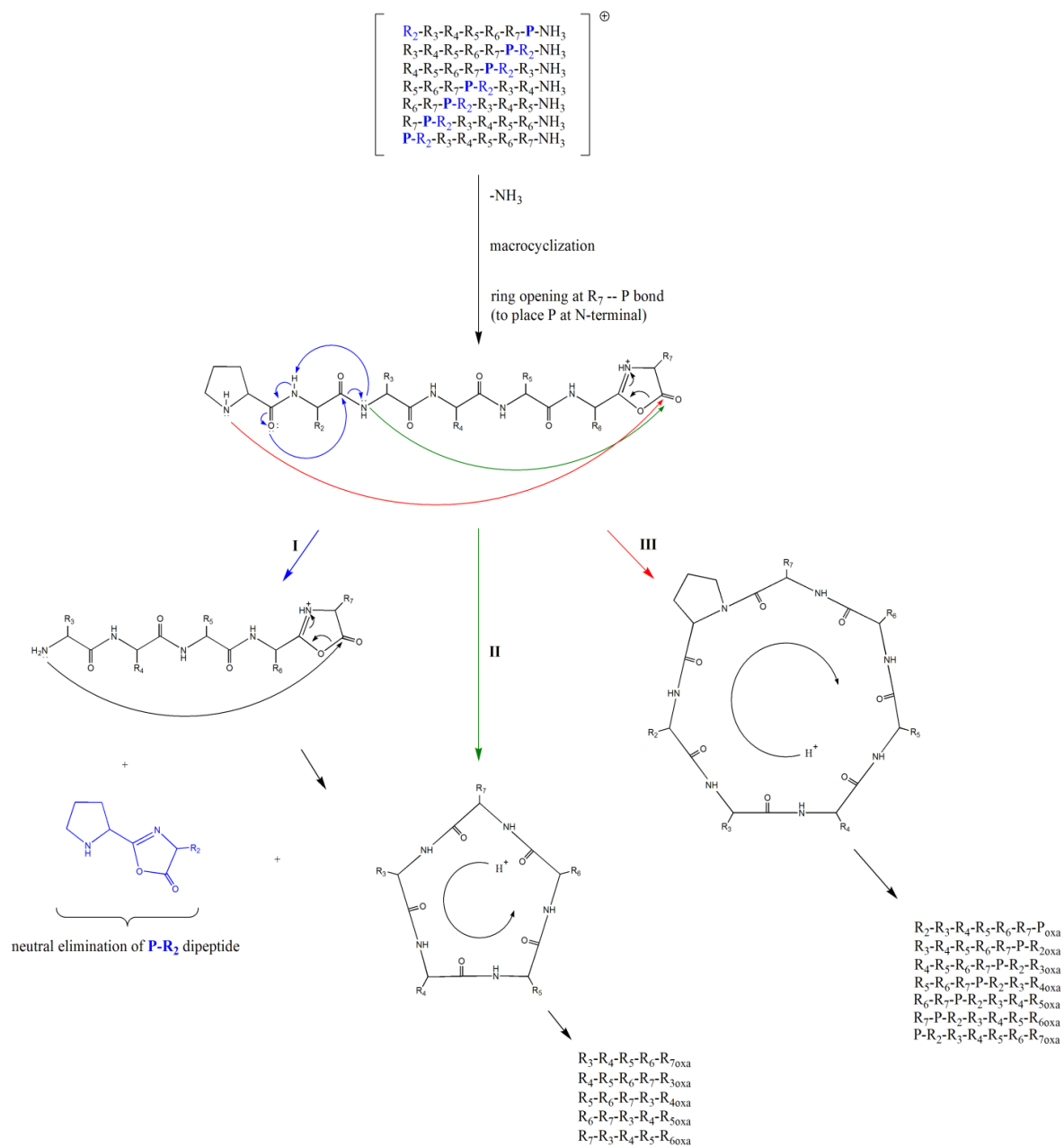


Figure 5.10. Breakdown graphs of  $b_7$  of AAXPAAA-NH<sub>2</sub> series (X= C, D, F, L, V, and Y)





Scheme 5.1. Proposed reaction mechanism and pathways for the formation of  $P+R_2$  dipeptide and its loss from  $b_7$  ion

## CHAPTER 6

# EFFECT OF BASIC RESIDUES ON PEPTIDE FRAGMENTATION

### 6.1. Fragmentation Behavior of Histidine Residue

#### 6.1.1. Introduction

Histidine is the third most basic residue among twenty common amino acids. A number of studies has been published to show how histidine side-chain influences the course of fragmentation. Respective studies of Wysocki and coworkers (76-78) have showed selective cleavages as well as enhanced dissociations facilitated by histidine residue when C-terminally positioned. Besides effect of basic residues on cyclization reaction has taken particular interest such that one of the leading groups working on this subject is that of Harrison who has published a very recent study (79) on the role of histidine residue in cyclization and sequence scrambling of *b* ions using model hexapeptides containing five alanine and single histidine residues with histidine position varied. They reported the presence of cyclization/sequence scrambling reaction, and thus *nondirect* sequence ions at all the isomeric forms of  $b_4$ , and  $b_5$ , except isomers with histidine near the N-terminus.

#### 6.1.2. Experimental

The histidine work utilized the following model peptides: HAAAAAA-NH<sub>2</sub>, AAAHAAA-NH<sub>2</sub>, HYAGFLV-NH<sub>2</sub>, YAGHFLV-NH<sub>2</sub>, and YAGFLVH-NH<sub>2</sub>. The details of MS conditions and all other parameters are given in Chapter 3.

### 6.1.3. Results and Discussion

CID mass spectra obtained for the  $b_7$  ions derived from protonated HAAAAAA-NH<sub>2</sub>, AAAHAAA-NH<sub>2</sub>, and AAAAAAH-NH<sub>2</sub> by neutral loss of C-terminal amine group are given in Figure 6.1 (a). The most dominant product ions for all of the seven heptapeptides involve loss of H<sub>2</sub>O ( $b_7^{\circ}$ , 546  $m/z$ ), CO ( $a_7$ , 536  $m/z$ ) as a base peak, and alanine (493  $m/z$ ) corresponding to  $b_6$  ion for all isomers except AAAAAAH-NH<sub>2</sub>. What is most noticeable about those  $b_7$  spectra is essential similarity between fragmentation patterns such that all seven isomers produced eliminations of A (493  $m/z$ ), 2A (422  $m/z$ ), 3A (351  $m/z$ ), 4A (280  $m/z$ ), 5A (209  $m/z$ ), H (427  $m/z$ ), H + A (356  $m/z$ ), H + 2A (285  $m/z$ ) from  $b_7$ . Even though some of these peaks are identified as expected sequential losses from C-terminus such as -A, -2A, -3A, -4A, and -5A for HAAAAAA-NH<sub>2</sub> isomer corresponding to the  $b_6$ ,  $b_5$ ,  $b_4$ ,  $b_3$ , and  $b_2$ , respectively, same eliminations cannot be explained directly by regular pathways of  $b$  ion formation for

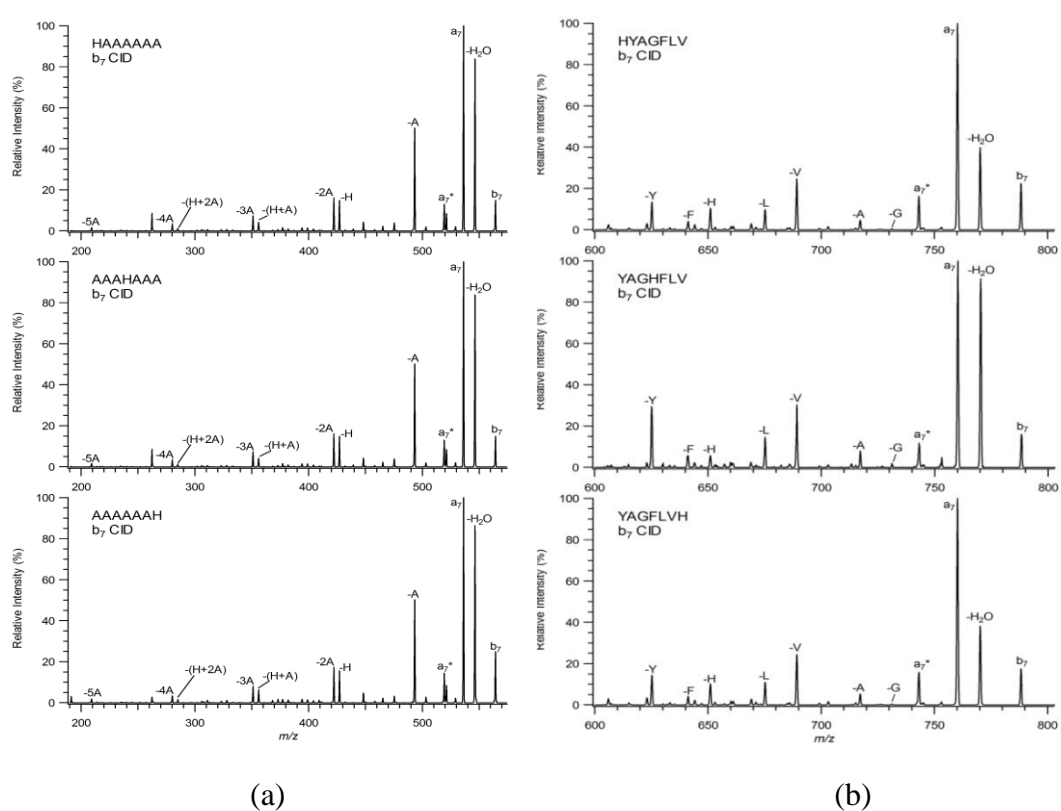
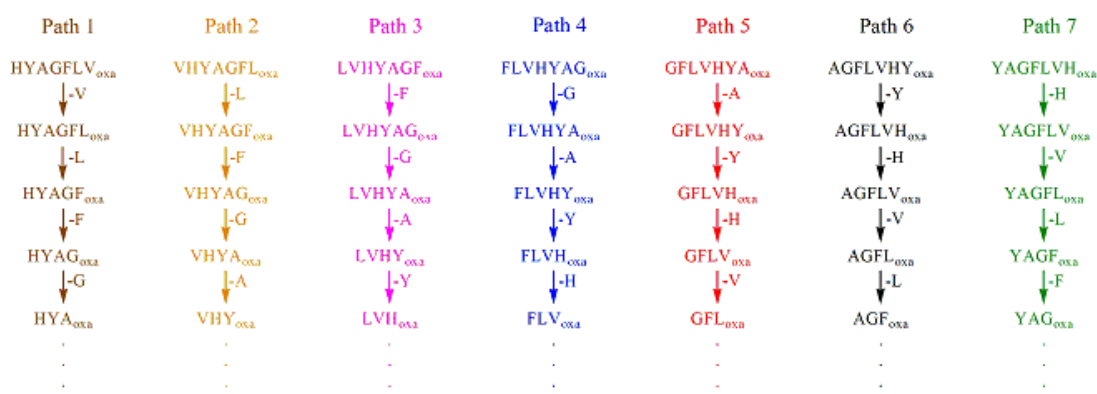
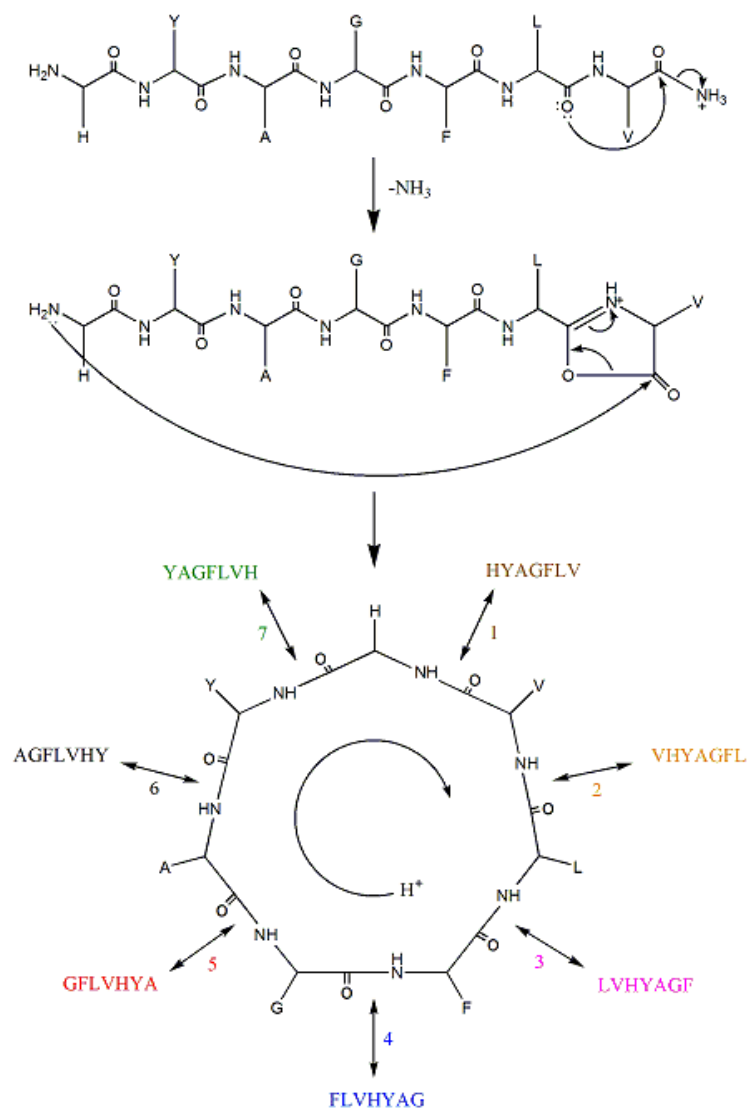


Figure 6.1. CID spectra of  $b_7$  of (a) HAAAAAA-NH<sub>2</sub> isomers, (b) HYAGFLV-NH<sub>2</sub> isomers

AAAAAAH-NH<sub>2</sub> isomer. In a similar manner, the neutral loss of H, and its further fragmentation products that are losses of H + A, and H + 2A from *b*<sub>7</sub> are direct sequence ions for AAAAAAH-NH<sub>2</sub> isomer whereas they are all assigned as abnormal fragmentation products for HAAAAAA-NH<sub>2</sub> isomer. As a matter of fact, these observed losses of amino acid residues from interior and almost the same fragment ion intensity distributions among the seven isomers point out an apparent macrocyclization reaction of initial *b*<sub>7</sub> oxazolone structure leading to scrambling of sequence (permuted sequence) prior to fragmentation. Accordingly, a number of nondirect sequence ions are generated from each isomer and their significant abundance is likely to trigger complications in the interpretation of CID mass spectra of *b*<sub>7</sub> ions. In addition, elimination peaks of H, H + A, and H + 2A indicate that fragmentation path is directly affected by the basic histidine residue.

Sustaining study involves the similar product ion mass spectra of *b*<sub>7</sub> ions generated from HYAGFLV-NH<sub>2</sub>, YAGHFLV-NH<sub>2</sub>, and YAGFLVH-NH<sub>2</sub> isomers. Focusing on mass range above 600 *m/z* for all the isomers in Figure 6.1 (b), it is observed that each of the seven different amino acid residues were singly eliminated from *b*<sub>7</sub> ion as -G (731 *m/z*), -A (717 *m/z*), -V (689 *m/z*), -L (675 *m/z*), -H (651 *m/z*), -F (641 *m/z*), and -Y (625 *m/z*) which are as abundant as direct sequence ions. Similar to the case of mono-histidine hexa-alanine isomers, it seems impossible to interpret these single eliminations in the absence of macrocyclization reaction of initially-oxazolone *b*<sub>7</sub> ions. This cyclic form then reopens at various sites to produce permuted sequences of seven different oxazolone structures which in turn generate those neutral losses of single amino acid residues upon CID (Scheme 6.1). Although all isomers yielded in the same fragmentation products, YAGHFLV-NH<sub>2</sub> differs from the other two models in terms of increased abundances of -Y, -A, -G and -H<sub>2</sub>O (*b*<sub>7</sub><sup>o</sup>, 770 *m/z*) eliminations in addition to lowered abundance of -H elimination peaks. This is mainly due to the change of amino acid sequence when histidine is located between glycine and phenylalanine. When C-terminally-located to Y-A-G fragment, histidine appears to favor the elimination of these residues. For the cases of HYAGFLV-NH<sub>2</sub> and YAGFLVH-NH<sub>2</sub> histidine stays between tyrosine and valine residues in the macrocyclic *b*<sub>7</sub> structure; thus, CID spectra and distribution of product ion intensities are nearly identical. This finding is an additional indication of macrocyclization reaction of *b*<sub>7</sub> ion prior to fragmentation.



Scheme 6.1. Mechanism of macrocyclization and formation of nondirect sequence ions for HYAGFLV-NH<sub>2</sub>

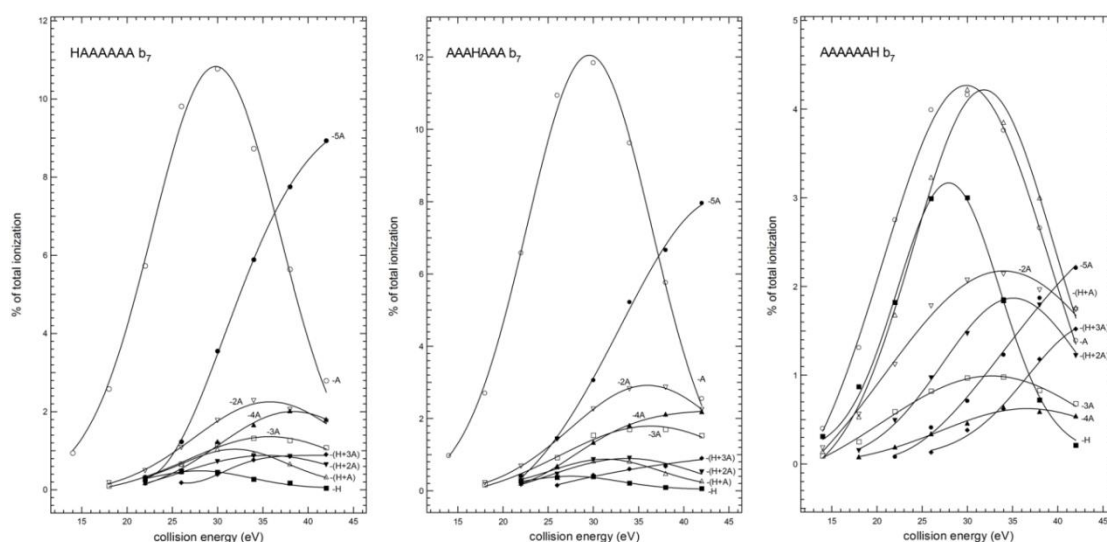


Figure 6.2. Breakdown graphs of  $b_7$  of HAAAAAA-NH<sub>2</sub> isomers

Figure 6.2 shows the breakdown graph for  $b_7$  ion of HAAAAAA-NH<sub>2</sub>, AAHAAA-NH<sub>2</sub>, and AAAAAAH-NH<sub>2</sub>, which were plotted by considering the direct sequence and nondirect sequence ions only. As can be seen from the relevant plots, the first two isomers give virtually identical fragmentation patterns while the third isomer AAAAAAH-NH<sub>2</sub> behaves differently. Some of the direct sequence ions for any of these isomers can constitute nondirect sequence ions for other isomer at the same time. Apparently, elimination of single alanine residue (-A) from  $b_7$  ion of HAAAAAA-NH<sub>2</sub> and AAHAAA-NH<sub>2</sub> is the major fragmentation route at low energy CID conditions. Increase in collision energy (> 37 eV) primarily favors the loss of penta-alanine (-5A) from  $b_7$  ion of both models to a greater extent while there are relatively minor eliminations of 2A, 3A, 4A, H, (H + A), (H + 2A), and (H + 3A) from  $b_7$  ions. However, when histidine is located at the C-terminus, there are some differences in profiles of product ion intensities. The  $b_7$  ion originated from AAAAAAH-NH<sub>2</sub> isomer showed dominant losses of A, H, and H + A at lower collision energies while similar patterns of product ions with HAAAAAA-NH<sub>2</sub> and AAHAAA-NH<sub>2</sub> were observed for the remaining eliminations. Especially, C-terminal histidine residue leads to an increase in fragmentation profiles of histidine-linked eliminations from  $b_7$ , which are -H, -(H + A), -(H + 2A), -(H + 3A). Based on these observations, it is clear to conclude

that direct sequence pathway is highly favored when histidine is located at the C-terminal end of the peptide.

Figure 6.3 gives the breakdown graph of single amino acid residue eliminations from  $b_7$  ion of HYAGFLV-NH<sub>2</sub>, YAGHFLV-NH<sub>2</sub>, and YAGFLVH-NH<sub>2</sub> isomers. Independent of the histidine position, all isomers have followed very similar fragmentation behavior in terms of single residue eliminations. This collision energy dependence study has revealed that every single residue except glycine (due to its relatively simple side chain) is lost from the macrocyclic  $b_7$  ion separately following to the selective ring opening. Looking at the distributions of product ion intensities of three isomers which are in accord with each other, these nondirect sequence ions have showed preferential elimination order of V > Y > L > F > A~H from macrocyclic  $b_7$  ion at higher collision energies.

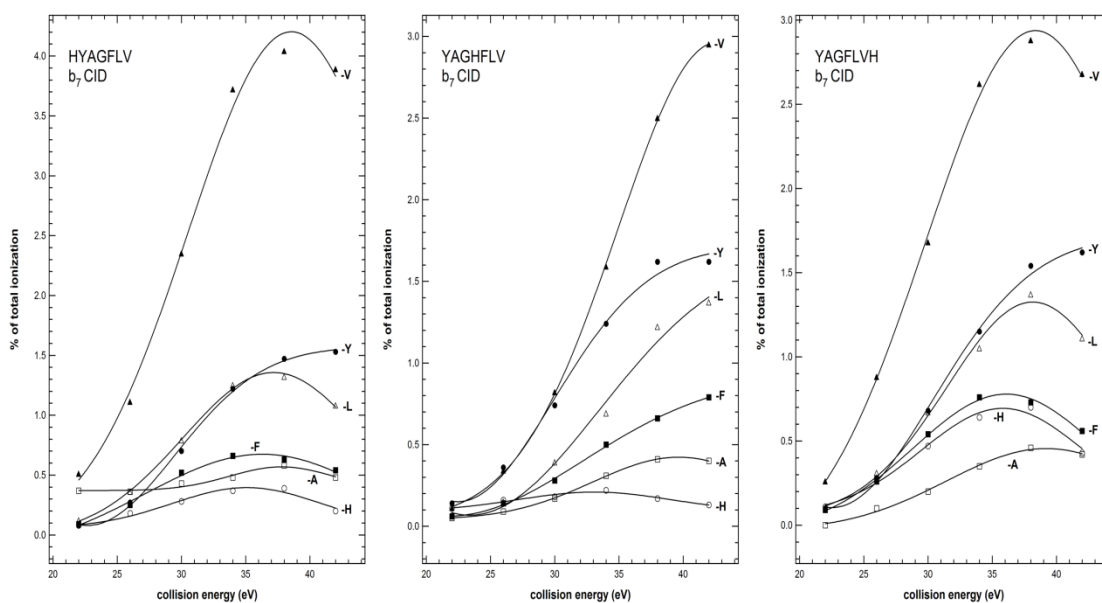


Figure 6.3. Breakdown graphs of  $b_7$  of HYAGFLV-NH<sub>2</sub> isomers

## 6.2. Fragmentation Behavior of Lysine Residue

### 6.2.1. Introduction

Principal approach in mass spectrometry-based proteomics is enzymatic cleavage (tryptic usually) of peptide bonds exclusively C-terminal to lysine or arginine in order to convert protein mixtures into more preferably analyzable peptide populations. In this way, highly basic lysine or arginine stays at the C-terminus of the peptides which in turn produces highly informative b/y ion series for ease of interpretation of tandem mass spectra. However, tryptic digestion can sometimes cause cleavages at other residues than lysine or arginine producing non-tryptic or half-tryptic peptides. Thus, decrease in reliability of database search algorithms in finding the sequence of protein of interest is highly possible. At this point, chemistry lying behind the fragmentation course of peptides containing basic amino acid residues has to be investigated to help algorithms improving.

### 6.2.2. Experimental

The study used the following peptide models: KAAAAAA-NH<sub>2</sub>, AKAAAAA-NH<sub>2</sub>, AAKAAAA-NH<sub>2</sub>, AAAKAAA-NH<sub>2</sub>, AAAAKAA-NH<sub>2</sub>, AAAAAKA-NH<sub>2</sub>, AAAAAAK-NH<sub>2</sub>, KYAGFLV-NH<sub>2</sub>, YAGKFLV-NH<sub>2</sub>, YAGFLVK-NH<sub>2</sub>, YAGFLVK(Ac)-NH<sub>2</sub>, YAGFLVKK-NH<sub>2</sub>, YAGFLVKKK-NH<sub>2</sub>, YAGFLVKKKK-NH<sub>2</sub>, YAGFLVKKKKK-NH<sub>2</sub>, YAGFLVKKKKKK-NH<sub>2</sub>, and YAGFLVKKKKKKK-NH<sub>2</sub>. The details of MS conditions and all other parameters are given in Chapter 3.

### 6.2.3. Results and Discussion

We first focused on the lysine residue and designed peptide models with a single lysine and six alanine residues where the position of lysine is varying systematically. Figure 6.4 represents the CID spectra of *b*<sub>7</sub> ions produced from isomeric forms of KAAAAAA-NH<sub>2</sub>. For the first six isomers, the fragmentation patterns look similar including the major eliminations of H<sub>2</sub>O (*b*<sub>7</sub><sup>o</sup>, 537 *m/z*), CO (*a*<sub>7</sub>, 527 *m/z*), A (484 *m/z*), K (427 *m/z*), 2A (413 *m/z*), K+A (356 *m/z*), 3A (342 *m/z*), K+2A (285 *m/z*), 4A



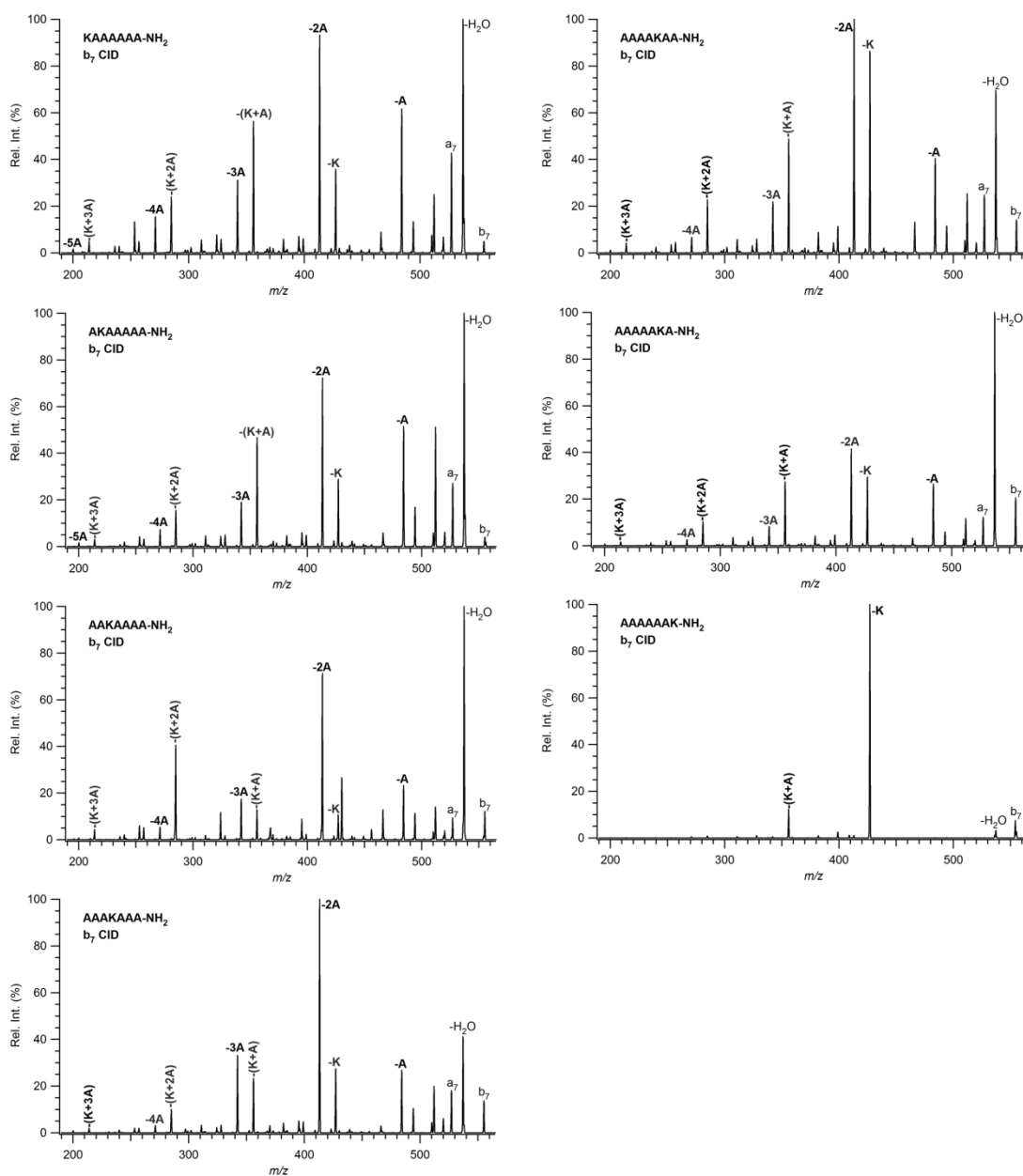


Figure 6.4. CID spectra of  $b_7$  ions derived from isomers of KAAAAAA-NH<sub>2</sub>

(271  $m/z$ ), K+3A (214  $m/z$ ). Similarity of fragmentation products and presence of internal losses indicate the macrocyclization reaction prior to scrambling of sequence while intensity fluctuations in the spectra show that original sequence and thus original position of lysine affect in some way the course of fragmentation. The most interesting thing is, however, completely different fragmentation behavior of  $b_7$  produced from AAAAAK-NH<sub>2</sub>. Compared to the first six isomers, very simple spectra was obtained

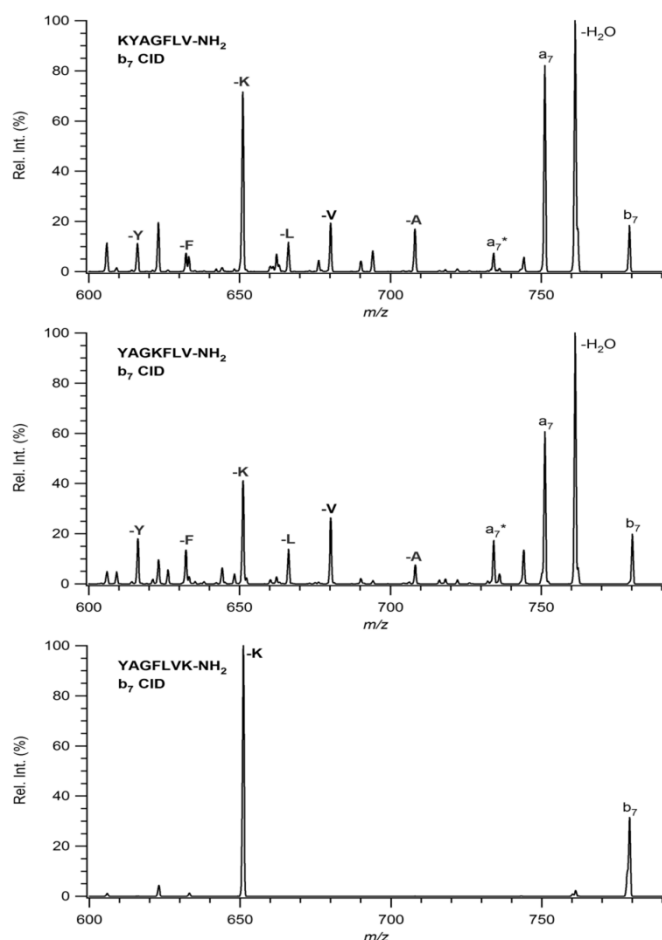


Figure 6.5. CID spectra of  $b_7$  ions derived from isomers of KYAGFLV-NH<sub>2</sub>

with a dominant elimination of lysine (K) as a base peak and following the loss of (K+A), which correspond to  $b_6$  and  $b_5$  ions, respectively. To check whether this unexpected behavior is valid independent of amino acid composition, we performed CID studies of  $b_7$  of KYAGFLV-NH<sub>2</sub>, YAGKFLV-NH<sub>2</sub>, and YAGFLVK-NH<sub>2</sub>. As apparent in Figure 6.5., we only focused on high mass range and obtained internal losses of A (708  $m/z$ ), L (666  $m/z$ ), K (651  $m/z$ ), F (632  $m/z$ ), and Y (616  $m/z$ ) in addition to direct sequence ions as elimination of V ( $b_6$ , 680  $m/z$ ), H<sub>2</sub>O ( $b_7^0$ , 761  $m/z$ ), CO ( $a_7$ , 751  $m/z$ ), and CO+NH<sub>3</sub> ( $a_7^*$ , 734  $m/z$ ) for the first two isomers. On the other hand, YAGFLVK-NH<sub>2</sub> shows very different fragmentation characteristics where only major elimination is lysine corresponding to  $b_6$  in high mass range similar to the AAAAAAK-NH<sub>2</sub> case. So it seems that lysine, when positioned at the C-terminus, inhibits the macrocyclization reaction and thus sequence-scrambling. At first glance,

high basicity of lysine side chain seemed to cause different fragmentation mechanism and be responsible for this strange behaviour. In 1996, Yalcin et al. (80) clearly proved that amino group of lysine side chain interacts with lysine carbonyl group to produce “ $\alpha$ -amino- $\epsilon$ -caprolactam” in protonated lysine derivatives. This finding forced us to think that formation of lactam might affect the course of fragmentation when lysine is at C-terminus. To verify our idea, we first intended to block the amino group of lysine side chain through acetylation to prevent the formation of  $\alpha$ -amino- $\epsilon$ -caprolactam. In Figure 6.6, we compared CID spectra of  $b_7$  ions produced from YAGFLVK-NH<sub>2</sub> and YAGFLVK(Ac)-NH<sub>2</sub>. Obviously, acetylation of lysine amino group de-functionalized lysine side chain, and single internal residue losses from  $b_7$  were observed, indicating that macrocyclic structure was formed.

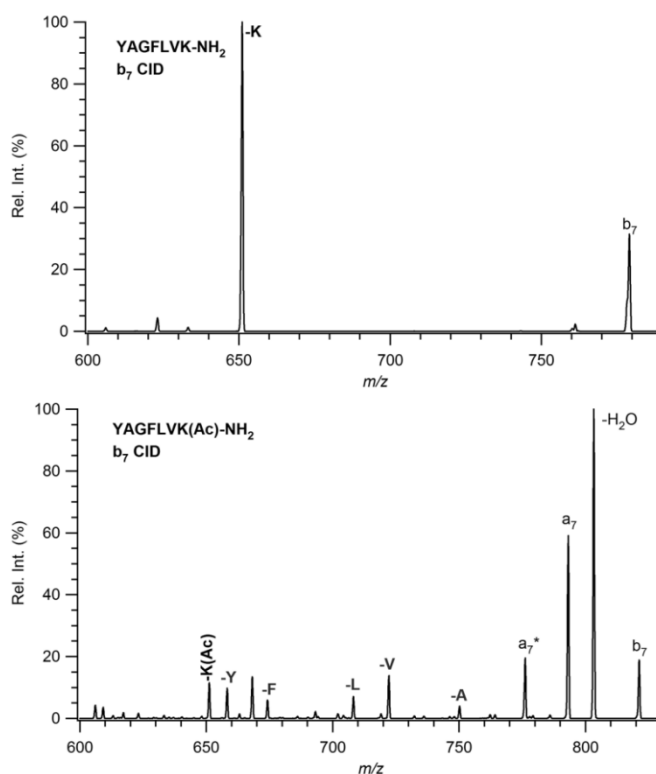


Figure 6.6. Comparison of CID spectra of  $b_7$  ions derived from YAGFLVK-NH<sub>2</sub> and YAGFLVK(Ac)-NH<sub>2</sub>

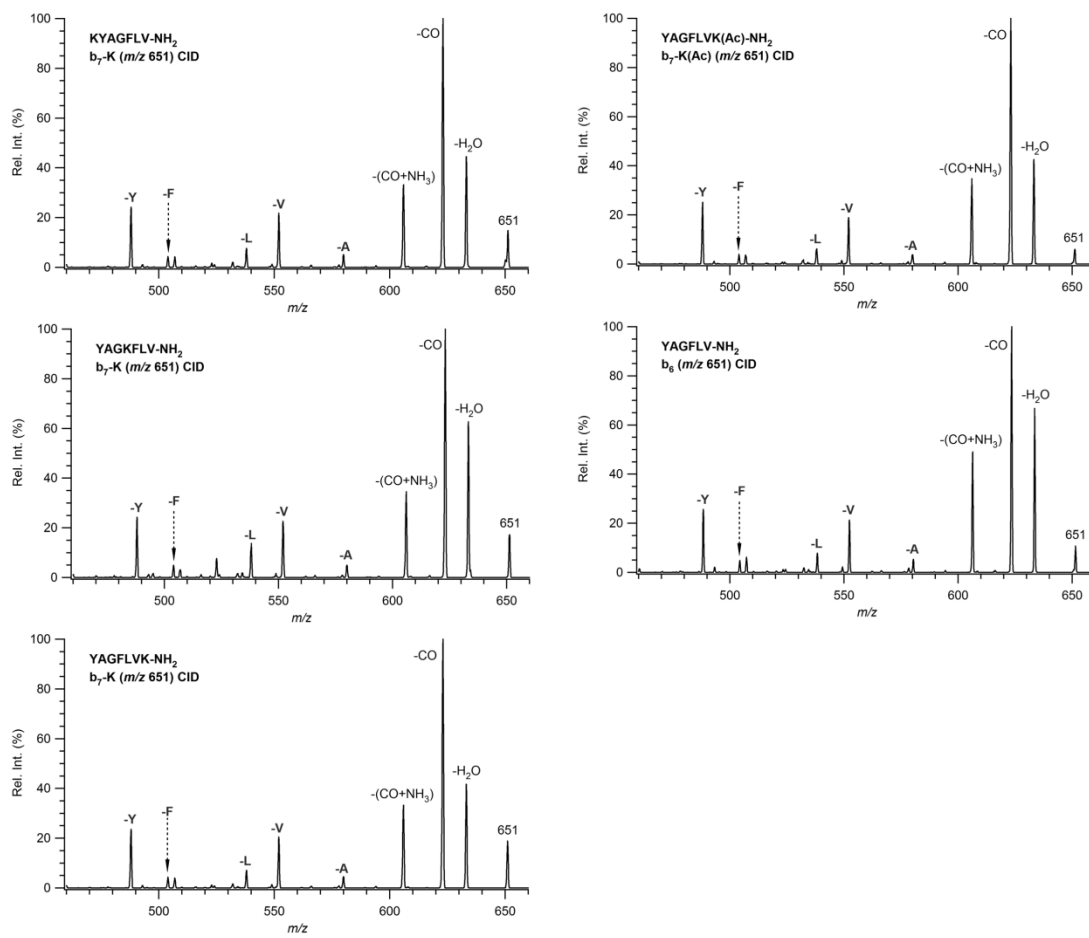
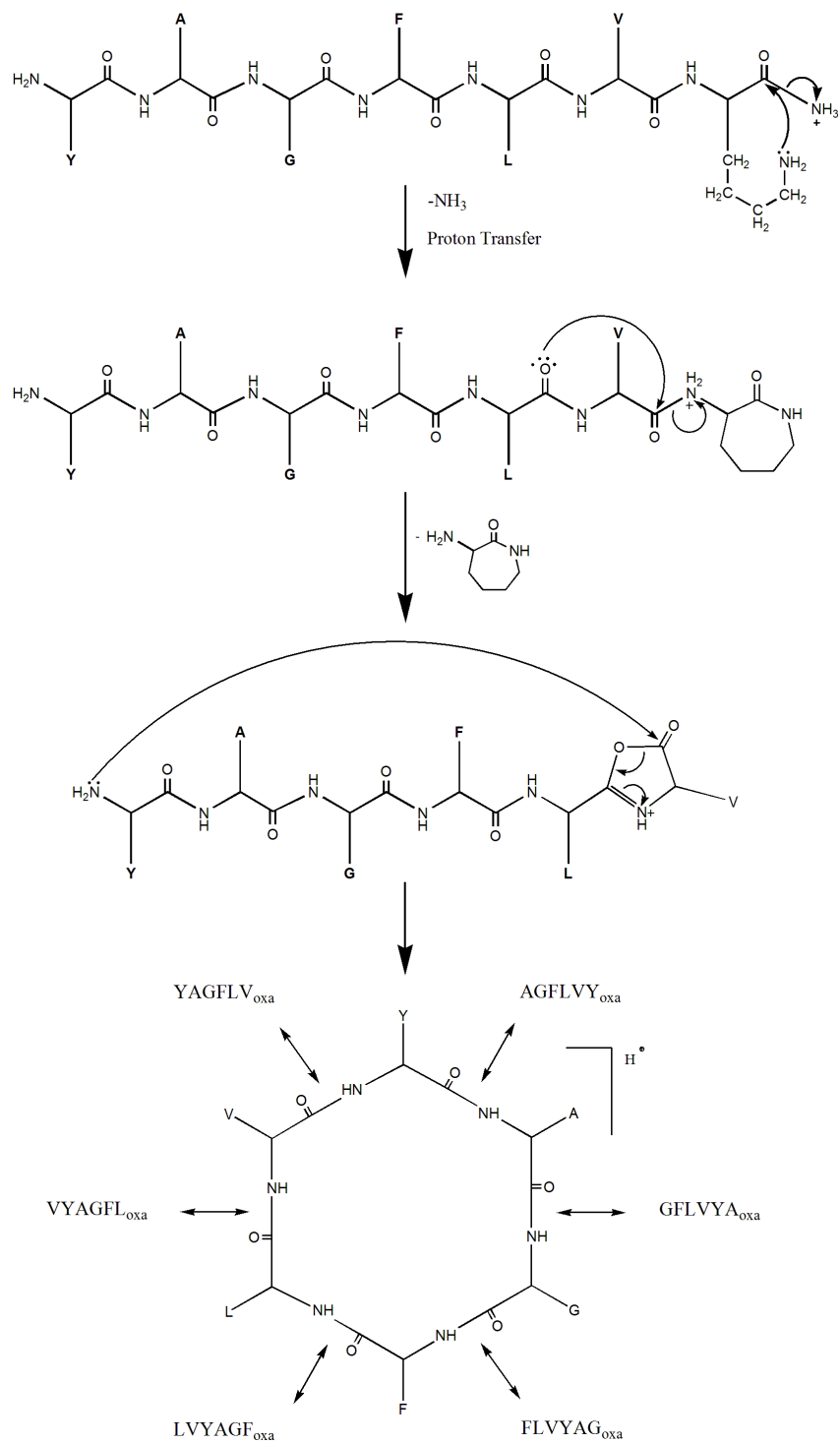


Figure 6.7. CID spectra of 651 *m/z* from different peptide series



Scheme 6.2. Proposed mechanism for CID of  $b_7$  produced from YAGFLVK-NH<sub>2</sub>

To further support this mechanism, we carried out CID experiments of 651  $m/z$  ion that corresponds to the sequence YAGFLV following the loss of K from KYAGFLV-NH<sub>2</sub>, YAGKFLV-NH<sub>2</sub>, YAGFLVK-NH<sub>2</sub>, loss of K(Ac) from YAGFLVK(Ac)-NH<sub>2</sub>. As can be seen in Figure 6.7, they all yielded exactly the same fragmentation pattern with and  $b_6$  of YAGFLV-NH<sub>2</sub> stating that peptide part remaining, YAGFLV, goes into macrocyclization following to the elimination of lysine or acetylated-lysine.

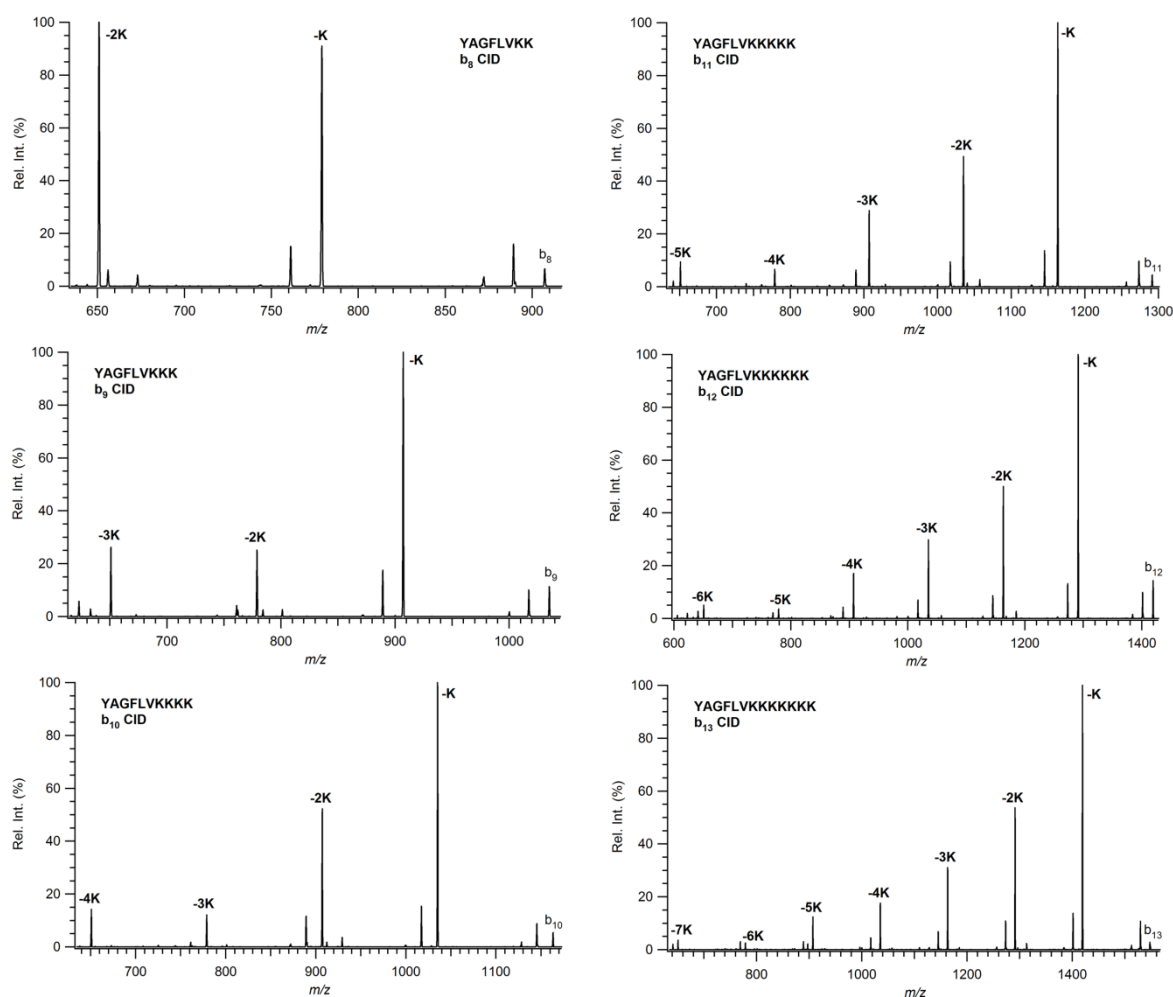


Figure 6.8. CID spectra of largest  $b$  ions of YAGFLVK<sub>n</sub> series ( $n = 2$  to 7)

In the consequence of our findings so far, we suggest that  $\alpha$ -amino- $\epsilon$ -caprolactam formation at the side chain of lysine prevents macrocyclization reaction of  $b_7$  when K is positioned at the C-terminus as in the cases of AAAAAAK-NH<sub>2</sub> and YAGFLVK-NH<sub>2</sub>. Because carbonyl group of lysine is blocked, oxazolone ring cannot be formed so that there is no oxazolone carbonyl to which N-terminal amine group can attack nucleophilically to produce seven membered-macrocyclic structure. By contrast, elimination of lysine as  $\alpha$ -amino- $\epsilon$ -caprolactam generates YAGFLV<sub>oxa</sub>, which can then undergo macrocyclization to produce sequence-scrambled  $b$  ions. This proposed mechanism is summarized in Scheme 6.2. CID studies of largest  $b$  ions derived from YAGFLVK<sub>n</sub> ( $n = 1$  to  $7$ ) also give additional mechanistic information. As shown in Figure 6.8, each model peptide produces sequential losses of lysine residues from C-terminus according to the number of lysine that the related peptide contains. Therefore, we can conclude that lysine residue is eliminated in the form of  $\alpha$ -amino- $\epsilon$ -caprolactam while remaining peptide becomes ready to form  $\alpha$ -amino- $\epsilon$ -caprolactam again to be lost, and so on. This elimination trend is continued until no lysine remains in the C-terminal side of the peptide.

## 6.3. Fragmentation Behavior of Arginine Residue

### 6.3.1. Introduction

Among twenty common amino acid residues, arginine possesses the highest proton affinity so that it has significant influence on peptide fragmentation with its high potential to retain mobile proton. Molesworth group (81) reported a recent study about fragmentation of  $b_5$  ions produced from hexapeptides with a single arginine residue and concluded that presence of arginine in peptides inhibits the formation of macrocyclic  $b_5$  ion. However, they did not consider the possible effects of neighbor residues and peptide length which are under study in detail by our group.

### 6.3.2. Experimental

The study used the following peptide models: RAAAAAA-NH<sub>2</sub>, ARAAAAA-NH<sub>2</sub>, AARAAAA-NH<sub>2</sub>, AAARAAA-NH<sub>2</sub>, AAAARAA-NH<sub>2</sub>, AAAAAARA-NH<sub>2</sub>,

AAAAAAR-NH<sub>2</sub>, RYAGFLV-NH<sub>2</sub>, YRAGFLV-NH<sub>2</sub>, YARGFLV-NH<sub>2</sub>, YAGRFLV-NH<sub>2</sub>, YAGFRLV-NH<sub>2</sub>, YAGFLRV-NH<sub>2</sub>, YAGFLVR-NH<sub>2</sub>, YAGFLVRR-NH<sub>2</sub>, YAGFLVRRR-NH<sub>2</sub>, YAGFLVRRRR-NH<sub>2</sub>, YAGFLVRRRRR-NH<sub>2</sub>, and YAGFLVRRRRRRR-NH<sub>2</sub>. The details of MS conditions and all other parameters are given in Chapter 3.

### 6.3.3. Results and Discussion

The first model peptide series we designed are mono arginine-hexaalanine isomers with varying position of arginine. As can be seen in Figure 6.9, CID spectra of *b*<sub>7</sub> generated from seven isomers are different both in pattern and ions. When R is at the N-terminus, direct sequence ions exist and peaks of ammonia elimination from *b* ions dominate the spectrum, however; internal losses such as eliminations of A (512 *m/z*), 2A (441 *m/z*), 3A (370 *m/z*), 4A (299 *m/z*), and 5A (228 *m/z*) are noticed when arginine is getting closer to the C-terminus.

Similar behavior was observed when the model peptide series were RYAGFLV-NH<sub>2</sub> and its isomers (Figure 6.10). CID spectra of *b*<sub>7</sub> ions are again completely different, and nondirect sequence ions are obtained when arginine is near to C-terminus. Contrary to Molesworth report suggesting that arginine inhibits the formation of *b*<sub>5</sub> macrocycle, our findings indicate that macrocyclization reaction occurs for *b*<sub>7</sub> ions when arginine is close to the C-terminal end of the peptide interested. The mechanism lying behind this interesting behavior is not exactly known for now, and it needs to be investigated in detail using a different set of model peptides.



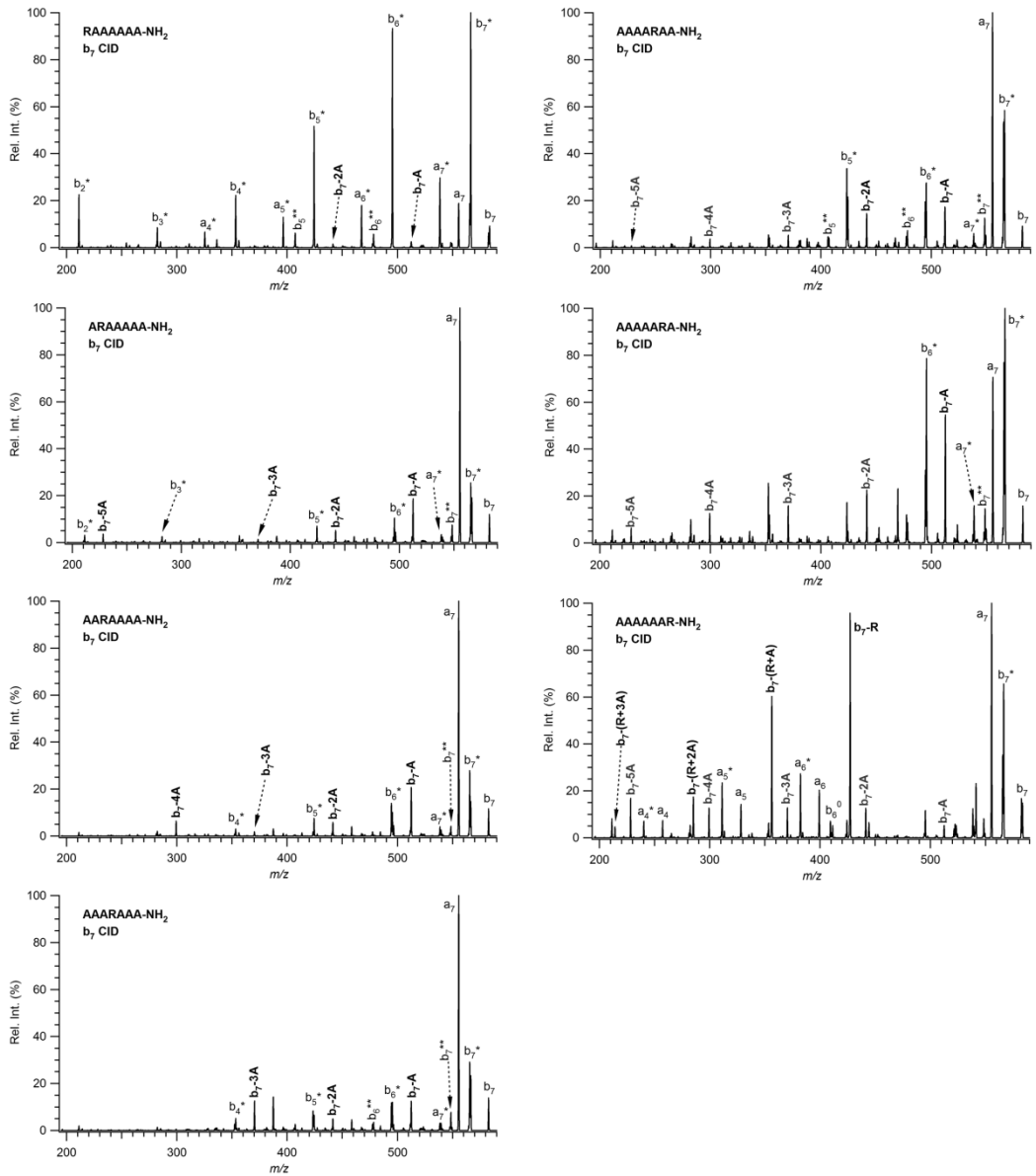


Figure 6.9. CID spectra of  $b_7$  ions derived from isomers of RAAAAAA-NH<sub>2</sub>

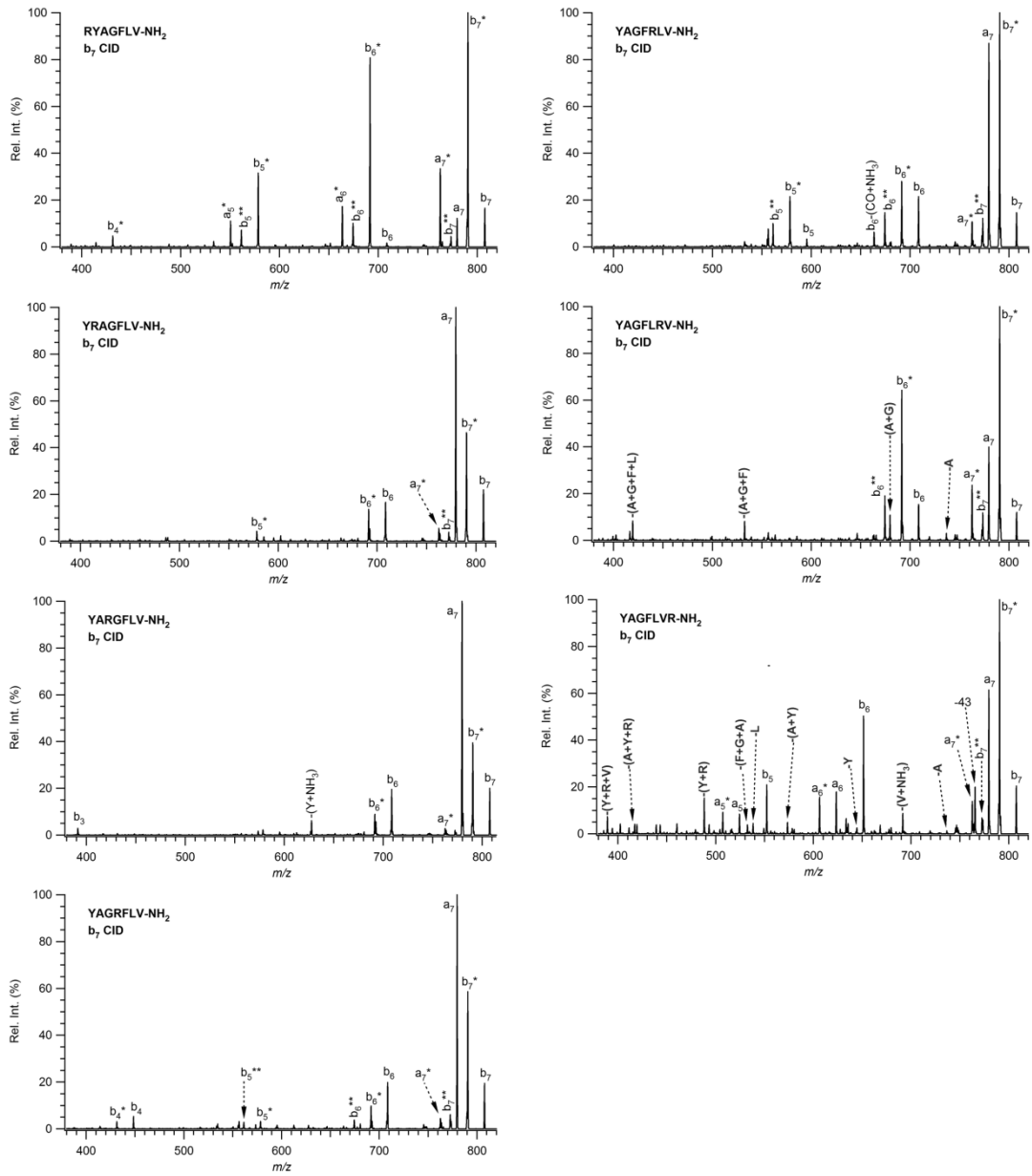


Figure 6.10. CID spectra of  $b_7$  ions derived from isomers of RYAGFLV-NH<sub>2</sub>

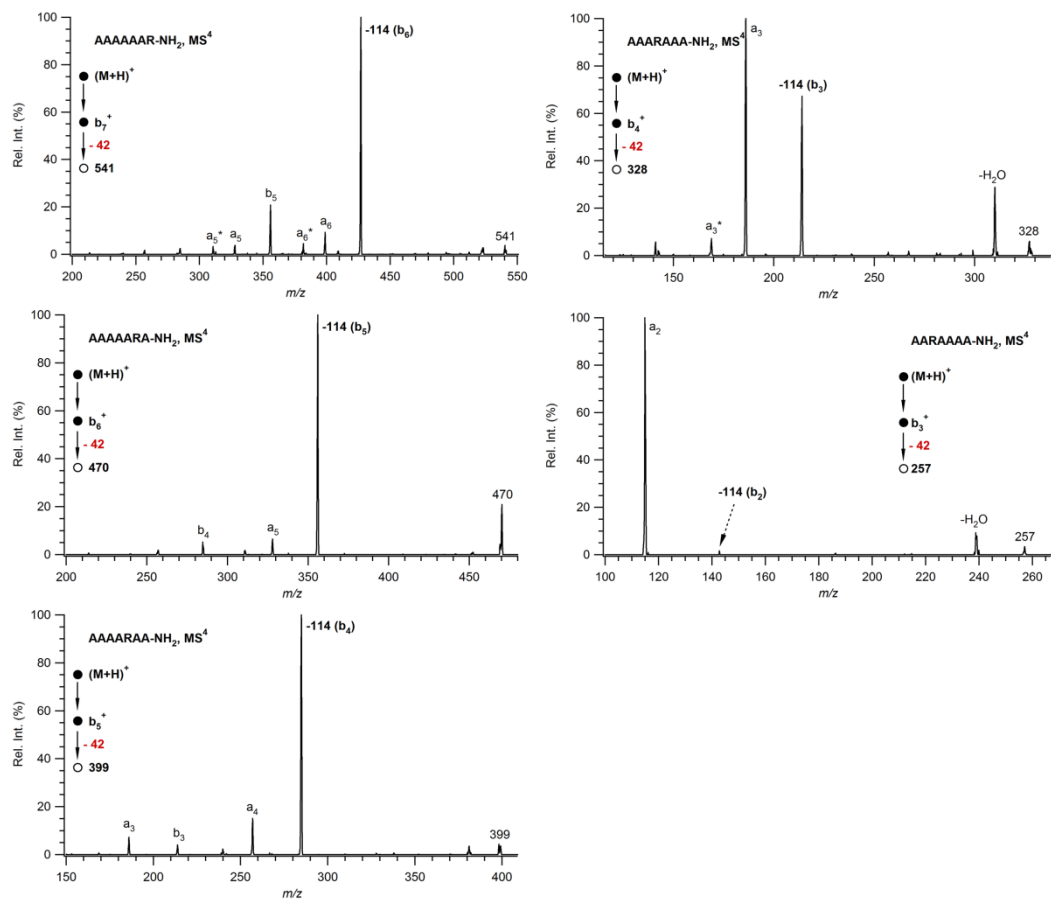


Figure 6.11. CID spectra of  $b_n - 42$  ion from isomers of AAAAAAR-NH<sub>2</sub>

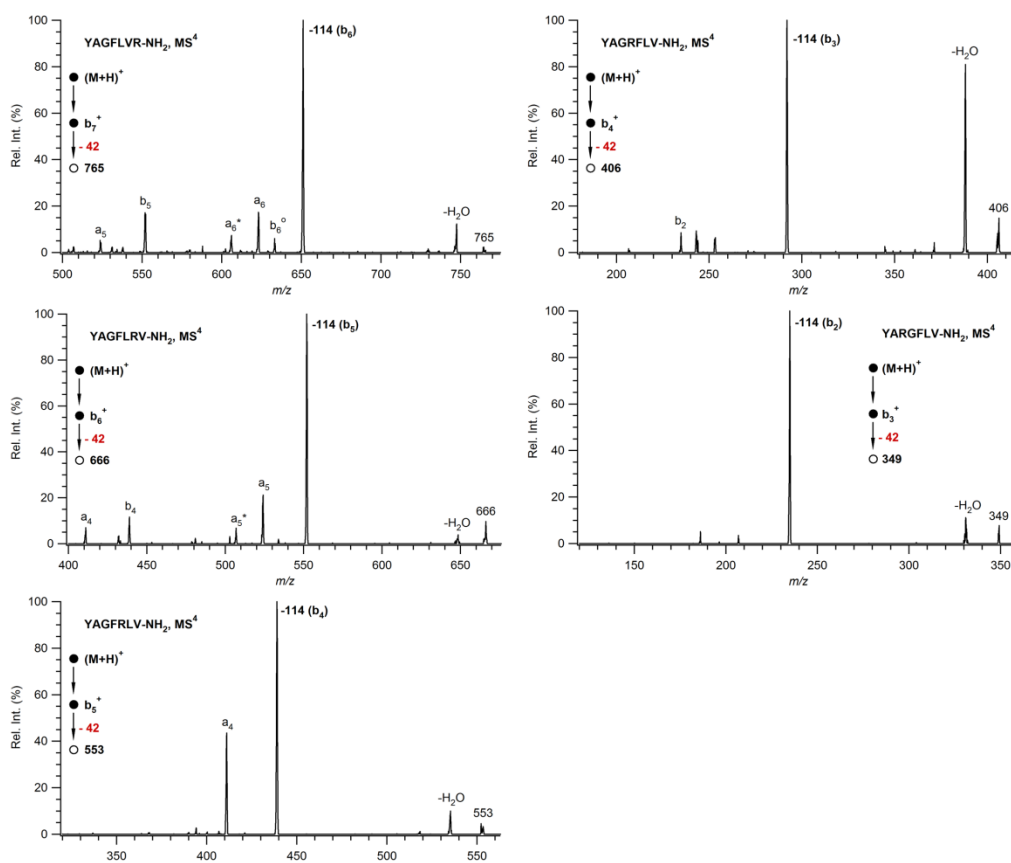


Figure 6.12. CID spectra of  $b_n - 42$  ion from isomers of YAGFLVR-NH<sub>2</sub>

Another interesting observation is the elimination of 42 u from  $b$  ions when the arginine is at C-terminus. This loss does not correspond to a common fragmentation route that is why we carried out CID studies of  $(b_n - 42)$  peaks generated from mono arginine - polyalanine isomers where arginine stays at the C-terminal end of the peptide (Figure 6.11). Surprisingly, we obtained a loss of 114 u from all  $(b_n - 42)$  corresponding to the mass of a lower  $b$  ion ( $b_{n-1}$ ). To verify whether this behavior is sequence-specific or not, similarly we performed CID analysis of  $(b_n - 42)$  peaks produced from isomers of YAGFLVR-NH<sub>2</sub>. As seen in Figure 6.12, loss of 114 u is the most dominant ion for all series similar to AAAAAAR-NH<sub>2</sub> case. At this point, we focused on the side chain of arginine residue. As can be seen from the relevant structures (Figure 6.13), lysine and arginine have similar side chain groups in chemical terms which makes us consider arginine might behave like lysine when located at C-terminus, forming a caprolactam-like structure which is called ‘ornithine’. In the view of these ideas, we propose a

mechanism to explain the loss of 42 u which is followed by an elimination of ornithine with 114 u, respectively in Scheme 6.3. As a result of charge delocalization in guanidinium group of arginine, cyanamide with 42 u is lost neutrally and a transition structure is formed where the remaining part of the arginine side chain behaves like lysine.  $\text{NH}_2$  group at the side chain attacks carbonyl group of arginine nucleophilically and forms a six-membered cyclic structure, which is then lost neutrally as ornithine. Finally, oxazolone *b* structure is produced and converted to macrocycle as described in previous sections. Increasing the number of arginine residues in the C-terminus did not inhibit the elimination of cyanamide (- 42) as can be seen in Figure 6.14.

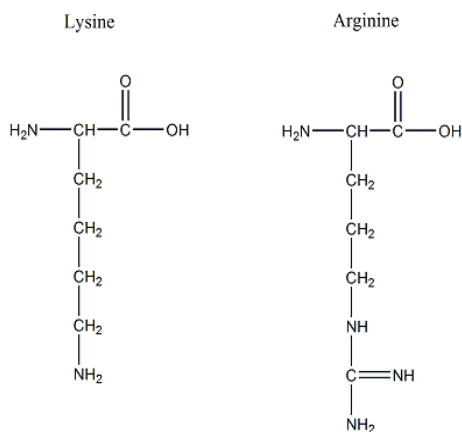
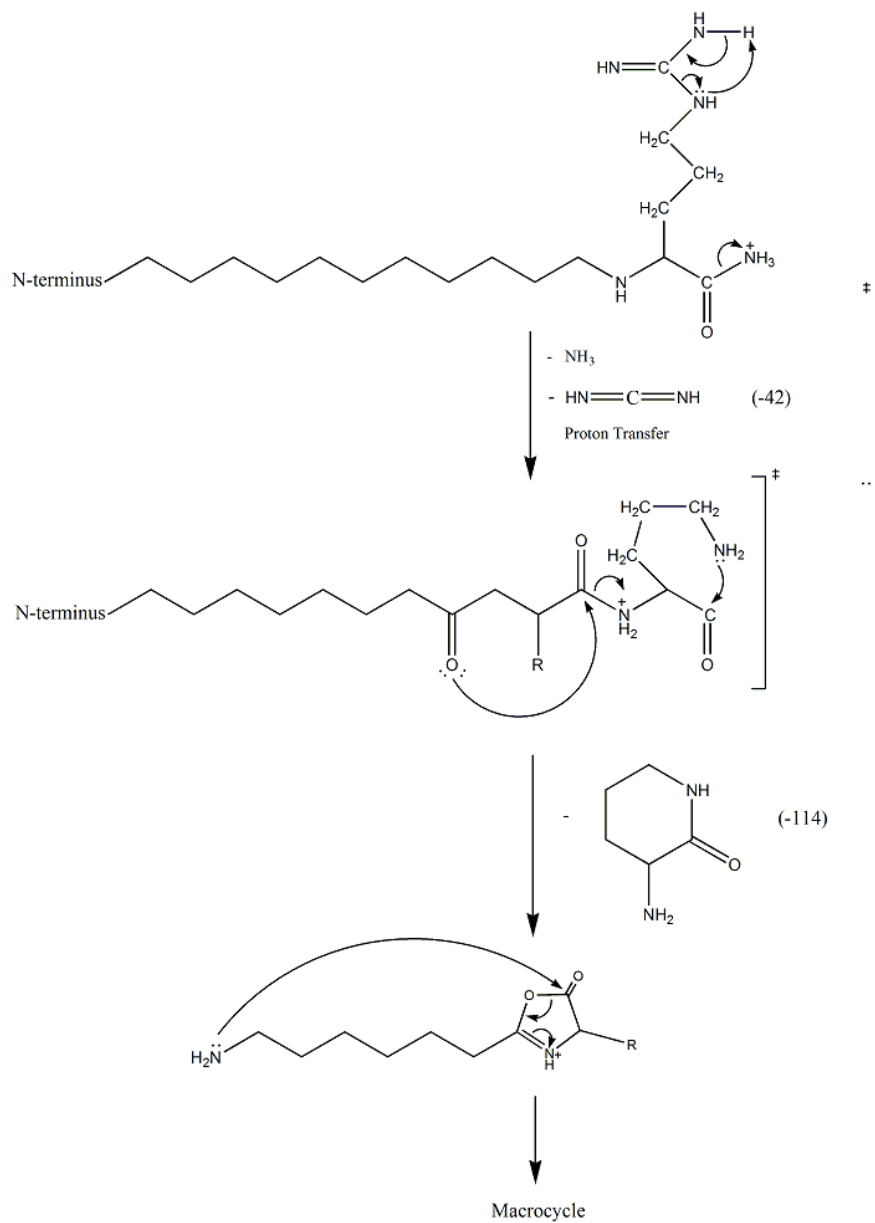


Figure 6.13. Structures of Lysine and Arginine



Scheme 6.3. Proposed mechanism for loss of 42 from *b* ions with C-terminal arginine

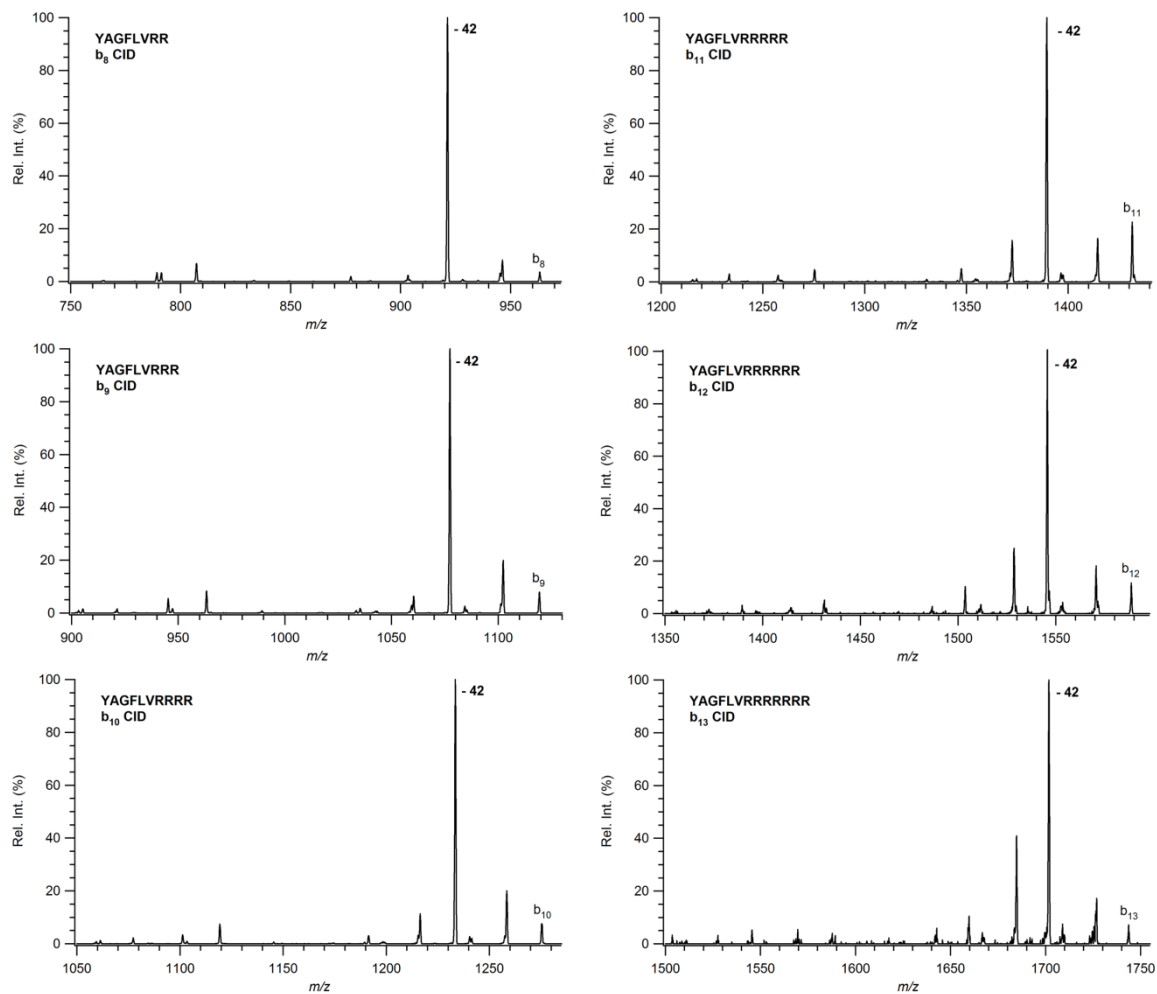


Figure 6.14. CID spectra of largest *b* ions of YAGFLVR<sub>n</sub> series (n = 2 to 7)

## CHAPTER 7

### CONCLUSION

In this thesis study, we mainly examined CID and collision energy dependency of a variety of different model peptides to gain further insight into the fragmentation characteristics of peptides with specific residues.

The systematic study of isomeric peptides of YAGFLV series clearly indicates that  $b_6$  and  $b_7$  ions have higher tendency of macrocyclization compared to  $b_5$  ions with the exception of QYAGFLV-NH<sub>2</sub> showing higher tendency of macrocyclization of  $b_5$  ion compared to that of  $b_7$  ion where  $b_5\text{-Q} > b_7\text{-Q}$ . It was showed that neighbor amino acid has influenced the selective opening of macrocyclic  $b_6$  ion. The selective ring opening also depends on the size of  $b$  ions and the position of the amino acid residue. Next, it is found that no preferential cleavage order can be specified depending on nature of amino acid side chain. Finally, Q, W, K, and M are found to be more favored eliminations from macrocyclic  $b_6$  ion.

In the next section, we mainly examined CID of a series of different model peptides to expand our understanding of the fragmentation characteristics of proline-containing peptides. All isomers of C-terminally-amidated PAAAAAA, PYAGFLV, and AAPXAAA undergo head-to-tail macrocyclization/re-opening reaction prior to fragmentation. Moreover, it was evident that the position of proline is not important as long as other residues are all alanine since the CID of  $b_7$  produced from PAAAAAA isomers gave nearly the same product ion distribution. The surprising observation from the data was a unique fragmentation reaction pathway which was observed as dipeptide elimination from N-terminal position of all proline-containing peptides. Highly-abundant P+X eliminations from  $b_7$  of AAPXAAA series were obtained whereas this peak was not seen for AAXPAAA models. Accordingly, we provide very strong evidence that proline containing peptides have high tendency to place the proline residue in the N-terminal position during the ring opening of macrocyclic structure which is then followed by dipeptide elimination of proline plus its adjacent C-terminal



residue. The obtained results are of particular importance in order to highlight the typical behavior of proline so that bioinformatics tools can be improved for more accurate protein identification.

Histidine study showed that scrambling of sequence occurs in all histidine-containing peptides regardless of the position and neighbor residue. We found that direct sequence pathway is highly favored when histidine is located at the C-terminal end of the peptide. Furthermore, residues of interest have showed preferential elimination order of  $V > Y > L > F > A \sim H$  from macrocyclic  $b_7$  ion at higher collision energies

Regarding to the influence of lysine on peptide fragmentation, it was demonstrated that  $\alpha$ -amino- $\epsilon$ -caprolactam formation at the side chain of lysine prevents macrocyclization reaction of  $b_7$  when K is positioned at the C-terminus of the peptide while macrocyclization prior to sequence-scrambling takes place for the other positions of lysine in the peptide backbone. Because carbonyl group of lysine is blocked, oxazolone ring cannot be formed so that there is no oxazolone carbonyl to which N-terminal amine group can attack nucleophilically to produce seven membered-macrocyclic structure. By contrast, elimination of lysine as  $\alpha$ -amino- $\epsilon$ -caprolactam generates  $YAGFLV_{\text{oxa}}$ , which can then undergo macrocyclization to produce sequence-scrambled  $b$  ions.

Last, we focused on the behavior of arginine on peptide fragmentation and concluded that macrocyclization reaction takes place for  $b_7$  ions when arginine gets closer to the C-terminal end of the peptide. Interestingly, ornithine effect was observed for the side-chain of arginine residue when located at the C-terminus. Neutral loss of cyanamide (- 42 u) initializes the formation of ornithine which is then lost as 114 u, respectively. Increasing the number of arginine residues in the C-terminus did not inhibit the elimination of cyanamide.

In general, the obtained results are of particular importance in order to highlight the effects of specific residues as much as the position and neighbor residue effects in gas-phase peptide fragmentation. Incorporation of this information into bioinformatics tools will certainly improve their capability of more accurate protein identification.

## LITERATURE CITED

1. Thomson JJ. 1897. Cathode Rays. *Philosophical Magazine* 44:293-316
2. Dole MM, L. L.; Hines, R. L. 1968. Molecular beams of macroions. *Journal of Chemical Physics* 49:2240-2249
3. Yamashita M, Fenn JB. 1984. Electrospray Ion-Source - Another Variation on the Free-Jet Theme. *Journal of Physical Chemistry* 88:4451-4459
4. Banerjee S, Mazumdar S. 2012. Electrospray ionization mass spectrometry: a technique to access the information beyond the molecular weight of the analyte. *International Journal of Analytical Chemistry* 2012:282574
5. Karas M, Hillenkamp F. 1988. Laser Desorption Ionization of Proteins with Molecular Masses Exceeding 10000 Daltons. *Analytical Chemistry* 60:2299-2301
6. Tanaka K, Waki H, Ido Y, Akita S, Yoshida Y, et al. 1988. Protein and polymer analyses up to m/z 100 000 by laser ionization time-of-flight mass spectrometry. *Rapid Communications in Mass Spectrometry* 2:151-153
7. Dass C. 2001. *Principles and Practice of Biological Mass Spectrometry*. pp 84. New York: Wiley Interscience
8. Paul WS, H. 1953. Ein neues Massenspektrometer ohne Magnetfeld. *Z. Naturforschg* 8A:448-450
9. Biemann K, Scoble HA. 1987. Characterization by Tandem Mass-Spectrometry of Structural Modifications in Proteins. *Science* 237:992-998
10. Stafford Jr GC, Kelley PE, Syka JEP, Reynolds WE, Todd JFJ. 1984. Recent improvements in and analytical applications of advanced ion trap technology. *International Journal of Mass Spectrometry and Ion Processes* 60:85-98
11. Gobezie R, Millett PJ, Sarracino DS, Evans C, Thornhill TS. 2006. Proteomics: Applications to the study of rheumatoid arthritis and osteoarthritis. *Journal of the American Academy of Orthopaedic Surgeons* 14:325-332

12. Stephens WE. 1946. A Pulsed Mass Spectrometer with Time Dispersion. *Physical Review A* 69:691
13. Comisar.Mb, Marshall AG. 1974. Fourier-Transform Ion-Cyclotron Resonance Spectroscopy. *Chemical Physics Letters* 25:282-283
14. Whitehouse CM, Dreyer RN, Yamashita M, Fenn JB. 1985. Electrospray Interface for Liquid Chromatographs and Mass Spectrometers. *Analytical Chemistry* 57:675-679
15. Cole R. 1997. *Electrospray Ionization Mass Spectrometry. Fundamentals, Instrumentation, and Applications.* pp 577. Wiley
16. Pramanik BNG, A.K.; Gross, M.L. 2002. *Applied Electrospray Mass Spectrometry.* pp 434. New York: Marcel Dekker
17. Beavis RC, Chait BT. 1996. Matrix-assisted laser desorption ionization mass-spectrometry of proteins. *High Resolution Separation and Analysis of Biological Macromolecules, Pt A* 270:519-551
18. Roepstorff P, Fohlman J. 1984. Proposal for a Common Nomenclature for Sequence Ions in Mass-Spectra of Peptides. *Biomedical Mass Spectrometry* 11:601-601
19. Biemann K. 1988. Contributions of Mass-Spectrometry to Peptide and Protein-Structure. *Biomedical and Environmental Mass Spectrometry* 16:99-111
20. Dongre AR, Jones JL, Somogyi A, Wysocki VH. 1996. Influence of peptide composition, gas-phase basicity, and chemical modification on fragmentation efficiency: Evidence for the mobile proton model. *Journal of the American Chemical Society* 118:8365-8374
21. Wysocki VH, Tsaprailis G, Smith LL, Breci LA. 2000. Special feature: Commentary - Mobile and localized protons: a framework for understanding peptide dissociation. *Journal of Mass Spectrometry* 35:1399-1406
22. Paizs B, Suhai S. 2005. Fragmentation pathways of protonated peptides. *Mass Spectrometry Reviews* 24:508-548
23. Eng JK, McCormack AL, Yates JR. 1994. An Approach to Correlate Tandem Mass-Spectral Data of Peptides with Amino-Acid-Sequences in a Protein Database. *Journal of The American Society for Mass Spectrometry* 5:976-989

24. Perkins DN, Pappin DJC, Creasy DM, Cottrell JS. 1999. Probability-based protein identification by searching sequence databases using mass spectrometry data. *Electrophoresis* 20:3551-3567
25. Steen H, Mann M. 2004. The ABC's (and XYZ's) of peptide sequencing. *Nature Reviews Molecular Cell Biology* 5:699-711
26. Nesvizhskii AI, Vitek O, Aebersold R. 2007. Analysis and validation of proteomic data generated by tandem mass spectrometry. *Nature Methods* 4:787-797
27. Mueller DR, Eckersley M, Richter WJ. 1988. Hydrogen Transfer-Reactions in the Formation of Y+2 Sequence Ions from Protonated Peptides. *Organic Mass Spectrometry* 23:217-222
28. Cordero MM, Houser JJ, Wesdemiotis C. 1993. The Neutral Products Formed during Backbone Fragmentations of Protonated Peptides in Tandem Mass-Spectrometry. *Analytical Chemistry* 65:1594-1601
29. Johnson RS, Martin SA, Biemann K. 1988. Collision-Induced Fragmentation of (M+H)+Ions of Peptides - Side-Chain Specific Sequence Ions. *International Journal of Mass Spectrometry and Ion Processes* 86:137-154
30. Biemann K. 1990. [25] Sequencing of peptides by tandem mass spectrometry and high-energy collision-induced dissociation. In *Methods in Enzymology*, ed. AM James, Volume 193:455-479: Academic Press. Number of 455-479 pp.
31. Papayannopoulos IA. 1995. The Interpretation of Collision-Induced Dissociation Tandem Mass-Spectra of Peptides. *Mass Spectrometry Reviews* 14:49-73
32. Yalcin T, Khouw C, Csizmadia IG, Peterson MR, Harrison AG. 1995. Why are B ions stable species in peptide spectra? *Journal of The American Society for Mass Spectrometry* 6:1165-1174
33. Yalcin T, Csizmadia IG, Peterson MR, Harrison AG. 1996. The structure and fragmentation of B-n ( $n \geq 3$ ) ions in peptide spectra. *Journal of The American Society for Mass Spectrometry* 7:233-242
34. Nold MJ, Wesdemiotis C, Yalcin T, Harrison AG. 1997. Amide bond dissociation in protonated peptides. Structures of the N-terminal ionic and neutral fragments. *International Journal of Mass Spectrometry and Ion Processes* 164:137-153

35. Vachet RW, Ray KL, Glish GL. 1998. Origin of product ions in the MS/MS spectra of peptides in a quadrupole ion trap. *Journal of The American Society for Mass Spectrometry* 9:341-344
36. Harrison AG, Csizmadia IG, Tang TH. 2000. Structure and fragmentation of b(2) ions in peptide mass spectra. *Journal of The American Society for Mass Spectrometry* 11:427-436
37. Reid GE, Simpson RJ, O'Hair RAJ. 1999. Probing the fragmentation reactions of protonated glycine oligomers via multistage mass spectrometry and gas phase ion molecule hydrogen/deuterium exchange. *International Journal of Mass Spectrometry* 191:209-230
38. Somogyi A. 2008. Probing Peptide Fragment Ion Structures by Combining Sustained Off-Resonance Collision-Induced Dissociation and Gas-Phase H/D Exchange (SORI-HDX) in Fourier Transform Ion-Cyclotron Resonance (FT-ICR) Instruments. *Journal of The American Society for Mass Spectrometry* 19:1771-1775
39. Bythell BJ, Somogyi A, Paizs B. 2009. What is the Structure of b(2) Ions Generated from Doubly Protonated Tryptic Peptides? *Journal of The American Society for Mass Spectrometry* 20:618-624
40. Rodriguez CF, Cunje A, Shoeib T, Chu IK, Hopkinson AC, Siu KWM. 2001. Proton migration and tautomerism in protonated triglycine. *Journal of the American Chemical Society* 123:3006-3012
41. Chen XH, Turecek F. 2005. Simple b ions have cyclic oxazolone structures. A neutralization-reionization mass spectrometric and computational study of oxazolone radicals. *Journal of The American Society for Mass Spectrometry* 16:1941-1956
42. Polfer NC, Oomens J, Suhai S, Paizs B. 2005. Spectroscopic and theoretical evidence for oxazolone ring formation in collision-induced dissociation of peptides. *Journal of the American Chemical Society* 127:17154-17155
43. Polfer NC, Oomens J, Suhai S, Paizs B. 2007. Infrared spectroscopy and theoretical studies on gas-phase protonated leu-enkephalin and its fragments: Direct experimental evidence for the mobile proton. *Journal of the American Chemical Society* 129:5887-5897
44. Yoon SH, Chamot-Rooke J, Perkins BR, Hilderbrand AE, Poutsma JC, Wysocki VH. 2008. IRMPD Spectroscopy Shows That AGG Forms an Oxazolone b(2)(+) Ion. *Journal of the American Chemical Society* 130:17644-+

45. Oomens J, Young S, Molesworth S, van Stipdonk M. 2009. Spectroscopic Evidence for an Oxazolone Structure of the b(2) Fragment Ion from Protonated Tri-Alanine. *Journal of The American Society for Mass Spectrometry* 20:334-339
46. Perkins BR, Chamot-Rooke J, Yoon SH, Gucinski AC, Somogyi A, Wysocki VH. 2009. Evidence of Diketopiperazine and Oxazolone Structures for HA b(2)(+) Ion. *Journal of the American Chemical Society* 131:17528-17529
47. Polce MJ, Ren D, Wesdemiotis C. 2000. Special feature: Commentary - Dissociation of the peptide bond in protonated peptides. *Journal of Mass Spectrometry* 35:1391-1398
48. Farrugia JM, O'Hair RAJ, Reid GE. 2001. Do all b2 ions have oxazolone structures? Multistage mass spectrometry and ab initio studies on protonated N-acyl amino acid methyl ester model systems. *International Journal of Mass Spectrometry* 210-211:71-87
49. Yague J, Paradela A, Ramos M, Ogueta S, Marina A, et al. 2003. Peptide rearrangement during quadrupole ion trap fragmentation: Added complexity to MS/MS spectra. *Analytical Chemistry* 75:1524-1535
50. Harrison AG, Young AB, Bleiholder C, Suhai S, Paizs B. 2006. Scrambling of Sequence Information in Collision-Induced Dissociation of Peptides. *Journal of the American Chemical Society* 128:10364-10365
51. Jia CX, Qi W, He ZM. 2007. Cyclization reaction of peptide fragment ions during multistage collisionally activated decomposition: An inducement to lose internal amino-acid residues. *Journal of The American Society for Mass Spectrometry* 18:663-678
52. Mouls L, Aubagnac JL, Martinez J, Enjalbal C. 2007. Low energy peptide fragmentations in an ESI-Q-ToF type mass spectrometer. *Journal of Proteome Research* 6:1378-1391
53. Bleiholder C, Osburn S, Williams TD, Suhai Sn, Van Stipdonk M, et al. 2008. Sequence-Scrambling Fragmentation Pathways of Protonated Peptides. *Journal of the American Chemical Society* 130:17774-17789
54. Riba-Garcia I, Giles K, Bateman RH, Gaskell SJ. 2008. Evidence for structural variants of a- and b-type peptide fragment ions using combined ion mobility/mass spectrometry. *Journal of The American Society for Mass Spectrometry* 19:609-613

55. Harrison AG. 2008. Peptide sequence scrambling through cyclization of b(5) ions. *Journal of The American Society for Mass Spectrometry* 19:1776-1780
56. Harrison AG. 2009. Cyclization of peptide b9 ions. *Journal of The American Society for Mass Spectrometry* 20:2248-2253
57. Molesworth S, Osburn S, Van Stipdonk M. 2009. Influence of size on apparent scrambling of sequence during CID of b-type ions. *Journal of The American Society for Mass Spectrometry* 20:2174-2181
58. Molesworth S, Osburn S, Van Stipdonk M. 2010. Influence of amino acid side chains on apparent selective opening of cyclic b5 ions. *Journal of The American Society for Mass Spectrometry* 21:1028-1036
59. Chen X, Yu L, Steill JD, Oomens J, Polfer NC. 2009. Effect of Peptide Fragment Size on the Propensity of Cyclization in Collision-Induced Dissociation: Oligoglycine b2–b8. *Journal of the American Chemical Society* 131:18272-18282
60. Bythell BJ, Knapp-Mohammady M, Paizs B, Harrison AG. 2010. Effect of the His residue on the cyclization of b ions. *Journal of The American Society for Mass Spectrometry* 21:1352-1363
61. Afonso C, Modeste F, Breton P, Fournier F, Tabet JC. 2000. Proton affinities of the commonly occurring L-amino acids by using electrospray ionization-ion trap mass spectrometry. *European Journal of Mass Spectrometry* 6:443-449
62. Hunt DF, Yates JR, Shabanowitz J, Winston S, Hauer CR. 1986. Protein Sequencing by Tandem Mass-Spectrometry. *Proceedings of the National Academy of Sciences of the United States of America* 83:6233-6237
63. Schwartz BL, Bursey MM. 1992. Some Proline Substituent Effects in the Tandem Mass-Spectrum of Protonated Pentaalanine. *Biological Mass Spectrometry* 21:92-96
64. Loo JA, Edmonds CG, Smith RD. 1993. Tandem Mass-Spectrometry of Very Large Molecules .2. Dissociation of Multiply Charged Proline-Containing Proteins from Electrospray Ionization. *Analytical Chemistry* 65:425-438
65. Vaisar T, Urban J. 1996. Probing Proline Effect in CID of Protonated Peptides. *Journal of Mass Spectrometry* 31:1185-1187

66. Brexi LA, Tabb DL, Yates JR, Wysocki VH. 2003. Cleavage N-Terminal to Proline: Analysis of a Database of Peptide Tandem Mass Spectra. *Analytical Chemistry* 75:1963-1971
67. Huang YY, Triscari JM, Tseng GC, Pasa-Tolic L, Lipton MS, et al. 2005. Statistical characterization of the charge state and residue dependence of low-energy CID peptide dissociation patterns. *Analytical Chemistry* 77:5800-5813
68. Bleiholder C, Suhai S, Harrison AG, Paizs B. 2011. Towards Understanding the Tandem Mass Spectra of Protonated Oligopeptides. 2: The Proline Effect in Collision-Induced Dissociation of Protonated Ala-Ala-Xxx-Pro-Ala (Xxx = Ala, Ser, Leu, Val, Phe, and Trp). *Journal of The American Society for Mass Spectrometry* 22:1032-1039
69. Unnithan AG, Myer MJ, Veale CJ, Danell AS. 2007. MS/MS of protonated polyproline peptides: The influence of N-terminal protonation on dissociation. *Journal of The American Society for Mass Spectrometry* 18:2198-2203
70. Grewal RN, El Aribi H, Harrison AG, Siu KWM, Hopkinson AC. 2004. Fragmentation of protonated tripeptides: The proline effect revisited. *Journal of Physical Chemistry B* 108:4899-4908
71. Harrison AG, Young AB. 2005. Fragmentation reactions of deprotonated peptides containing proline. The proline effect. *Journal of Mass Spectrometry* 40:1173-1186
72. Eckart K, Holthausen MC, Koch W, Spiess J. 1998. Mass spectrometric and quantum mechanical analysis of gas-phase formation, structure, and decomposition of various b(2) ions and their specifically deuterated analogs. *Journal of The American Society for Mass Spectrometry* 9:1002-1011
73. Smith LL, Herrmann KA, Wysocki VH. 2006. Investigation of gas phase ion structure for proline-containing b(2) ion. *Journal of The American Society for Mass Spectrometry* 17:20-28
74. Gucinski AC, Chamot-Rooke J, Steinmetz V, Somogyi A, Wysocki VH. 2013. Influence of N-terminal Residue Composition on the Structure of Proline-Containing b(2)(+) Ions. *Journal of Physical Chemistry A* 117:1291-1298
75. Harrison A. 2012. Fragmentation Reactions of b5 and a5 Ions Containing Proline—The Structures of a5 Ions. *Journal of The American Society for Mass Spectrometry* 23:594-601



76. Huang YY, Wysocki VH, Tabb DL, Yates JR. 2002. The influence of histidine on cleavage C-terminal to acidic residues in doubly protonated tryptic peptides. *International Journal of Mass Spectrometry* 219:233-244
77. Tabb DL, Huang YY, Wysocki VH, Yates JR. 2004. Influence of basic residue content on fragment ion peak intensities in low-energy - collision-induced dissociation spectra of peptides. *Analytical Chemistry* 76:1243-1248
78. Tsaprailis G, Nair H, Zhong W, Kuppannan K, Futrell JH, Wysocki VH. 2004. A mechanistic investigation of the enhanced cleavage at histidine in the gas-phase dissociation of protonated peptides. *Analytical Chemistry* 76:2083-2094
79. Bythell BJ, Knapp-Mohammady M, Paizs B, Harrison AG. 2010. Effect of the His Residue on the Cyclization of b Ions. *Journal of The American Society for Mass Spectrometry* 21:1352-1363
80. Yalcin T, Harrison AG. 1996. Ion chemistry of protonated lysine derivatives. *Journal of Mass Spectrometry* 31:1237-1243
81. Molesworth SP, Van Stipdonk MJ. 2010. Apparent inhibition by arginine of macrocyclic b ion formation from singly charged protonated peptides. *Journal of The American Society for Mass Spectrometry* 21:1322-1328

# VITA

## PERSONAL INFORMATION

**Date / Place of Birth:** 19.05.1982 / Milas - Türkiye

**E-mail:** ctasoglu@gmail.com

## EDUCATION

<b>2013</b>	<b>Ph.D. in Chemistry</b>	İzmir Institute of Technology
<b>2008</b>	<b>M.Sc. in Chemistry</b>	İzmir Institute of Technology
<b>2005</b>	<b>B.Sc. in Chemistry</b>	İzmir Institute of Technology
<b>2000</b>	<b>High School</b>	İzmir Atatürk Lisesi

## WORK EXPERIENCE

<b>2007-2014</b>	<b>Teaching Assistant</b>	İzmir Institute of Technology
<b>2004</b>	<b>Trainee</b>	İzmir Bölge Hıfzıssıhha Enst.

## PUBLICATIONS

Alex G. Harrison, Cagdas Tasoglu, Talat Yalcin. ‘‘Non-Direct Sequence Ions in the Tandem Mass Spectrometry of Protonated Peptide Amides - an Energy-Resolved Study’’. *Journal of The American Society for Mass Spectrometry*. **2013**, 24: 1565-1572.

Cagdas Tasoglu, Guvenc Gorgulu, Talat Yalcin. ‘‘Investigation of peptide size, residue position, neighbor amino acid and side chain effect on macrocyclization of  $b_n$  ( $n = 5-7$ ) ions’’. *International Journal of Mass Spectrometry*. **2012**, 316-318: 108-116.